

---

# **PEPTIDES AS MODULATORS OF PROTEIN-PROTEIN INTERACTIONS**

---

**Annamaria Sandomenico**

Dottorato in Scienze Biotechologiche – XXI ciclo  
Indirizzo Biotecnologie industriali  
Università di Napoli Federico II



Dottorato in Scienze Biotechologiche – XXI ciclo  
Indirizzo Biotecnologie industriali  
Università di Napoli Federico II



---

# **PEPTIDES AS MODULATORS OF PROTEIN-PROTEIN INTERACTIONS**

---

**Annamaria Sandomenico**

**Dottoranda: Dott.ssa Annamaria Sandomenico**

**Relatore: Prof. Ettore Benedetti**

**Correlatore: Dott. Menotti Ruvo**

**Coordinatore: Prof. Giovanni Sannia**

## **“LENTAMENTE MUORE”**

*Lentamente muore,*

*chi diventa schiavo dell'abitudine, ripetendo ogni giorno gli stessi percorsi,*

*chi non cambia la marcia,*

*chi non rischia e cambia colore dei vestiti,*

*chi non parla a chi non conosce.*

*Muore lentamente chi evita una passione,*

*chi preferisce il nero su bianco e i puntini sulle “i” piuttosto che un insieme di emozioni,*

*proprio quelle che fanno brillare gli occhi, quelle che fanno di uno sbadiglio un sorriso,*

*quelle che fanno battere il cuore davanti all'errore e ai sentimenti.*

*Lentamente muore,*

*chi non capovolge il tavolo,*

*chi e' infelice sul lavoro,*

*chi non rischia la certezza per l'incertezza per inseguire un sogno,*

*chi non si permette almeno una volta nella vita di fuggire ai consigli sensati.*

*Lentamente muore chi non viaggia,*

*chi non legge,*

*chi non ascolta musica,*

*chi non trova grazia in se stesso.*

*Muore lentamente chi distrugge l'amor proprio,*

*chi non si lascia aiutare;*

*chi passa i giorni a lamentarsi della propria sfortuna o della pioggia incessante.*

*Lentamente muore chi abbandona un progetto prima di iniziarlo,*

*chi non fa domande sugli argomenti che non conosce,*

*chi non risponde quando gli chiedono qualcosa che conosce.*

*Evitiamo la morte a piccole dosi,*

*ricordando sempre che essere vivo richiede uno sforzo di gran lunga maggiore del semplice fatto di respirare.*

*Soltanto l'ardente pazienza porterà al raggiungimento di una splendida felicità.*

**Pablo Neruda**

**“SLOWLY DYING”**

*Slowly dying,*

*who becomes a slave of habit*

*who repeating every day the same routes,*

*who does not change the march,*

*who does not speak to those do not Know.*

*Dies slowly who avoids a passion,*

*Who prefers black and white and dot the “i” rather than a set of emotions,*

*those who make their eyes light up, those who are a yawn of a smile,*

*those that make the heart beat before the error and feelings.*

*Slowly dying,*

*Who does not overturn the table,*

*Who unhappy at work,*

*Who does not risk certainty for the uncertainty to chase a dream,*

*Who would not at least once in life to flee to sensible advice.*

*Slowly dying,*

*Who do not travel,*

*Those who do not read,*

*Who does not listen to music,*

*Who does not find grace in himself.*

*He died slowly,*

*Who destroy the self-respect,*

*Who will not be helping;*

*Who passes the day to complain its bad luck or the incessant rain.*

*Slowly dying, who abandons a project before you start,*

*Who does questions on the subjects that do not know,*

*Those who do not respond when seeking something familiar.*

*Let's death in small doses,*

*Remembering always that being alive requires an effort far greater the sample act of breathing.*

*Only ardent patience leads to achieve a splendid happiness.*

**Pablo Neruda**

# INDEX

<b>RIASSUNTO</b>	pag. 1
<b>SUMMARY</b>	pag. 7
<b>I. PEPTIDES AS MODULATORS OF PROTEIN-PROTEIN INTERACTIONS</b>	pag. 8
<b>I.1 REFERENCES</b>	pag. 9
<b>II. PEPTIDES MIMICKING THE IgE HIGH AFFINITY RECEPTOR FcεRI</b>	pag. 10
<b>II.1 INTRODUCTION</b>	pag. 10
<b>II.1.2 The IgE high –affinity receptor: FcεRI</b>	pag. 12
<b>II.1.3 Structural insights into the interaction between IgE and its high affinity receptor FcεRI</b>	pag. 14
<b>II.2 PROJECT AIMS</b>	pag. 19
<b>II.3 EXPERIMENTAL PROCEDURES</b>	pag. 20
<b>II.3.1 Materials</b>	pag. 20
<b>II.3.2 Methods</b>	pag. 21
<b>II.3.2.1 Cloning of α-chain human FcεRI</b>	pag. 21
<b>II.3.2.2 Expression screening for the full-length human FcεRI α-chain</b>	pag. 22
<b>II.3.2.3 Purification of full-length His6x-αchain</b>	pag. 22
<b>II.3.2.4 Purification of full-length GST-αchain</b>	pag. 23
<b>II.3.2.5 Purification of full-length MBP-αchain</b>	pag. 23
<b>II.3.2.6 Purification of periplasmatic full-length His6x-αchain and full-length Dsb-His6x-αchain</b>	pag. 23
<b>II.3.2.7 Expression and purification of His6x-D1-D2 domain as inclusion bodies</b>	pag. 24
<b>II.3.2.8 Expression and purification of MBP-D2 domain</b>	pag. 25
<b>II.3.2.9 Expression and purification of His6x-D2 domain</b>	pag. 25
<b>II.3.2.10 Western blotting</b>	pag. 26
<b>II.3.2.11 Vinyl pyridine reaction</b>	pag. 26
<b>II.3.2.12 Gel filtration analysis</b>	pag. 26
<b>II.3.2.13 Protein characterization LC-MS</b>	pag. 26
<b>II.3.2.14 Circular Dichroism analysis</b>	pag. 27
<b>II.3.2.15 Peptide synthesis, purification and characterization</b>	pag. 27
<b>II.3.2.16 Immunoglobulins coating on sensor surface</b>	pag. 28
<b>II.3.2.17 SPR data fitting and analysis</b>	pag. 28
<b>II.3.2.18 ELISA assay</b>	pag. 29
<b>II.4 RESULTS AND DISCUSSION</b>	pag. 31
<b>II.4.1 Molecular design of FcεRI receptor mimicking polypeptides</b>	pag. 31

<b>II.4.1.2 Synthesis, purification and characterization of polypeptides</b>	pag. 33
<b>II.4.1.3 Equilibrium affinity measurements between IgE-receptor mimicking peptides by SPR assay</b>	pag. 35
<b>II.4.1.4 Selectivity affinity measurements between IgE-receptor mimicking peptides by SPR assay</b>	pag. 45
<b>II.4.2 Expression of human FcεRI αchain as recombinant protein</b>	pag. 47
<b>II.4.2.1 Expression and purification of full length hαFcεRI</b>	pag. 47
<b>II.4.2.2 Expression and purification of D1-D2 domain</b>	pag. 50
<b>II.4.2.3 Expression and purification of D2 domain</b>	pag. 51
<b>II.4.2.4 Expression, purification and characterization of His6x-D2 domain</b>	pag. 52
<b>II.4.2.4a Expression and purification of His6x-D2 domain</b>	pag. 52
<b>II.4.2.4b Refolding of His6x-D2 domain</b>	pag. 53
<b>II.4.2.4c Characterization of His6x-D2 domain</b>	pag. 54
<b>II.4.2.5 His6x-D2 domain – Immunoglobulins E binding assay</b>	pag. 55
<b>II.4.3 ELISA Competition assay with synthetic peptides</b>	pag. 60
<b>II.5 CONCLUSIONS AND PERSPECTIVES</b>	pag. 62
<b>II.6 REFERENCES</b>	pag. 64
<b>III. IDENTIFICATION OF A BCL-10 INHIBITORY PEPTIDE</b>	pag. 67
<b>III.1 INTRODUCTION</b>	pag. 67
<b>III.1.2 The family of CARD containing proteins</b>	pag. 68
<b>III.1.3 BCL10: a modular protein</b>	pag. 69
<b>III.2 PROJECT AIMS</b>	pag. 71
<b>III.3 EXPERIMENTAL PROCEDURES</b>	pag. 72
<b>III.3.1 Materials</b>	pag. 72
<b>III.3.2 Methods</b>	pag. 72
<b>III.3.2.1 BCL10-CARD domain cloning, expression and purification</b>	pag. 72
<b>III.3.2.2 Circular Dichroism analysis</b>	pag. 73
<b>III.3.2.3 Biotinylation of the BCL10-CARD domain</b>	pag. 73
<b>III.3.2.4 Protein digestion with trypsin and peptide fractionation</b>	pag. 73
<b>III.3.2.5 BCL10-CARD domain self-association and binding competition ELISA assays</b>	pag. 74
<b>III.3.2.6 Peptide synthesis, purification and characterization</b>	pag. 75
<b>III.3.2.7 Size Exclusion Chromatography analysis</b>	pag. 75
<b>III.3.2.8 Serum stability</b>	pag. 75
<b>III.3.2.9 Cell culture</b>	pag. 76
<b>III.3.2.10 Immunoblot analysis and co-immunoprecipitation</b>	pag. 76

<b>III.3.2.11 Fluorescence peptide assay</b>	pag. 76
<b>III.3.2.12 NFκB luciferase reporter gene assay</b>	pag. 76
<b>III.4 RESULTS AND DISCUSSION</b>	pag. 78
<b>III.4.1 Expression, purification and characterization of BCL10-CARD domain</b>	pag. 78
<b>III.4.2 Identification of BCL10-CARD regions involved in self-association</b>	pag. 79
<b>III.4.2.1 BCL10–CARD domain self-association assay</b>	pag. 79
<b>III.4.2.2 Protein digestion with trypsin and peptide fractionation</b>	pag. 80
<b>III.4.2.3 Protein fragments characterization and screening competition assay</b>	pag. 80
<b>III.4.3 Molecular design of BCL10 peptides</b>	pag. 81
<b>III.4.3.1 Synthesis, purification and characterization of BCL10 peptides</b>	pag. 82
<b>III.4.3.2 Competitive ELISA assay with BCL10-CARD peptides</b>	pag. 83
<b>III.4.3.3 Characterisation of the oligomeric state of Peptide I and Peptide II by SEC analysis</b>	pag. 83
<b>III.4.3.4 Ala-scanning assay</b>	pag. 84
<b>III.4.4 Cellular assays</b>	pag. 85
<b>III.4.4.1 Synthesis, purification, serum stability and characterization of TAT-conjugated and FITC-TAT-conjugated Peptide VIII</b>	pag. 85
<b>III.4.4.2 Immunoblotting and co-precipitation analysis</b>	pag. 86
<b>III.4.4.3 Assessment of peptide entry into HEK 293 cells</b>	pag. 87
<b>III.4.4.4 NFκB luciferase reporter gene assay</b>	pag. 88
<b>III.5 CONCLUSIONS AND PERSPECTIVES</b>	pag. 90
<b>III.6 REFERENCES</b>	pag. 92
<b>IV. ABBREVIATIONS INDEX</b>	pag. 95
<b>V. SCIENTIFIC PRESENTATIONS</b>	pag. 97
<b>VI. PUBLICATIONS</b>	pag. 98

## RIASSUNTO

Uno degli aspetti più importanti nella moderna ricerca biotecnologica riguarda lo studio a livello molecolare delle interazioni proteina-proteina essenziali per una corretta comprensione dei meccanismi fisio-patologici che regolano i processi cellulari.

Tali interazioni possono scatenare eventi quali il reclutamento di specifiche proteine segnale, richieste per svolgere una determinata funzione nei compartimenti cellulari, oppure l'induzione di stati conformazionali in grado di cambiare l'attività e/o modificare l'accessibilità di una proteina ad altri domini di legame, permettendo ulteriori interazioni proteina-proteina. Pertanto, la conoscenza dettagliata dei meccanismi biomolecolari responsabili di interazioni proteina-proteina, rappresenta il primo traguardo per la modulazione dell'attività biologica di proteine target che controllano i processi cellulari.

Attualmente, l'identificazione di molecole capaci di inibire o promuovere interazioni proteina-proteina o proteina-ligandi rappresenta lo scopo ultimo nel processo di "*drug discovery*". Diversamente dal tradizionale approccio, basato soprattutto sul design di inibitori modellati su substrati molecolari specifici per siti attivi enzimatici, lo sviluppo di inibitori capaci di modulare interazioni proteina-proteina si presenta come un processo più complesso in quanto subordinato a numerosi fattori. In primo luogo, l'ampia interfaccia di interazione (750–1500 Å<sup>2</sup>) necessaria per lo specifico riconoscimento, implica l'uso di molecole più grandi rispetto ai piccoli ligandi usati come inibitori enzimatici. Inoltre, la presenza di regioni multiple e non contigue responsabili del legame, piuttosto che un unico sito di legame ben definito, e l'adattabilità delle superfici proteiche che sono in grado di riarrangiare la loro struttura in seguito ad interazioni, rendono più complicato e articolato il "*rational design*". Tuttavia, negli ultimi anni sono stati identificati numerosi ligandi di varie dimensioni capaci di modulare e/o distruggere un'interazione proteina-proteina che hanno portato lo sviluppo e la commercializzazione di potenti inibitori impiegabili in patologie come il cancro e HIV.

L'obiettivo principale dello studio condotto durante questo lavoro di tesi è stato proprio l'identificazione di molecole capaci di modulare interazioni proteina-proteina.

E' noto che numerose patologie sono associate alla trasduzione di segnali biochimici dall'esterno della cellula fino ai compartimenti subcellulari in cui avvengono reazioni biomolecolari cruciali per la sopravvivenza della cellula stessa. La regolazione dei segnali di trasduzione può avvenire a monte (*upstream regulation*), modulando interazioni proteina-recettore di membrana, e/o a valle (*downstream regulation*), modulando interazioni proteina-proteina che portano all'attivazione di fattori di trascrizione attraverso complesse cascate di amplificazione del segnale.

La prima parte della tesi è stata incentrata sull'identificazione di molecole capaci di modulare l'interazione IgE-FcεRI, uno dei principali target molecolari per bloccare le reazioni allergiche di ipersensibilità immediata di tipo I.

La recente determinazione della struttura cristallografica del complesso, formato dalla catena α extracellulare del recettore FcεRI e la porzione Fc delle IgE, ha consentito di chiarirne sia il meccanismo molecolare che la stechiometria di interazione, aprendo così la strada alla progettazione di molecole di tipo peptidico e

peptidomimetico che possano modulare tale interazione. Data la crescente incidenza (oltre il 20% della popolazione mondiale), di malattie di natura allergica, questo tipo di molecole avrebbero un enorme interesse industriale per lo sviluppo di nuove classi di farmaci non di tipo sintomatico come gli antistaminici, ma eziologico. Pertanto, l'obiettivo è stato quello di selezionare delle nuove molecole di sintesi, mimanti il recettore, capaci di legare specificamente le IgE, da usare come punto di partenza per lo sviluppo di modulatori potenti e selettivi della reazione allergica.

Inoltre, lo stesso recettore in forma ricombinante solubile e attiva può trovare applicazione come agente terapeutico oltre a rappresentare il presupposto per l'allestimento di saggi biochimici di legame con le IgE da impiegare per la selezione di molecole di sintesi, disegnate *ad hoc* o preparate in maniera "random", che siano capaci di interferire con tale interazione.

Il progetto è stato sviluppato seguendo due differenti approcci: i) progettazione e sintesi di recettore-mimetici ("*synthetic receptor*") e ii) preparazione per via ricombinante della porzione extracellulare del recettore. La validità della prevenzione del legame delle IgE al recettore FcεRI come target è clinicamente dimostrata dall'efficacia riscontrata con l'anticorpo monoclonale anti-IgE rhu-Mab E25 (Omalizumab), già in commercio da qualche anno.

La regione extracellulare della catena α del recettore FcεRI, costituita da due "Ig-like domains", denominati D1 e D2, interagisce con la porzione Fc-IgE attraverso due siti di legame. La determinazione della struttura cristallografica del complesso αFcεRI-Fc-IgE ad alta affinità ( $K_D=10^{-9}$ - $10^{-10}$ M) ha permesso di identificare in maniera dettagliata gli amminoacidi che sono coinvolti nei due siti di interazione. Utilizzando questi dati strutturali è stato disegnato un polipeptide, denominato IgE-TRAP (M.W. 3474 amu), rappresentato schematicamente in Fig.1, in cui sono stati mimati entrambi i siti di interazione.

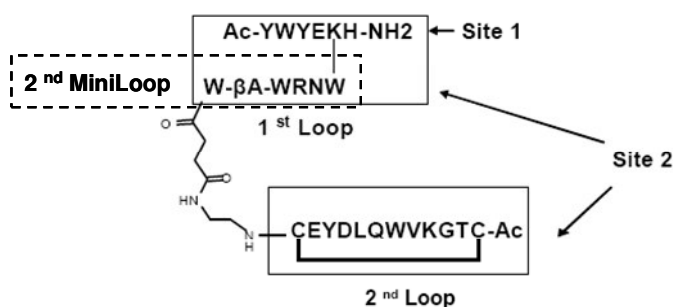


**Figura 1:** Rappresentazione schematica del polipeptide IgE-TRAP ossidato

Su entrambe le forme del polipeptide IgE-TRAP, ridotta ed ossidata, è stata condotta un'analisi strutturale preliminare in soluzione, mediante dicroismo circolare. Questa indagine ha evidenziato per il polipeptide ridotto una conformazione secondaria prevalentemente di tipo β-sheet. L'affinità dei peptidi per le IgE è stata determinata mediante saggi di legame utilizzando la tecnica SPR.

I dati SPR sono stati accuratamente analizzati assumendo una stechiometria 1:1 e utilizzando un modello bifasico. In tal modo, per ogni fase, è stata estrapolata una costante di affinità ( $K_{D1}$  e  $K_{D2}$ ) ed è stata calcolata una costante di affinità globale ( $K_D$ ). Pertanto è stato possibile analizzare il contributo dei singoli siti e il loro effetto globale nell'interazione. Entrambi i polipeptidi IgE-TRAP hanno mostrato affinità per le IgE. In particolare, per il polipeptide ciclico, sono state estrapolate una  $K_{D1} = 65$

$\mu\text{M}$ ,  $KD_2 = 60 \mu\text{M}$  e  $KD$  globale di  $16 \mu\text{M}$ , mentre per la forma ridotta una  $KD_1 = 19 \mu\text{M}$ , una  $KD_2 = 37 \mu\text{M}$  ed una  $KD$  globale di  $6.2 \mu\text{M}$ . Per entrambi la costante di affinità globale è risultata essere più bassa delle singole costanti separate, confermando in tal modo la presenza di un meccanismo cooperativo dei due siti. Sebbene per entrambi la  $KD$  risulta nell'ordine micromolare, il polipeptide ridotto mostra una affinità globale 2.5 volte più alta rispetto alla forma ossidata. Tale aumento è il risultato complessivo di una maggiore flessibilità conformazionale dovuta all'assenza del ponte disolfuro che consente al polipeptide ridotto di adattarsi più facilmente alla superficie delle immunoglobuline. Questo effetto si riflette soprattutto sul sito 1, in cui la  $KD_1$  diminuisce da  $65 \mu\text{M}$  (nella forma ossidata) a  $19 \mu\text{M}$  (nella forma ridotta), e solo parzialmente sul sito 2. Per aumentare l'affinità del polipeptide IgE-TRAP, abbiamo esplorato una possibile correlazione struttura-attività utilizzando un set di peptidi derivanti dallo stesso, che riproducono i due siti anche separatamente. Mediante analisi SPR è stato confermato che il peptide denominato 1° Loop (Fig.1) riconosce ancora le IgE e sono state estrapolate una  $KD_1 = 65 \mu\text{M}$ ,  $KD_2 = 19 \times 10^{-5} \text{M}$  e  $KD$  globale di  $19 \mu\text{M}$ , mentre per il peptide denominato 2° Loop (Fig.1), nelle varianti forma ossidata e ridotta, non è stato osservato nessun legame. Questi dati evidenziano che il 1° Loop è responsabile del legame, media il riconoscimento e promuove il successivo legame del 2° Loop. Infatti, il 1° Loop mostrando una  $KD_1 = 65 \mu\text{M}$  (uguale a quella estrapolata per il polipeptide IgE-TRAP ossidato) conferma che la presenza o l'assenza del 2° Loop influenza lo stato conformazionale incidendo soprattutto sul riconoscimento mediato dal sito 1. Inoltre, dall'analisi di peptidi riproducenti separatamente i due siti di legame, è stato evidenziato che solo il peptide denominato 2° MiniLoop (Fig.1), che riproduce essenzialmente il sito 2, è in grado di riconoscere, sebbene con una debole affinità ( $KD = 8.3 \times 10^{-4} \text{M}$ ), le IgE. I dati SPR, in questo caso, sono stati analizzati assumendo una stechiometria 1:1 e utilizzando un modello monofasico. Ciò conferma che il sito 2 è stato riprodotto con efficienza, e che il 2° MiniLoop rappresenta la sequenza amminoacidica responsabile dell'ancoraggio alle IgE, contenuta anche nel 1° Loop (Fig.1). La selettività dei peptidi selezionati (IgE-TRAP, 1° Loop e 2° MiniLoop) di riconoscere esclusivamente le IgE è stata verificata mediante saggi di legame con altre immunoglobuline, IgG e IgA, le più abbondanti nel siero, utilizzando ancora la tecnica SPR, dimostrando che i peptidi legano esclusivamente le immunoglobuline di tipo E.

Parallelamente è stata messa a punto l'espressione della catena  $\alpha$  del recettore Fc $\epsilon$ RI in forma ricombinante da usare sia per allestire saggi di legame con le IgE per lo screening di molecole di sintesi e di librerie peptidiche, sia come antagonista solubile delle stesse IgE.

La catena  $\alpha$  del recettore hFc $\epsilon$ RI è stata espressa in forma ricombinate sia come proteina intera (1-257), sia come dominio D1-D2 (1-170) che come singolo dominio D2 (84-170) della porzione extracellulare (ECD). Le varie forme ricombinanti della proteina intera e del dominio D1-D2 sono risultate inattive a causa delle difficoltà incontrate nella rinaturazione della proteina che contiene 4 cisteine. La presenza delle cisteine ha portato quasi sempre alla formazione di aggregati covalenti insolubili. Invece, la forma ricombinante del dominio D2, recante al N-terminale una coda di 6xHis, è stata purificata in condizioni denaturanti e rinaturata con successo. La proteina rinaturata presenta una struttura secondaria prevalentemente di tipo  $\beta$ -sheet, come atteso dalla struttura cristallografica nota, mentre un'analisi dello stato oligomerico, mediante cromatografia ad esclusione molecolare, ha evidenziato una forte tendenza della proteina a formare oligomeri di natura non covalente. Il dominio

His6x-D2 rinaturato, sebbene oligomero, è risultato attivo, infatti il legame alle IgE è stato confermato sia mediante tecnica SPR che ELISA. Da un'analisi preliminare del legame del dominio alle IgE, mediante SPR, sono state estrapolate una  $KD_1 = 8.3 \mu\text{M}$ ,  $KD_2 = 11.1 \mu\text{M}$  e una  $KD$  globale di  $1.8 \mu\text{M}$ . Anche in questo caso, la cooperatività dei due siti è stata confermata dalla costante di affinità globale più bassa delle singole costanti separate. Tuttavia, il dominio His6x-D2 ricombinante mostra una affinità dell'ordine micromolare per le IgE, più bassa rispetto a quella del recettore intero nativo ( $KD=10^{-9} \text{M}$ ), prevedibilmente sia per la mancanza del dominio D1 (il quale pur non essendo direttamente coinvolto nell'interazione contribuisce strutturalmente al mantenimento dell'alta affinità) sia a causa dello stato oligomero che rende la proteina meno disponibile al riconoscimento. Inoltre, il legame è stato confermato, mediante saggio ELISA, ed è stato ottimizzato variando condizioni di pH e di concentrazione salina. È stato verificato che l'uso di un tampone leggermente più acido (Bis-Tris 25 mM pH 6.5, NaCl 150 mM) rende la proteina più disponibile al riconoscimento. Mediante saggio ELISA in tali condizioni, sono stati evidenziati i due siti di interazione e sono state estrapolate una  $KD_1 = 112 \text{ nM}$  per il primo sito, la cui saturazione avviene per concentrazioni superiori a  $1 \mu\text{M}$ , e una  $KD_2 = 4.1 \mu\text{M}$  per il secondo sito, la cui saturazione avviene per concentrazioni superiori a  $20 \mu\text{M}$ . La messa a punto del saggio biochimico di legame ha consentito di verificare la capacità dei polipeptidi IgE-TRAP, 1° Loop e 2° MiniLoop (selezionati come "binders" delle IgE) di spiazzare l'interazione His6x-D2 ricombinante - IgE. Saggi ELISA di competizione hanno confermato che il polipeptide IgE-TRAP ridotto riesce a spiazzare l'interazione con una  $IC_{50} = 36 \mu\text{M}$ ; il 1° Loop e il 2° MiniLoop, prevedibilmente, competono ma con  $IC_{50} = 103 \mu\text{M}$  e  $IC_{50} = 864 \mu\text{M}$ , rispettivamente, in ottimo accordo con le  $KD$  determinate per legame diretto. Questi dati indicano che le molecole disegnate soddisfano il requisito della selettività per le IgE con un'affinità di interazione dell'ordine micromolare. Pertanto, il peptide 1° Loop potrebbe rappresentare il punto di partenza per lo sviluppo di nuove molecole più affini. La messa a punto del saggio biochimico di legame tra il dominio His6x-D2 ricombinante e le IgE consente la selezione di competitori mediante lo screening di librerie di composti.

La seconda parte del lavoro di tesi è stata incentrata sull'identificazione di un peptide capace di inibire il processo di oligomerizzazione della proteina BCL10. BCL10 (B-cell lymphoma 10) è un fattore proteico con una struttura bipartita, costituita da un dominio CARD N-terminale e da un dominio C-terminale ricco in residui di treonina e serina. Sebbene il completo "pathway" di attivazione della proteina non è ancora del tutto chiaro, molti studi hanno confermato che BCL10, attraverso interazioni omofile con altre proteine, mediate dal dominio CARD N-terminale, promuove l'attivazione del fattore NF- $\kappa$ B. BCL10 è un importante modulatore della risposta immunitaria, infatti l'attivazione dei recettori TCR (localizzati sulle cellule T e B) induce, mediante interazioni CARD-CARD, la formazione del complesso CBM (CARMA1-BCL10-MALT1) che, attraverso la fosforilazione del complesso IKK, promuove l'attivazione del fattore NF- $\kappa$ B. Modificazioni morfologiche o mutazioni a livello del dominio CARD si riflettono nella perdita di capacità da parte della proteina di agire correttamente. Recenti dati di letteratura dimostrano, infatti, che la sovraespressione di BCL10 è correlata allo sviluppo di linfomi di tipo MALT ed è determinata da una traslocazione genica t(1;14)(p22;q32) che pone il gene BCL10 sotto il controllo del gene promotore delle catene pesanti delle immunoglobuline. La condizione di sovraespressione

favorisce un processo di omodimerizzazione tra domini CARD di molecole contigue di BCL10 che sono in grado di assemblarsi in filamenti. Tali filamenti portano all'inappropriata attivazione del fattore NF- $\kappa$ B. Pertanto, l'identificazione di un inibitore del processo di oligomerizzazione può aprire la strada allo sviluppo di molecole capaci di modulare l'attivazione del fattore NF- $\kappa$ B.

I domini CARD sono costituiti da sei  $\alpha$ -eliche con un arrangiamento tipico a chiave greca ed hanno una lunghezza di circa 110 residui amminoacidici.

Il pre-requisito fondamentale per lo sviluppo di inibitori basati sull'interfaccia di interazione, è l'identificazione delle regioni direttamente coinvolte nel processo di oligomerizzazione di BCL10-CARD.

Per questo studio, un mutante del dominio CARD di BCL10, in cui le due cisteine presenti nella sequenza sono state sostituite da serine, è stato ottenuto per via ricombinate; un'analisi conformazionale preliminare in soluzione mediante dicroismo circolare ha evidenziato una conformazione secondaria di tipo  $\alpha$  elicoidale.

Avvalendoci del sistema di rivelazione biotina-streptavidina, per verificare l'interazione CARD-CARD, è stato allestito un saggio tipo ELISA utilizzando la stessa proteina biotinilata. E' stato verificato che il dominio BCL10-CARD riconosce sé stesso con una costante di auto-associazione pari a 1.3  $\mu$ M.

La messa a punto del saggio di auto-associazione è stato pertanto il punto di partenza per identificare le regioni della sequenza di CARD responsabili dell'interazione. Mediante un semplice ed efficiente approccio basato sulla proteolisi limitata della proteina, abbiamo selezionato "frammenti proteici" capaci di interferire nell'auto-associazione.

Il dominio mutato CARD-BCL10 è stato idrolizzato con tripsina e i frammenti triptici prodotti sono stati separati mediante RP-HPLC in frazioni, che sono state analizzate mediante LC-MS e usate per allestire saggi ELISA di competizione. La frazione F8 è risultata essere la più efficace nell'inibire l'auto-associazione del 45%. L'analisi LC-MS ha rivelato che la frazione conteneva essenzialmente il frammento BCL10[91-98]. L'analisi di un modello teorico predittivo della struttura del dominio CARD di BCL10, ha suggerito che il frammento BCL10[91-98] è localizzato in prossimità dell'elica 6, pertanto, per investigare l'influenza della regione contigua del frammento 91-98 interna al dominio CARD, sono stati disegnati due analoghi di sequenza più estesa, contenenti anche le eliche 4 e 5 (Tabella I). I tre peptidi, denominati Peptide I BCL10[91-98], Peptide II BCL10[78-98] e Peptide III BCL10[68-98] sono stati sintetizzati e sottoposti a saggi di tipo ELISA di competizione analogamente a quanto fatto per il saggio di screening. Il Peptide I BCL10[91-98], sebbene più corto, è risultato l'unico in grado di inibire ancora l'auto-associazione della proteina, esibendo una  $IC_{50}$  di circa 70 nM. I peptidi sintetici II e III invece, pur contenendo la sequenza 91-98, sono risultati del tutto inefficaci.

Indagini relative allo stato oligomerico dei peptidi sintetici, eseguite mediante SEC, hanno evidenziato che in soluzione il Peptide I BCL10[91-98] è stabile nello stato monomero fino a concentrazioni pari a 400  $\mu$ M, mentre il peptide BCL10[78-98] è in forma dimerica già a 5  $\mu$ M. Sulla base di tali informazioni, abbiamo ipotizzato che il Peptide II BCL10[78-98], alle concentrazioni usate, risulta meno efficace perché i residui 78-90 favoriscono la formazione di oligomeri rendendo in tal modo i residui 91-98 non disponibili per il riconoscimento.

Partendo dal Peptide I BCL10[91-98] abbiamo condotto uno studio mirato all'identificazione degli aminoacidi cruciali per l'interazione. Per tale scopo sono stati progettati e saggiati dei peptidi mutati denominati Peptide IV, V, VI, VII caratterizzati dalla presenza di doppie mutazioni contigue ad alanina (Tabella I).

**Tabella I**

	<b>PEPTIDE</b>	<b>SEQUENCE</b>
I	BCL10[91-98]	TQNFLIQK
II	BCL10[78-98]	GLDTLVESIRREKTQNFLIQK
III	BCL10[68-98]	LLDYLQENPKGLDTLVESIRREKTQNFLIQK
IV	BCL10[91-98]T91A,Q92A	AANFLIQK
V	BCL10[91-98]N93A,F94A	TQAALIQK
VI	BCL10[91-98]L95A,I96A	TQNFAAQK
VII	BCL10[91-98]Q97A,K98A	TQNFLIAA
VIII	Tat-BCL10[91-98]	-*GRKKRRQRRRPPQ-βA-βA-TQNFLIQK
IX	Tat-BCL10[91-98]T91A,Q92A	-*GRKKRRQRRRPPQ-βA-βA-AANFLIQK

L'analisi funzionale di questi peptidi ha dimostrato che:

- la sostituzione dei primi due aminoacidi Thr91 e Gln92 con Ala ha reso il peptide completamente inattivo
- la sostituzione della Asn93 e Phe94 con Ala ha fatto diminuire l'efficacia mostrando una IC<sub>50</sub> di circa 10<sup>-6</sup> M.
- la sostituzione della Leu95 e Ile96 con Ala, invece, ha portato ad una netta diminuzione della capacità di competere.
- la sostituzione degli ultimi due aminoacidi Gln97 e Lys98 è risultata totalmente ininfluente.

Questi dati suggeriscono che i residui di BCL10 [91-98] possono avere un ruolo rilevante nel processo di auto-associazione e che le catene laterali della Thr91, Gln92, Leu95 e Ile96 possono rappresentare i punti di contatto tra proteine monomeriche.

Inoltre, la capacità inibitoria del Peptide I è stata valutata con esperimenti cellulari sia come effetto diretto che indiretto. A tal fine, il Peptide I è stato opportunamente coniugato con la sequenza basica della TAT (Peptide VIII) e ne è stata valutata la stabilità in siero e, mediante esperimenti di immunoprecipitazione, è stato verificato che in cellule HEK293, sovraesprimenti l'intera proteina BCL10 (1-127), il Peptide VIII inibisce in maniera dose-dipendente l'auto-associazione mostrando la massima attività a 100 μM. Mediante microscopia a fluorescenza è stata anche valutata la capacità di penetrazione della membrana cellulare e la localizzazione cellulare. Come effetto a valle, è stata valutata la capacità del Peptide VIII di inibire l'attivazione del fattore NF-κB, indotta sia dalla sovraespressione di BCL10 che dall'attivazione della PKC. In entrambi i casi, il Peptide VIII inibisce in maniera dose-dipendente l'attivazione del fattore NF-κB mostrando, alla concentrazione di 50 μM, un'inibizione del 50% e del 70%, rispettivamente.

Pertanto, il Peptide VIII può rappresentare il punto di partenza per lo sviluppo di nuove molecole da usare per il trattamento di specifiche condizioni patologiche associate con l'attivazione del fattore NF-κB.

## SUMMARY

One of the major challenges for the comprehension of physiological and pathological functions regulating the cellular processes, is the elucidation of molecular mechanisms underlining protein–protein interactions.

Protein–protein interactions indeed play a key role in a variety of biological processes and are therefore important targets for the design of novel therapeutics. Unlike the design of enzyme inhibitors, the disruption of protein–protein interactions is far more challenging, due to large interfacial areas involved in protein recognition and to the relatively flat topologies of these surfaces. Nevertheless, in spite of such difficulties, there has been considerable progress in the recent years.

The purpose of this PhD thesis is the identification of small peptides acting as modulators of protein–protein interactions playing a crucial role in pathological processes, such as allergy and cancer.

Different strategies have been employed: in one case, starting from a crystallographic structure, the rational design of short polypeptides mimicking the receptor binding surface has been achieved. In a second case, potent inhibitors of a protein have been identified following an approach of screening of peptide pools generated from the protein itself.

In the first part of the study, we have dealt with *de novo* designed inhibitors of the IgE-FcεRI interaction, one of the main target for blocking the IgE-mediated allergic reactions. We have selected several short peptides interacting with IgE with a dissociation constant in the low micromolar range but with a very high selectivity for this immunoglobulin subclass. We have evaluated their kinetic and thermodynamic properties and assessed the capacity to block the interaction of IgE with a recombinant variant of the receptor second domain. Despite the relatively low affinity, these peptides have a potential applicability as modulators of the IgE-FcεRI interaction and therefore as new molecules to be developed for contrasting allergy.

In a second study, we have studied a homotypic protein-protein interaction mediated by specific α-helical domains, known as **C**apase **R**ecruitment **D**omains (CARD). We have studied the CARD of the protein BCL10, a main regulator of the innate immune response that is a component of the CBM (CARMA1-BCL10-MALT1) protein complex, by which it promotes the activation of the NF-κB transcription factor.

In this case, we have studied a very short peptide derived from the protein structure, which is able to block the protein self-interaction. The peptide has been selected by functionally ranking CARD-CARD antagonists by a binding competition assay between differently tagged recombinant domains. The antagonists have been prepared by enzymatically digesting the CARD itself and fractionating the resulting peptides. Using synthetic peptides, we have been able to identify single residues involved in CARD-CARD contacts. The peptide appears to mimic the protein binding interface and is a useful and effective inhibitor of the BCL10 activity in cellular assays.

# **CHAPTER I**

## **I.1 PEPTIDES AS MODULATORS OF PROTEIN-PROTEIN INTERACTIONS**

Protein-protein interactions play a central role in many cellular functions, including DNA replication, DNA transcription and translation, signal transduction, and in metabolic pathways [1].

One of the main challenges in biotechnological research is the use of enzyme active sites as templates for the design of antagonists. Developing inhibitors of protein-protein interactions is a far more complicated process that involves a numerous factors. Firstly, the interfacial surface area necessary for specific recognition is typically large (approximately 750–1500 Å<sup>2</sup>), suggesting that large ligands may be required to compete effectively with the natural protein partner, as opposed to ‘*drug-like*’ small molecules that have been successfully utilized in enzyme inhibition. Secondly, interaction surfaces are often shallow and relatively featureless, rather than the well-defined binding pockets present in enzyme active sites, making the design of selective inhibitors difficult. Thirdly, the binding regions of protein-protein interactions are often non-contiguous, so that mimicry of these domains is not possible by simple synthetic peptides or peptidomimetics. In addition, the adaptively of the protein surfaces involved in protein-protein interactions suggests that there may be binding conformations suitable for small molecules that are invisible in a single crystal structure, thereby the design of suitable and effective binders can be a very difficult task. Finally, unlike enzyme activity that may simply be monitored by commercially available assays, novel and efficient screening assays must be developed for the interaction between proteins [1-6].

The identification of peptides based on the amino acid sequences found at protein-protein interfaces can be an excellent and straightforward way to obtain new leads for antagonist development, indeed a lot of inhibitors based on the design of molecular scaffolds, on protein surface mimetics, alpha-helical mimetics, beta-sheet or beta-strand mimetics, as well as beta-turn mimetics, have been successfully utilized to modulate protein-protein interactions involved in a number of diseases, including cancer and HIV [3,4].

The topic of the present thesis work is focused on the identification of small peptides that modulate protein-protein interactions.

The first part of the study is focused on the design of inhibitors of the IgE-FcεRI interaction, one of the main target for blocking the IgE-mediated allergic reactions. Indeed, the determination of Fc-IgE-αFcεRI complex crystal structure has elucidated their interactions at the atomic level and has provided a detailed description of the complex interaction interface and the role of any single amino acid in complex formation, thus opening the way to the design of peptides and “peptidomimetics” antagonists [7]. Following a *de novo* design approach, based on the complex crystal structure, we have selected several peptides interacting with the IgE with an activity in the low micromolar range. We have evaluated their binding activity assessing affinity and selectivity and have assessed their potential applicability as modulators of the IgE-FcεRI interaction.

In the second part, we have studied a homotypic protein-protein interaction mediated by specific  $\alpha$ -helical domains, known as **C**apase **R**ecruitment **D**omains (CARD). We have studied the CARD of the protein BCL10, a main regulator of the innate immune response that is a component of the CBM (CARMA1-BCL10-MALT1) protein complex by which it promotes the activation of the NF- $\kappa$ B transcription factor [8]. In this case, we have selected a peptide mimetic of the protein self-interaction interface by enzymatically producing CARD fragments which have been functionally ranked as CARD-CARD antagonists by a binding competition assay between differently tagged recombinant domains. By this method, coupled with the use of synthetic peptides, we have been able to identify single residues involved in CARD-CARD contacts and we have proved the concept that the peptides mimicking the interface are useful and effective inhibitors of the protein-protein self-interaction.

## I.2 REFERENCES

1. Fletcher S. and A.D. Hamilton Targeting protein-protein interactions by rational design: mimicry of protein surfaces. *J. R. Soc. Interface* (2006) 22; 3(7):215-33
2. Sillerud L.O. and R.S. Larson Design and structure of peptide and peptidomimetic antagonists of protein-protein interaction. *Curr. Protein Pept. Sci.* (2005) 6(2):151-69
3. Che Y., Brooks B.R. and G.R. Marshall Development of small molecules designed to modulate protein-protein interactions. *J. Comput. Aided Mol. Des.* (2006) 20(2):109-30
4. Hershberger S.J., Lee S.G. and J. Chmielewski Scaffolds for blocking protein-protein interactions. *Curr. Top Med. Chem.* (2007) 7(10):928-42
5. González-Ruiz D. and H. Gohlke Targeting protein-protein interactions with small molecules: challenges and perspectives for computational binding epitope detection and ligand finding. *Curr. Med. Chem.* (2006)13(22):2607-25.
6. Moreira I.S., Fernandes P.A. and M.J. Ramos Hot spots: a review of the protein-protein interface determinant amino-acid residues. *Proteins* (2007) 1;68(4):803-12
7. Garman S.C., Wurzburg B.A., Tarchevskaya S.S., Kinet J.P. and T.S. Jardetzky Structure of the Fc fragment of human IgE bound to its high-affinity receptor Fc $\epsilon$ RI. *Nature* (2000) 406:259–266
8. Langel F.D., Jain N.A, Rossman J.S., Kingeter L.M., Kashyap A.K. and B.C. Schaefer Multiple protein domains mediate interaction between Bcl10 and MALT1. *J. Biol. Chem.* (2008) Epub ahead of print

## CHAPTER II

# II. PEPTIDES MIMICKING THE HIGH-AFFINITY IgE RECEPTOR FcεRI

## II.1 INTRODUCTION

The human immune system has been designed to protect the integrity of the host by maintaining homeostasis. When this homeostatic mechanism is disturbed through challenge from foreign invaders or altered self tissue, the immune system is activated to protect the host.

A large spectrum of pathologies listed as allergic or atopic diseases are associated with the inappropriate activation of the immune system by environmental factors and affect nearly 20% of the world population [1].

In the past two decades an increase in cases has been observed predominantly in young people and linked to the Western lifestyle [2].

The reason why many patients are affected from particular hypersensitivities remains an open debate, but it is generally accepted that genetic and environmental factors synergistically influence patients' susceptibility.

The immune response involves the coordination of cellular and molecular defence mechanisms. The stimulation of the antibody response leads to the production of antibody isotypes that are responsible in stimulating a variety of cellular responses from the activation of inflammatory pathways to the targeted killing of infected or cancerous cells. Fc receptors, expressed on all hemopoietic cells, play a crucial role in immune defense by providing a link between antibody-antigen complexes and cellular effector machinery [3]. The diversification in immune responses depends on the type of Fc receptor, their cellular localization and their affinities for various classes of antibodies. Several Fc receptors are belonging to the Immunoglobulins superfamily (Ig-like domain) and include FcεRI, specific for IgE antibodies. FcεRI has the highest affinity of all Fc Ig-like receptors with a binding constant in the  $10^{-9}$  to  $10^{-10}$  range for its ligand.

Immunoglobulins E play a central role in allergic inflammatory processes such as anaphylaxis, allergic rhinitis, asthma and atopic dermatitis, but they are also associated with other different immune responses.

Activation of eosinophils by FcεRI provides defence mechanisms against parasitic infection, whereas FcεRI on antigen-presenting cells can deliver IgE-bound antigen into MHC class II antigen-presentation pathways.

Instead the binding of IgE to its high affinity receptor FcεRI, on mast cells and basophils, is a key step for allergic reactions.

In the first phase of an allergic reaction, called *sensitization phase*, the contact with allergens leads to the abnormal production of allergen-specific IgE molecules by B cells and this depends partially on genetic predisposition. In normal people the serum concentration of IgE, 50–300 µg/mL, is the lowest of all antibodies.

The produced allergen-specific IgE circulate in the body in a free form able to bind cell surface receptors. In a further step, the clustering of multivalent antigens leads to the crosslinking of the receptor-bound IgE that induces (its activation) the immediate phosphorylation of ITAM motifs in its β and γ chains. In fact, cellular activation is brought about by the rapid release of chemical mediators, such as histamine and the

biosynthesis of leukotrienes and prostaglandins acting later in the inflammatory cascade [4].

FcεRI plays an important role in both phases of the allergic reaction. The presence of FcεRI-bound IgE may affect mast cell physiology, even in the absence of antigen. Recently, it has been observed that monomeric IgE can stimulate mast cell survival through signalling pathways that are distinct from those activated by receptor cross-linking [5,6]. The mechanisms adopted by monomeric IgE to bind to FcεRI stimulating mast cell survival is still far from being fully clarified.

Current pharmacological therapy suggests the use of corticosteroids to control inflammation, antihistamines and sympathomimetics to treat other symptoms. They are not always effective in allergic diseases and have some side effects [6].

Allergen immunotherapy (*desensitisation*) is effective for some allergic disorders too, such as pollenosis and insect allergy, but not for others, such as eczema, food allergy and asthma. However the use of the immunotherapy is recently decreasing.

The broad spectrum of different allergy reactions and the side effects caused by many symptomatic anti-allergic drugs have increased the interest in the development of new alternative therapeutic strategies.

A challenging strategy consists in the identification of molecules able to prevent IgE-FcεRI binding and, consequently, activation of the FcεRI receptor. The proof-of-concept that an anti-IgE therapy has a strong efficacy for the treatment of allergic asthma has been demonstrated by the commercialization of the humanized recombinant monoclonal anti-IgE antibody, rhu Mab 25 (generic name, Omalizumab; trade name, Xolair). Omalizumab is a monoclonal antibody identified using conventional somatic cell hybridization techniques. Through this process, researchers have identified a murine monoclonal anti-human IgE antibody, MAE11, directed specifically toward the IgE-Cε3 domain which is involved in receptor engagement. MAE11 was then humanized in a process involving transplantation of the complementarity-determining regions (CDRs) onto a human IgG1 antibody framework. Additional MAE11 amino acid sequences were also incorporated into the humanized antibody to maintain the correct CDR conformational arrangement. This process resulted in a humanized monoclonal antihuman IgE antibody, rhuMAb-E25, containing approximately 5% non-human amino-acid residues [7-9]. This biotechnological drug has been approved for the treatment of moderate and severe forms of IgE-mediated allergic asthma and represents a new class of mast cell-stabilizing drugs that inhibit IgE function by blocking or reducing their binding to cellular receptors.

Considerable interest is currently focused on the study of FcεRI as regards the antigen-independent FcεRI-mediated biological responses (*upstream regulation*) and the distinct signalling of FcεRI-activated pathways and its tight control through inhibitory mechanisms (*downstream regulation*) [10].

Most of our knowledge is provided by structural biology. The crystal structures of the high affinity IgE receptor, the Fc-IgE and the complex of these two proteins have clarified their interactions at the atomic level [11] and the mechanisms adopted by this family of antibody receptors to achieve specificity and affinity has been elucidated unveiling an individual residue involved in the interaction. All of this information allows a targeted manipulation of the Fc specificity and affinity for receptors and, most importantly, the engineering of new antagonistic molecules of potential therapeutic interest.

The main goal in this field would thereby be the design of inhibitors of the IgE-FcεRI interaction that block the IgE-mediated allergic reactions and the identification of

small peptides reproducing the binding interface and interacting with either the Fc-IgE or the receptor could be a valuable starting point for further development in combination with medicinal chemistry strategies [12,13]. Attempts of using the soluble extracellular domain (ECD) of the FcεRI receptor have also been reported and the data indicate that it is a promising candidate for this application [14-19].

## II.1.2 The high-affinity IgE receptor: FcεRI

FcεRI is a multimeric cell-surface receptor that binds the Fc fragment of IgE with high affinity ( $K_D=10^{-9}$ - $10^{-10}$ ). It plays a central role as the initial “docking station”, providing the starting signal for the allergic signal transduction cascade.

Two isoforms have been described for FcεRI, a tetrameric and a trimeric complex, with different cellular distribution and biological function (Fig.1).

The  $\alpha\beta\gamma_2$  isoform is constitutively expressed on mast cells and basophils and activate the immediate-type hypersensitivities associated with the allergic responses.

The  $\alpha\gamma_2$  isoform, expressed on monocytes, eosinophils, Langerhans cells in the pancreas and on the surface of dendritic cells, is responsible of for antigen presentation (anti-parasitic immunity).

Although rodent FcεRI has obligatory  $\alpha\beta\gamma_2$  tetrameric structure, both tetrameric and trimeric structures are expressed for the human variant [10,20,21].

FcεRI is specific for the ε isotype immunoglobulin, but it is not completely species specific. Murine IgE indeed bind to both murine and human FcεRI, whereas human IgE bind only to human FcεRI [10,22].

The FcεRI tetrameric receptor complex consists of one alpha ( $\alpha$ FcεRI), one beta ( $\beta$ FcεRI), and a homodimer of disulphide linked  $\gamma$ -chains ( $\gamma$ FcεRI).

A combination of hydrophobic and electrostatic non covalent interactions builds up the complex in the plasma membrane by keeping  $\alpha$ ,  $\beta$ , and dimeric  $\gamma$  together and involves lipids binding.

The  $\alpha$ -chain belongs to the immunoglobulin super-family and comprises two extracellular immunoglobulin-related domains binding a single IgE molecule, a transmembrane domain containing a conserved aspartic acid residue and a short cytoplasmatic tail. The human  $\alpha$ -chain contains seven potential N-glycosylated sites. These sites are not intrinsically necessary for proper folding of the  $\alpha$ -chain but are required in the endoplasmic reticulum to mediate the proper interaction between the  $\alpha$ -chain and the ER folding machinery [23]. The intracellular tail of the  $\alpha$ -chain has no apparent signalling function.

The FcεRI  $\beta$  and  $\gamma$ -chains possess an immunoreceptor tyrosine-based activation motif (ITAM). The tyrosine residues, contained in this motif, are phosphorylated when antigen crosslinking of receptor-bound IgE molecules occurs. ITAM motifs activate down-stream signal propagation by recruiting and activating the Src kinase family [10].

Despite numerous studies on the structure and function of the FcεRI its physiological relevance is still an open question.

Tetrameric FcεRI ( $\alpha\beta\gamma_2$ ), expressed in mast cells and basophils, is well known as a key regulator of IgE-mediated immediate-type allergic reactions and late-phase allergic reactions (Fig.1). Upon crosslinking of FcεRI by IgE and antigen, a signalling cascade leads within minutes, through degranulation, to the release of preformed mediators, such as histamine, and lipid-mediator synthesis. These events produce an immediate-type allergic reaction characterized by vasodilatation, increased vascular permeability, up-regulation of vascular adhesion molecules and bronchoconstriction.

Upon prolonged stimulation, a late-phase allergic reaction is induced, leading in addition to cytokine and chemokine production and inducing the recruitment of inflammatory cells and T-cell activation [24,25].

On the other hand, the antigen-independent effects, mediated by IgE binding to tetrameric FcεRI, may result in increased survival of the cell [26,27].

Trimeric FcεRI (αγ<sub>2</sub>), expressed by professional APCs (as Langerhans cells), monocytes and macrophages, has a role in the process of allergen presentation and a pro-inflammatory function in allergic patients (Fig.1). Crosslinking of trimeric FcεRI by IgE and antigen leads to the endocytosis of FcεRI and IgE-bound antigen, followed by their uptake in MHC-class-II-rich compartments. In this case the antigen processing and loading of antigenic peptides onto MHC class II molecules occurs, and ultimately, the presentation of the antigenic-peptide–MHC-class-II complexes to T cells.

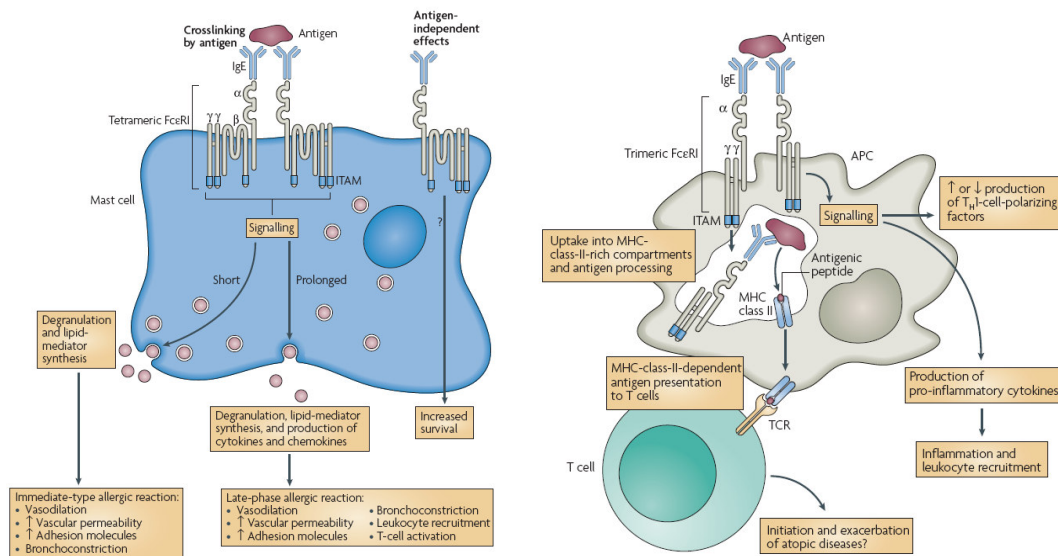


**Figure 1:** Composition of the tetrameric and trimeric FcεRI complex and biological functions: A) The tetrameric form consists of one IgE-binding α-chain with two immunoglobulin-like domains in the extracellular part, one β-chain and two γ-chains with intracellular immunoreceptor tyrosine-based activation motifs (ITAMs) for signal transduction. Tetrameric FcεRI is expressed by mast cells and basophils. B) The trimeric form lacks the β-chain and is expressed by APCs and eosinophils [10].

On the mast-cells and basophils the antigen crosslinking of FcεRI-bound IgE, initiates a complex intracellular signalling cascade, which ultimately leads to effector functions [28,29].

Recent works have been focused on the separation of proximal FcεRI signalling into a primary pathway and a complementary pathway that mainly regulates FcεRI-induced degranulation (Fig.2). In the basic proximal FcεRI signalling events the β- and γ-chains of FcεRI, after tyrosine phosphorylation of ITAMs motifs, bind the SH<sub>2</sub> domains of protein tyrosine kinases (PTKs), mainly those of the SRC kinase family as LYN, FYN and SYK.

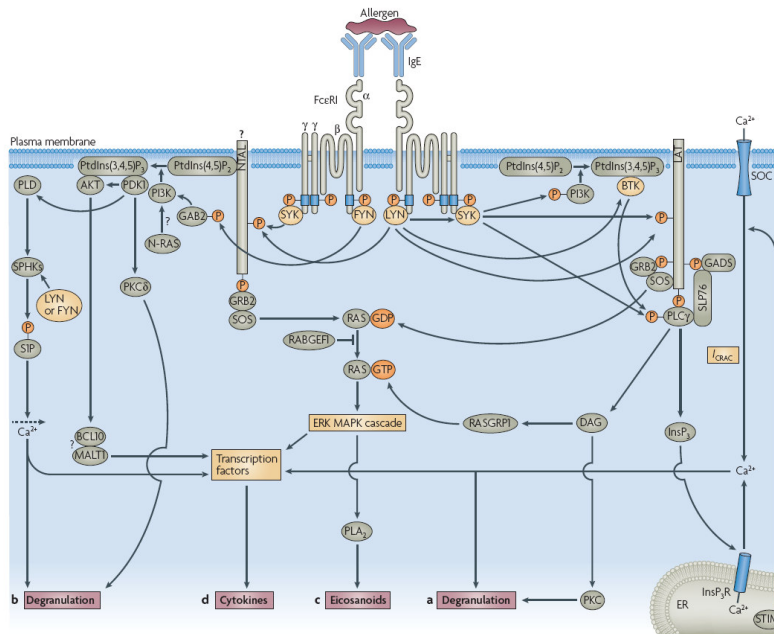


**Figure 2:** FcεRI signalling: A) In the primary pathway LYN activation leads to SYK association with  $\gamma$ -chains and subsequent SYK activation. Activated SYK allows classical PKC activation and  $Ca^{2+}$  mobilization which, ultimately leads to degranulation; B) In the complementary pathway, FYN and SYK activation induce a signalling complex which activates PKC $\delta$ , ultimately leading to degranulation [10].

### II.1.3 Structural insights into the interactions between human IgE and its tetrameric high affinity receptor FcεRI

Structural studies to elucidate the regions of FcεRI critical for the interaction with IgE molecules have been reported by Jardetzky *et al.* [11]

The crystal structure of Fc-IgE- $\alpha$ FcεRI shows that the N-terminal region of the  $\alpha$ FcεRI chain is made up of two “Ig-like domains” called D1 and D2 (Fig.3). These domains form a very pronounced acute angle like an inverse V, and the convex surface, comprising the D2 domain, constitutes the binding interface with the IgE [11].

D1 and D2 domains are oriented in a nearly anti-parallel arrangement, with the N- and C-terminal part on the same side of the receptor structure. This arrangement reveals an unusual grouping of four surface-exposed tryptophans at the top of the D1–D2 interface (“tryptophan ridge”) involved in antibody-binding interactions. An extensive packing interface forms part of the core fold of the overall structure and contributing to its stability.

Although the D1 domain is not directly involved in the binding with the IgE, it structurally contributes to the high affinity maintenance [30].

The structural analysis of the Fc-IgE- $\alpha$ FcεRI shows the two C $\epsilon$ 3 domains of the Fc-IgE interact with two different surfaces of  $\alpha$ FcεRI (referred to as binding site 1 and 2). Each IgE heavy chain contains four constant domains (C $\epsilon$ 1–C $\epsilon$ 4) but only C $\epsilon$ 3 domain and the linker C $\epsilon$ 2–C $\epsilon$ 3 domains are directly involved in the interaction with  $\alpha$ FcεRI. The C $\epsilon$ 4 domains of the Fc-IgE provide a structural dimerization scaffold that allows two C $\epsilon$ 3 domains to form the bivalent interaction with  $\alpha$ FcεRI. The C $\epsilon$ 2–C $\epsilon$ 3 IgE linker residues adopt an asymmetric, arch-like structure over the top of the

receptor, while the lower domains C $\epsilon$ 4 point away from the interaction site and possibly away from the membrane surface [11].

There are *N*-linked oligosaccharides in both the Fc-IgE and  $\alpha$ Fc $\epsilon$ RI, but they do not contribute significantly to interactions between the two molecules [31,32]. Carbohydrate attached to the conserved site (N394 in IgE), lies along the inner face of the C $\epsilon$ 3 domains (strands A, B and E) similar to that observed in structures of Fc-IgG. Carbohydrates attached to residue N42 in  $\alpha$ Fc $\epsilon$ RI extends upwards to the top of the D1–D2 interface approaching one of the Fc-IgE chains.

Carbohydrate residues are attached to N21 and N166 of  $\alpha$ Fc $\epsilon$ RI, projecting from the receptor surface away from the IgE-binding interface.

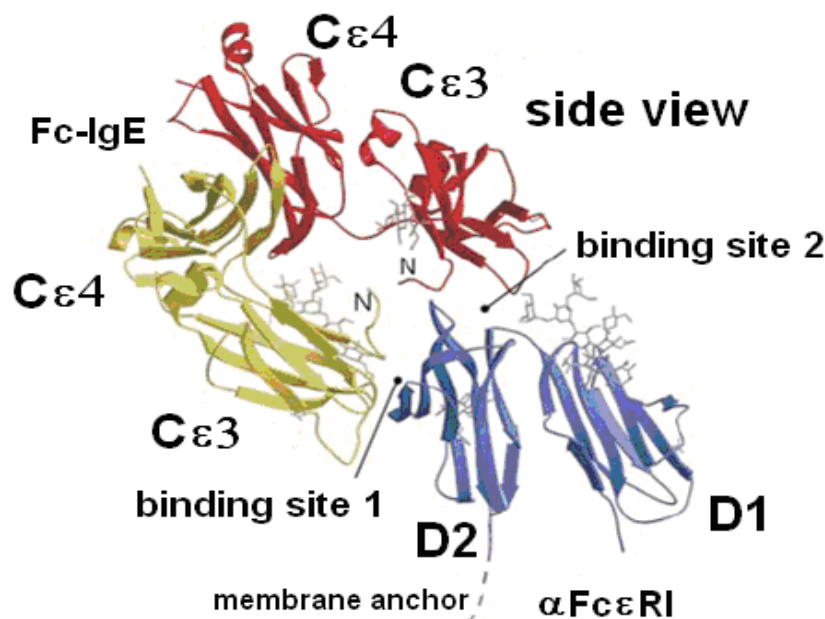


**Figure 3:** Side view of the crystal structure of the Fc-IgE- $\alpha$ Fc $\epsilon$ RI complex: the two Fc chains are in yellow and red, the  $\alpha$ Fc $\epsilon$ RI chain is in blue. Carbohydrate residues are shown as sticks in the same colour as the protein chain. Binding sites 1 and 2 are indicated. The cell membrane would lie below the receptor [11].

The two distinct binding sites use overlapping but non-identical sets of Fc-IgE residues (Fig.4).

**Site 1** refers to the interaction of one C $\epsilon$ 3 domain with the C–C' region of the receptor D2 domain, centered around receptor residue Y131. Twelve amino acids from the Fc-IgE and eight amino acids from the  $\alpha$ Fc $\epsilon$ RI form site 1, burying a total of about 860 Å<sup>2</sup> of surface area. The IgE residues are from four distinct regions of the IgE-Fc sequence, including the C $\epsilon$ 2–C $\epsilon$ 3 linker (residues 334–336), the B–C loop (362–365), the D–E loop (393–396) and the F–G loop (residue 424) of C $\epsilon$ 3 domain. The receptor residues derive from two regions of the D2 domain, involving the C strand (residues K117, I119 and Y121) and the C'–E loop (residues A126, Y129, W130, Y131 and E132). Two potential salt bridges ( $\alpha$ K117–C $\epsilon$ 3D362 and  $\alpha$ E132–C $\epsilon$ 3R334) and four potential hydrogen bonds ( $\alpha$ K117–C $\epsilon$ 3G335,  $\alpha$ Y129–C $\epsilon$ 3D362,  $\alpha$ Y131–C $\epsilon$ 3D364 and  $\alpha$ Y131–C $\epsilon$ 3H424) are formed across the site 1 interface. Y131 from the receptor

projects into a pocket on the Fc-IgE formed by the B-C, D-E and F-G loops of C $\epsilon$ 3 and the C $\epsilon$ 2–C $\epsilon$ 3 linker [11].

**Site 2** refers to the interaction of the second C $\epsilon$ 3 domain with the D1–D2 interface, and involves the cluster of four surface-exposed tryptophans (W87, W110, W113 and W156). Interactions at site 2 bury about 970Å<sup>2</sup>, including ten amino acids from IgE and eight from  $\alpha$ Fc $\epsilon$ RI. The IgE residues are localized to two distinct segments of C $\epsilon$ 3: the C $\epsilon$ 2–C $\epsilon$ 3 linker region (residues 332–337) and the F-G loop (424–427). The  $\alpha$ Fc $\epsilon$ RI contributes residues from three regions: the D1–D2 linker region (85–87); B-C loop (residues 110 and 113) and F-G loop (156–158) of D2 domain. Residues from the D1 domain of the receptor do not form direct interactions with the Fc-IgE. Site 2 primarily contains hydrophobic amino acids with three potential hydrogen bonds across the interface ( $\alpha$ W156– C $\epsilon$ 3G335,  $\alpha$ Q157– C $\epsilon$ 3N332 and  $\alpha$ Q157– C $\epsilon$ 3R334) [11]. P426 from the Fc-IgE intercalates between receptor residues W87 and W110, forming a hydrophobic proline sandwich. Interactions with  $\alpha$ Fc $\epsilon$ RI cause the C $\epsilon$ 2–C $\epsilon$ 3 linker regions to point up and away from the complex interface. The C $\epsilon$ 4 domains are not directly involved in binding to  $\alpha$ Fc $\epsilon$ RI but act as a scaffold, allowing the C $\epsilon$ 3 domains to assume an appropriate orientation for  $\alpha$ Fc $\epsilon$ RI binding [11].

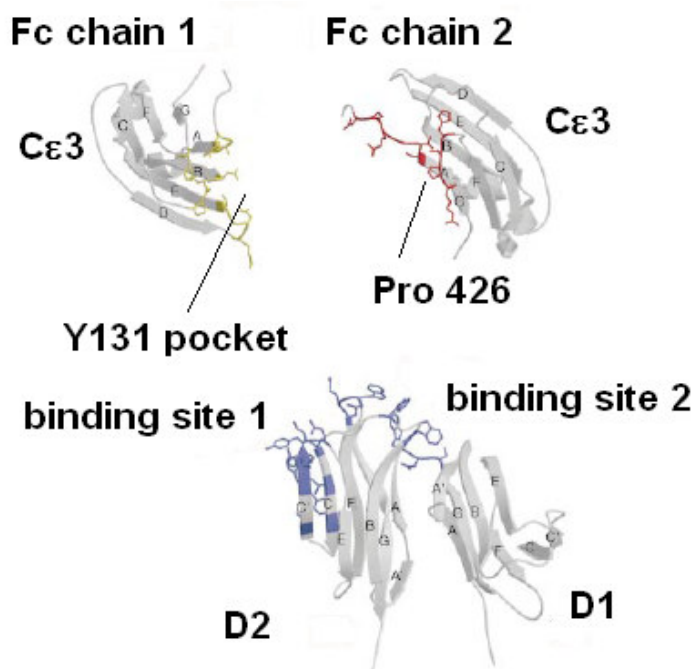


**Figure 4:** Structural basis for the 1:1 binding of Fc-IgE to  $\alpha$ Fc $\epsilon$ RI. The Fc-IgE- $\alpha$ Fc $\epsilon$ RI complex has been taken apart to display the interaction sites. Fc-IgE domain strands and  $\alpha$ Fc $\epsilon$ RI strands in D1 and D2 are labelled. The Fc-IgE binding residues are shown as sticks in yellow (site 1) and red (site 2); the D1-D2 linker and D2 binding residues are in blue [13].

Residues forming the Fc-IgE- $\alpha$ Fc $\epsilon$ RI interface in site 1 are generally poorly conserved (Fig.5A). Three residues are completely conserved (G335, D362 and N394 of IgE) in the Fc-IgE sequences, but there is poor conservation in the receptor sequences, except for the partial conservation of K117 and the relatively conserved Y129.

The conservation of K117 in three of the four FcγRs receptors matches the complete conservation of D362 and G335 in the Fc-IgE sequences, potentially preserving one of the two salt bridges and one of the hydrogen bonds of site 1.

The conservation of Y129 (αFcεRI) as tyrosine or phenylalanine in Fc-IgG, suggests that this interaction may be conserved in Fc-IgG complexes with the FcγRs.

However, Y131 of αFcεRI, which forms a large number of atomic contacts across the interface and is buried in a shallow surface pocket on the Fc-IgE, is not conserved in the FcγRs (changing to either histidine or arginine). Given the central location of Y131 in the site 1 interface, this residue may generally be important in immunoglobulin specificity. Four of the five residues that contact Y131 in IgE change in the Fc-IgG sequences.

In the site 2, G335, P426 and L425 in the antibody sequence are absolutely conserved (Fig. 5B). In particular P426 interacts with two absolutely conserved tryptophans in αFcεRI (W87 and W110), which form a hydrophobic pocket. These residues in the Fc-IgE (residues 332–334) interact with the F-G loop of αFcεRI. For site 2, the conservation of five residues and the additional functional data suggest a conserved binding mode across these members of the FcR family [11].

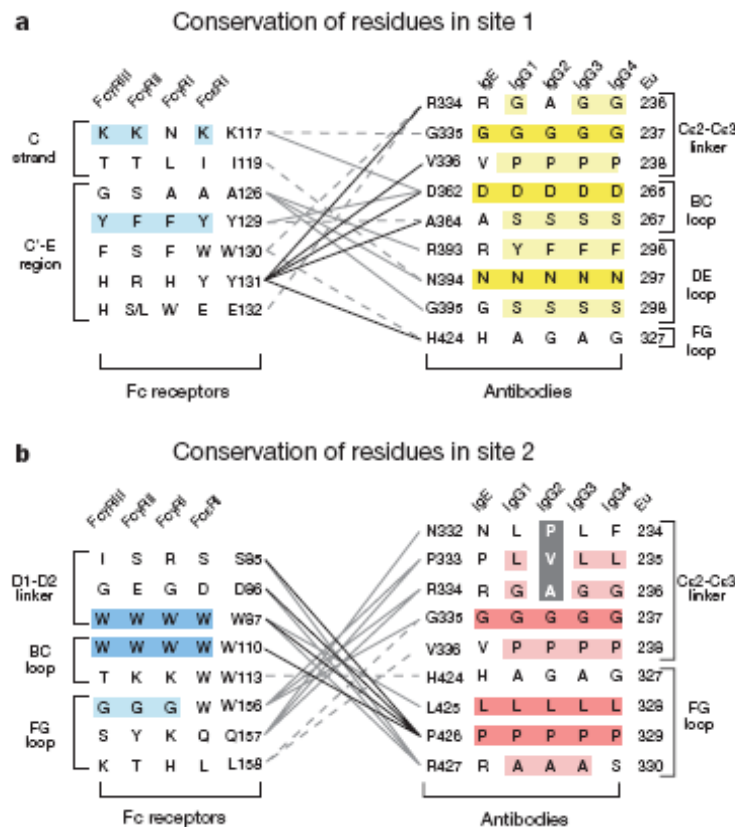


**Figure 5:** Conservation of amino-acid residues and contacts at the Fc-IgE-αFcεRI interfaces in IgG receptors and antibodies. Contacting residues are defined as inter-atomic distances less than 4 Å. **a)** Residues that interact in site 1, and their conservation in related human receptors and antibodies. Absolutely conserved residues are highlighted in bold, and partially conserved residues are lightly highlighted (yellow for IgE, blue for αFcεRI). Dark lines are drawn for residues making the largest number of contacts across the interface, lighter lines for intermediate numbers of contacts, and dashed lines for the fewest contacts [11]. **b)** Residues that interact in site 2, and their conservation in related human Fc receptors and antibodies. Receptor residues are highlighted in blue, antibody residues in red. Three residues in IgG2 (P, V, A) that affect binding to FcγRs are boxed in black [11].

The crystallographic structure of Fc-IgE- $\alpha$ Fc $\epsilon$ RI complex reveals a 1:1 stoichiometry, in contrast with models proposing a 1:2 stoichiometry for the homologous Fc-IgG receptors Fc $\gamma$ RIIa and Fc $\gamma$ RIIb [11,33-37].

The formation of complexes with 1:1 stoichiometry is supported by two structural keys: the induction of structural asymmetry in the C $\epsilon$ 2–C $\epsilon$ 3 linker of Fc-IgE and the steric hindrance blocking the binding of a second receptor.

The C $\epsilon$ 2–C $\epsilon$ 3 linker regions (residues 328–336) are constrained to an asymmetric arrangement by interactions with  $\alpha$ Fc $\epsilon$ RI. The amino acids of the C $\epsilon$ 2–C $\epsilon$ 3 linker form the top of an arch that conforms to the convex surface of  $\alpha$ Fc $\epsilon$ RI, creating an asymmetric binding site for a single receptor.

In addition, four IgE residues (R334, G335, V336 and H424) are common to both sites 1 and 2, preventing the simultaneous binding of two receptors to one Fc-IgE. Superposition of a second receptor onto the 1:1 complex shows significant steric overlap between receptors and the amino acids of the C $\epsilon$ 2–C $\epsilon$ 3 linker.

Thus, the binding of one receptor effectively prevents the binding of a second, owing to both the induced asymmetry of the C $\epsilon$ 2–C $\epsilon$ 3 linker of the Fc-IgE and the steric inhibition across the Fc dyad axis.

Furthermore the structure of free Fc-IgE shows that the IgE receptor-binding domains can undergo a large conformational rearrangement. The Fc domain conformational flexibility allows IgE to adopt an “open form” in Fc-IgE- $\alpha$ Fc $\epsilon$ RI complex and a “closed form” when it is free. In the free Fc-IgE crystal structure, the C $\epsilon$ 2–C $\epsilon$ 3 inter-domain angle is more acute than that observed in Fc-IgE- $\alpha$ Fc $\epsilon$ RI [38,39].

Analysis of the  $\alpha$ Fc $\epsilon$ RI structure, in several crystal forms, shows little conformational change in the angle between D1 and D2 in the absence of the Fc-IgE and on complex formation with the Fc-IgE [38]. The C' strand in the D2 domain (residues 127–133) shows an unusual conformational adaptability perhaps due to exposed aromatic residues (Y129, W130, Y131). The B-C loop in D1 also adopts different conformations in different crystal forms, but this region is distal to the Fc-IgE binding site [38].

Multiple binding and dissociation steps for the interaction of the Fc-IgE with  $\alpha$ Fc $\epsilon$ RI have been observed using surface plasmon resonance methods. Two association and dissociation steps (a fast on/off and a slow on/off) have been detected and investigated with substantial experimental controls, leading to the conclusion that the binding of the Fc-IgE to the  $\alpha$ Fc $\epsilon$ RI is better represented using a biphasic model [19,32,40,41].

The mechanism underlying the biphasic kinetics remains to be clarified. The interaction of each C $\epsilon$ 3 domain with distinct surfaces of the  $\alpha$ Fc $\epsilon$ RI structure suggests a kinetic scheme in which transient release of one of the C $\epsilon$ 3 domains may occur within the complex. This could lead to two distinct pathways for the association and dissociation of the complex, consistent with the experimental observation of two distinct kinetic off-rates. Transient opening of the complex may allow inhibitors to enhance the dissociation of receptor-bound IgE by preventing the rebinding of an exposed C $\epsilon$ 3 domain within the complex. These kinetics may reflect the observations that Fc-IgE may adopt both binding (open) and non-binding (closed) conformational states in solution [42,43]. For example, in solution the Fc $\epsilon$ RI-binding loop residues would be inaccessible in the closed Fc-IgE conformation, which could interfere with receptor binding. Initial interactions might be primarily through the flexible C $\epsilon$ 2–C $\epsilon$ 3 linker residues in this IgE conformation. In the open IgE conformation, the receptor

binding loops could engage the receptor directly, followed by adaptation of the linker region to the receptor, leading to a distinct kinetic rate.

Alternatively, the binding of IgE sequentially to binding site 1 and then to binding site 2 may have distinct kinetic rate as compared to sequential binding to binding site 2 and then to binding site 1. The two dissociation rates of the Fc-IgE may also result from distinct disassembly pathways in which bound C $\epsilon$ 3 domains are released sequentially, with individual microscopic rate constants. The observed flexibility of the Fc-IgE structure and the interaction sites on the receptor for each Fc chain are consistent with dynamic models for the local dissociation of each antibody chain in the complex. If the two C $\epsilon$ 3 domains bind independently, with transient exposure of each site in the complex, inhibitors for either site 1 or site 2 could potentially accelerate the dissociation of receptor-bound IgE.

## II.2 PROJECT AIMS

The demonstrated efficacy of the drug Omalizumab against allergic asthma is pushing research towards the identification of new molecules that can similarly regulate IgE-receptor signalling. Smaller molecules, with less antigenic properties and without the economical drawbacks typical of large molecules such as antibodies, are being studied and developed by combinatorial [12] as well as rational drug design approaches [13].

The atomic description of the receptor-immunoglobulin interaction interface has provided insights on the structural relevance of amino acids directly responsible of such interactions, opening the way to peptidic and peptidomimetic design [11].

The first part of this thesis is devoted to the selection of new molecules that specifically bind IgE and that displace its binding with the high affinity receptor. These molecules can indeed be used as efficient tools for the development of more potent and selective new chemical entities (NCE) for the modulation of allergic responses. Two parallel strategies have been employed.

The first was based on a *de-novo* design of IgE-binding polypeptides using the receptor structure as template. Several polypeptides have been designed, chemically prepared and tested as binders of the immunoglobulins, assessing affinity and selectivity. Furthermore, following an approach of progressive size reduction, the sites that underlie the recognition between IgE and the polypeptide will also be determined.

In a second approach, the extracellular domain of the  $\alpha$ Fc $\epsilon$ RI, was expressed as a soluble and active recombinant protein and evaluated as IgE binder and receptor antagonist. The soluble receptor or functional domains, produced as recombinant products in a stable form, could be employed as a high affinity biotechnological drug with antagonistic activity for the membrane-bound receptor. Binding assays between the soluble receptor and IgE can also be used as tools for the selection of new molecules by screening repertoires of synthetic molecules.

## II.3 EXPERIMENTAL PROCEDURES

### II.3.1 Materials

Human  $\alpha$ Fc $\epsilon$ RI cDNA was kindly provided by Prof. J.P. Kinet from the Harvard Institutes of Medicine (Boston, Massachusetts, USA).

pETM vectors for the expression of recombinant proteins are from EMBL (Heidelberg, Germany) and pGEX vector are from GE Healthcare (Uppsala, Sweden). Oligonucleotides were synthesized by Sigma-Genosys (Sigma-Aldrich, Milano, Italy). Pfu DNA polymerase is from Stratagene (Milano, Italy). Restriction enzymes are from New England Biolabs (Milano, Italy). All molecular biology kits are from Qiagen (Milano, Italy). *Escherichia coli* bacterial strains are from Novagen (Milano, Italy), except for TOP10F' that are from Invitrogen (Milano, Italy). Isopropyl-beta-D-thiogalactopyranoside (IPTG) is from Inalco (Milano, Italy). Reagents for bacterial medium are from Becton-Dickenson (Milano, Italy). Perfect Protein Marker is from Novagen and See Blue Pre-stained Marker is from Invitrogen. PreScission protease, SDS-PAGE reagents, chromatography columns and AKTA FPLC are from GE HealthCare (Milano, Italy). 4-Vinyl pyridine (4-VP), mouse monoclonal anti-dinitrophenol immunoglobulins E (IgE), 2,4-dinitrophenol-conjugated human serum albumin (DNP-HSA) and o-phenyldiamine (OPD) table sets, reduced and oxidized glutathione, are from Sigma-Aldrich (Milano, Italy). Anti-poly-Histidine (His-probe)-HRP conjugated is from Santa Cruz Biotechnology (California, USA). Trans Blot SD semi-dry, blotting grade blocker Non-Fat Dry Milk (NFDM) and Opti-4CN goat anti-mouse (GAM) detection Kit are from Biorad.

BIAcore system and reagents are from Pharmacia Biosensor AB (Uppsala, Sweden).

For peptide synthesis, protected N<sup>α</sup>-Fmoc-amino acid derivatives, succinic anhydride, ethylenediamine, coupling reagents and Rink amide MBHA resin have been purchased from Calbiochem-Novabiochem (Laufelfingen, Switzerland). DIEA is provided from Applied Biosystem (Foster City, CA). All other reagents and chemicals are commercially available from Sigma-Aldrich.

Analytical characterization of synthetic peptides and recombinant proteins have been performed on an LC-MS system comprising an LCQ DECA XP ion trap mass spectrometer (ThermoElectron, Milan, Italy) equipped with an OPTON ESI source (operating at a needle voltage of 4.2 kV and 320°C temperature) and a complete Surveyor HPLC system (including MS pump, autosampler and photo diode array [PDA]). Preparative purification of synthetic peptides has been carried out on a Shimadzu LC-8A, equipped with a SPD-M10 AV detector.

CD spectra were recorded using a Jasco J-810 spectropolarimeter (JASCO Corp) equipped with a Peltier-type temperature control system.

UV-VIS spectra were performed by using a UV-VIS Jasco (Easton, MD) model 440 spectrophotometer with a path length of 1 cm.

Other reagents and chemical suppliers are indicated in the section of methods.

## II.3.2 Methods

### II.3.2.1 Cloning of hFcεRI α-chain

hFcεRI was amplified as full-length [101-897nt], D1-D2 domains [176-685nt] and D2 domain [425-685nt] by PCR from the cDNA of hFcεRI (sequence code NM\_002001 from PubMed) using Pfu polymerase with the oligonucleotides reported in the Table XIV. The amplified DNA was hydrolyzed in the presence of BsmBI and XhoI enzymes for pET vectors and BamHI and XhoI for the pGEX vector [44]. The digested fragments were extracted from 1.2% agarose gel using QIAquick Gel Extraction Kit and cloned into the corresponding vectors reported in table I, previously digested and dephosphorylated. Ligation products were electroporated into TOP10F' and recombinant colonies were selected by PCR. Each expression vector from positive clones was isolated using QIAprepSpin Miniprep kit. All plasmids and expression vectors were generated by standard procedures and confirmed by sequencing.

hFcεRI full-length oligonucleotides sequence	vector	Tm
5'-CGCGCG <u>CGTCTCCC</u> ATGGCTCCTGCCATGGAATCCCCT-3' BsmBI	pETM11 pETM40 pETM52	54 °C
5'-CGCGCG <u>CTCGAG</u> TTACTAGTTGTTTTGGGGTTTGGCTTAGGA-3' XhoI * *		
5'-CGCGCG <u>CGATCCCC</u> ATGGCTCCTGCCATGGAATCCCCT-3' BamHI	pGEX	56 °C
5'-CGCGCG <u>CTCGAG</u> TTACTAGTTGTTTTGGGGTTTGGCTTAGGA-3' XhoI * *		
5'-CGCGCG <u>CGTCTCCC</u> ATGGCTCCTGCCATGGAATCCCCT-3' BsmBI	pET22	54 °C
5'-CGCGCG <u>CTCGAG</u> TTGTTTTGGGGTTTGGCTTAGGA-3' XhoI		

**A**

D1-D2 domain oligonucleotides sequence	vector	Tm
5'-CGCGCG <u>CTCGAG</u> TTACTATATTACAGTAATGTTGAGGGG-3' XhoI * *	pETM11	54 °C
5'-CGCGCC <u>CTCTCCC</u> ATGGTGTTAGCAGTCCCTCAG-3' BsmBI		

**B**

D2 domain oligonucleotides sequence	vector	Tm
5'-CGCGCG <u>CTCGAG</u> TTACTATATTACAGTAATGTTGAGGGG-3' XhoI * *	pETMA11 pETM40	56 °C
5'-CGCGCG <u>CTCTCCC</u> ATGTTCACTGACTGGCTGCT-3' BsmBI		

**C**

**Table I:** PCR primers used for the construction of expression of the: **A)** hFcεRI α chain full-length; **B)** D1-D2 domain of hFcεRI **C)** D2 domain of hFcεRI. The site of enzyme restriction is underline and the stop codons are asterisked.

### II.3.2.2 Expression screening for full-length hFcεRI α-chain

Optimal expression conditions were selected for each recombinant protein, by performing a complete screening in several *E.coli* strains, using different induction time, different temperatures and inducing agent concentration. 100 ng of expression vector were chemically transformed into *E. coli* competent cells from the following *E. coli* strains: BI21 (DE3), BI21 (DE3)pLysS, BI21star (DE3), BI21star (DE3)pLysS and Origami (DE3). Recombinant colonies were grown in 1.5 mL LB medium up to 0.6 OD/mL at 37°C and when expression was induced with different IPTG concentrations (0.1 mM, 0.2 mM, 0.5 mM and 1 mM) for different times and temperature (22°C and 37°C). Bacterial cultures were harvested, lysed and purified in batch using appropriate affinity resin. QIAgen Ni-NTA Magnetic Agarose Beads for His6x-tag, Amylose resin (Biolabs, New England) for MBP-tag and Glutathione Sepharose 4B resin (GE Healthcare) for GST-tag following the standard instructions of producers. 15 µL total and soluble fractions from the lysates were re-suspended in 5 µL SDS-Loading buffer (Tris-HCl 50 mM, SDS 1%, blue bromophenol 0.1%, glycerol 10%, pH 6.8) and analyzed on SDS-PAGE. For each recombinant protein the optimal expression conditions were selected.

### II.3.2.3 Purification of full-length His6x-αchain

Full-length hFcεRI α-chain was expressed with an N-terminal His6x-tag using the vector pETM11 and the recombinant protein expression was optimised in BI21star (DE3) inducing with 0.2 mM IPTG for 16 h at 22°C. The pellet obtained from 100 mL of bacterial culture was re-suspended in 5 mL cold lysis buffer (30 mM Tris-HCl, 150 mM NaCl, 6 M UREA, pH 8.0) supplemented with protease inhibitor mixture (1 mM PMSF, 1 µg/mL aprotinin, 1 µg/mL leupeptin, 1 µg/mL pepstatin and 1 mg/mL lysozyme) and incubated at R.T for 30 min. Cells were disrupted by sonication in ice using 10" on / 10" off cycles for 10 min. in total. The lysate was then centrifuged for 30 min. at 4°C at 15 krpm. The supernatant was loaded on a 1 mL His-Trap HP column, previously equilibrated with buffer 1 (30 mM Tris-HCl, 500 mM NaCl, 10 mM imidazole, 6 M urea, pH 8.0 buffer), using an AKTA FPLC chromatography system. The column was washed with buffer 1 and the bound protein was eluted using a linear gradient of imidazole from 10 mM to 500 mM in buffer 2 (30 mM Tris-HCl, 500 mM NaCl, 500 mM imidazole, 6M urea, pH 8) in 30 min. Protein elution was monitored by measuring the absorbance at 280 nm. His6x-αchain full-length was eluted at 21% buffer 2 (350 mM imidazole). The total cell protein fraction, the soluble fraction (supernatant of cell lysate) and the purified fraction were analyzed by 10% SDS-PAGE. The full-length His6x-αchain was recovered in 30 mM Tris-HCl, 500 mM NaCl, 1 mM DTT and 6 M urea pH 8.0 and dialyzed, slowly decreasing urea concentration, up to 30 mM Tris-HCl, 150 mM NaCl, 1 mM DTT, 2 M urea, pH 8.0 buffer. In order to increase the purity of full-length His6x-αchain, a further step of anionic exchange chromatography was performed on a Mono Q HR 5/5 column, integrated in an AKTA system, using a linear gradient from 10 mM to 500 mM NaCl in 30 min. The buffers are reported in table II:

<b>Buffer A</b>	<b>Buffer B</b>
30 mM Tris-HCl pH 8 10 mM NaCl 2 M UREA 1 mM DTT	30 mM Tris-HCl pH 8 500 mM NaCl 2 M UREA 1 mM DTT

**Table II**

Full-length His6x- $\alpha$ chain eluted at 350 mM NaCl and showed a 60% purity grade. Fractions were analyzed by 10% SDS-PAGE.

### **II.3.2.4 Purification of full-length GST- $\alpha$ chain**

Full-length hFc $\epsilon$ RI  $\alpha$ chain was expressed fused at its N-terminus with the GST-tag using the pGEX6P vector and the recombinant protein expression was optimised in BI21 (DE3)trxB induced with 0.1 mM IPTG for 16 h at 22°C. 100 mL bacterial culture was pelleted and re-suspended in 5 mL cold lysis buffer (30 mM Tris-HCl, 150 mM NaCl pH 8.0) supplemented with the protease inhibitor mixture (1 mM PMSF, 1  $\mu$ g/mL aprotinin, 1  $\mu$ g/mL leupeptin, 1  $\mu$ g/mL pepstatin and 1 mg/mL lysozyme) and incubated at room temperature for 30 min. Cells were disrupted by sonication in ice with 10" on / 10" off cycles for a total of 10 minutes. The lysate was then centrifuged for 30 min. at 4°C at 15 krpm and the supernatant loaded on a 1 mL Glutathione Sepharose 4B resin (GE Healthcare) in batch, previously equilibrated with buffer 1 (30 mM Tris-HCl, 500 mM NaCl) [45]. The resin was extensively washed with buffer 1 and the protein was eluted with 10 mM reduced Glutathione dissolved in 50 mM Tris-HCl pH 8.0. The total cell protein fraction, the soluble cytoplasmic fraction (supernatant of cell lysate), and the purified fraction were analyzed by 12% SDS-PAGE.

### **II.3.2.5 Purification of full-length MBP- $\alpha$ chain**

Full-length hFc $\epsilon$ RI  $\alpha$ chain was expressed with an N-terminal MBP-tag using the vector pETM40 and the recombinant protein expression was optimised in BI21 (DE3) inducing with 0.1mM IPTG for 16 h at 22°C. 100 mL bacterial culture was pelleted and re-suspended in 5 mL cold lysis buffer (30 mM Tris-HCl, 15 mM NaCl, pH 8.0) supplemented with protease inhibitor mixture (as described before) and incubated at room temperature for 30 min. Cells were disrupted by sonication in ice with 10" on / 10" off cycles for a total of 10 min. The lysate was then centrifuged for 30 min. at 4°C at 15 krpm and the supernatant loaded on 1 mL of amylose resin (Biolabs, New England), previously equilibrated with buffer 1 (30 mM Tris HCl, 500 mM NaCl) [46]. The resin was washed extensively with buffer 1 and the protein was eluted with 10 mM maltose dissolved in 30 mM Tris-HCl, 500 mM NaCl pH 8.0 buffer. The total cell protein fraction, the soluble fraction (supernatant of cell lysate) and purified fraction were analyzed by 10% SDS-PAGE.

### **II.3.2.6 Purification of the periplasmatic full-length His6x- $\alpha$ chain and full-length Dsb-His6x- $\alpha$ chain.**

Full-length hFc $\epsilon$ RI  $\alpha$ chain was expressed within the periplasmatic space with N-terminal His6x-tag and Dsb-His6x-tag using the pET22 and pETM50 vectors,

respectively [47]. Full-length His6x- $\alpha$ chain expression was optimised in Origami (DE3) inducing with 0.2 mM IPTG for 16 h at 22°C. A pellet from 500 mL bacterial culture was re-suspended in 10 mL cold lysis buffer (30 mM Tris-HCl, 20% sucrose, 1 mM EDTA pH 8.0), supplemented with protease inhibitor mixture (1 mM PMSF, 1  $\mu$ g/mL aprotinin, 1  $\mu$ g/mL leupeptin, 1  $\mu$ g/mL pepstatin) and incubated at R.T. for 20 min. After centrifugation at 8 krpm for 10 min. at 4°C, the resulting pellet was re-suspended in 5 mL of 30 mM Tris-HCl, 5 mM MgSO<sub>4</sub>, 10 mM DTT and 4 M urea, pH 8.0 buffer. The supernatant was loaded on a 1 mL His-Trap HP column, previously equilibrated with buffer 1 (30 mM Tris-HCl, 500 mM NaCl, 10 mM imidazole, 1 mM DTT, 4M urea pH 8.0), using an AKTA FPLC chromatography system. The column was washed with buffer 1 and the bound protein was eluted using a linear gradient from 10 mM to 500 mM imidazole in buffer 2 (30 mM Tris HCl, 500 mM NaCl, 500 mM imidazole, 1 mM DTT, 4 M urea pH 8.0) in 30 min. Protein elution was monitored by measuring the absorbance at 280 nm and the full-length His6x- $\alpha$ chain was eluted at 16% buffer 2 (80 mM imidazole). The purified fractions were analyzed by 15% SDS-PAGE. The periplasmatic full-length His6x- $\alpha$ chain recovered in 30 mM Tris-HCl, 500 mM NaCl, 1 mM DTT and 4 M urea pH 8.0 buffer was dialyzed, slowly decreasing urea concentration, up to 30 mM Tris-HCl, 150 mM NaCl, 1 mM DTT, 1 M urea pH 8.0 buffer. In order to increase the purity of the full-length His6x- $\alpha$ chain, a further step of anionic exchange chromatography was performed on a Mono Q HR 5/5 column, integrated in an AKTA system, using a linear gradient from 10 mM to 500 mM NaCl in 30 min. The buffers are reported in table III:

<b>Buffer A</b>	<b>Buffer B</b>
<b>30 mM Tris-HCl pH 8</b> <b>10 mM NaCl</b> <b>2 M UREA</b> <b>1 mM DTT</b>	<b>30 mM Tris-HCl pH 8</b> <b>500 mM NaCl</b> <b>2 M UREA</b> <b>1 mM DTT</b>

**Table III**

Full-length periplasmatic His6x $\alpha$ chain was eluted at 250 mM NaCl with 90% purity grade and fractions were analyzed by 15% SDS-PAGE.

The full length Dsb-His6x- $\alpha$ chain expression was optimised in BI21(DE3) bacterial strain induced with 0.2 mM IPTG for 16 h at 22°C. The purification was carried out using the protocol already described. The full-length periplasmatic Dsb-His6x- $\alpha$ chain recovered, in 30 mM Tris-HCl, 500 mM NaCl, 1 mM DTT and 4 M urea pH 8.0 buffer, was then dialyzed against 30 mM Tris-HCl, 150 mM NaCl, 1 mM DTT pH 8.0 maintaining its solubility in buffer with 1 M urea.

### **II.3.2.7 Expression and purification of His6x-D1-D2 domain as inclusion bodies**

100 ng of the expression vector D1-D2 domain/pETM11 was chemically transformed in BI21 (DE3), *E.coli* competent cells. The clone D1-D2/pETM11 was streaked onto LB agar plate containing kanamycin (50  $\mu$ g/mL) and incubated at 37°C for 16 h. A single colony was used to inoculate 10 mL of LB medium containing kanamycin (50  $\mu$ g/mL) followed by incubation at 37°C in a shaking incubator. Ten millilitres overnight culture was then used to inoculate a further 1 L of LB-kanamycin and the culture growth continued in a 37°C shaker for approximately 3 h. When the optical density (OD), measured at 600 nm, reached the value 0.8, 1 mM IPTG was added (1 mL 'uninduced' culture was taken for SDS-PAGE analysis). After 4 h induction at 37°C (1

mL 'induced' culture was taken for SDS-PAGE analysis), cells were harvested by centrifugation. The pellet obtained from 250 mL bacterial culture was re-suspended in 20 mL of lysis buffer (50 mM Tris-HCl, 150 mM NaCl, 10 mM EDTA, 0.5 mM PMSF, 2 mM DTT, 10% glycerol, and 1 mg/mL lysozyme pH 8.0). The cellular lysate, incubated at R.T. for 30 min., was sonicated in ice for 10 min. (10" on / 10" off) and centrifuged for 20 min. at 10 Krpm. The supernatant was decanted and the inclusion bodies pellet was resuspended in 20 mL of washing buffer 1 (150 mM Tris-HCl, 150 mM NaCl, Triton 1%, 5 mM DTT pH 8.0) and centrifuged 10 min. at 10 Krpm. This step was repeated by resuspending the inclusion bodies pellet in 20 mL washing buffer 2 (50 mM Tris-HCl, 150 mM NaCl, 10 mM EDTA, 2 M UREA, Triton 1%, 5 mM DTT, pH 8.0) and, for three times, in washing buffer 3 (50 mM Tris-HCl, 15 mM NaCl, 10 mM EDTA, 5 mM DTT). The final pellet was dissolved in 6 M guanidine chloride, 50 mM Tris-HCl, 100 mM NaCl, 10 mM EDTA and 2 mM DTT, pH 8.0 buffer and stirred at 4°C for 12 h till complete solubilization. The residual insoluble part was removed by centrifugation at 12 Krpm for 30 min. at 4°C and the soluble protein fraction was analyzed by 15% SDS-PAGE.

### **II.3.2.8 Expression and Purification of MBP-D2 domain**

100 ng expression vector D2-pETM40 were chemically transformed into BI21 (DE3), *E.coli* competent cells. Recombinant colonies were grown in 2 mL LB medium up to 0.6 OD/mL at 37°C and then expression was induced with 0.1 mM IPTG for 16 h at 22°C. 100 mL of bacterial culture were resuspended in 5 mL of lysis buffer (30 mM Tris-HCl, 150 mM NaCl, 1 mM PMSF, and 1 mg/mL lysozyme pH 8.0), left for 30 min. at RT and then sonicated 10" on / 10" off for 5 min. The lysate was then centrifuged for 30 min. at 4°C at 15 krpm and the soluble fraction was loaded on 1 mL amylose resin (Biolabs, New England), previously equilibrated with buffer 1 (30 mM Tris-HCl, 500 mM NaCl pH 8.0). The resin was washed extensively with buffer 1 and the protein was eluted with 10 mM maltose dissolved in 30 mM Tris-HCl, 500 mM NaCl pH 8.0 buffer. The total cell protein fraction, the soluble cytoplasmic fraction (supernatant of cell lysate), and the purified fraction were analyzed by 15% SDS-PAGE.

### **II.3.2.9 Expression and Purification of His6x-D2 domain**

100 ng expression vector D2-pETMA11 were chemically transformed into BI21 (DE3)trxB, *E. coli* competent cells. Recombinant colonies were grown in 2 mL of LB medium up to 0.6 OD/mL at 37°C and expression was induced with 0.2 mM IPTG for 16 h at 22°C. 100 mL bacterial culture was re-suspended in 5 mL of 30 mM Tris-HCl, 150 mM NaCl, 4M UREA, 5 mM DTT, 1 mg/mL lysozyme pH 8.0 buffer supplemented with protease inhibitor mixture (1 mM PMSF, 1 µg/mL aprotinin, 1 µg/mL leupeptin, 1 µg/mL pepstatin (lysis buffer), kept for 30 min. at R.T. and then sonicated for 10 min. (10" on, 10" off). After 20' centrifugation at 4°C and 15 Krpm, 500 mM NaCl and 10 mM imidazole were added to the soluble fraction. Thus the recovered fraction was loaded on a His-trap column (1 mL). The column was washed with buffer 1 (30 mM Tris-HCl, 500 mM NaCl, 10 mM imidazole, 1 mM DTT, 4M urea pH 8.0) and the bound protein was eluted using a linear gradient from 10 mM to 500 mM imidazole in buffer 2 (30 mM Tris-HCl, 500 mM NaCl, 500 mM imidazole, 1 mM DTT, 4M urea pH 8.0). Protein elution was monitored by measuring the absorbance

at 280 nm. Under these conditions, His6x-D2 domain was eluted in 30 mM Tris-HCl, 500 mM NaCl, 290 mM imidazole, 1 mM DTT, 4 M urea pH 8.0 buffer.

The purified protein dissolved in 30 mM Tris-HCl, 500 mM NaCl, 1 mM DTT, 290 mM imidazole and 4M urea pH 8.0 buffer was dialyzed against 30 mM Tris-HCl, 1 mM DTT, 500 mM NaCl, 2M urea pH 8.0 buffer over night at 4°C. The recombinant protein was refolded decreasing the urea concentration by rapid dilution in 30 mM Tris-HCl, 150 mM NaCl, 1mM DTT, pH 8.0. The last step of dialysis was carried out in 30 mM Tris-HCl, 150 mM NaCl, 5 mM reduced glutathione, 0.5 mM oxidized glutathione pH 8.0 buffer over night at 4°C. The precipitate formed during the refolding procedure was removed by centrifugation at 12 Krpm for 30' at 4°C. The recovered His6x-D2 domain was analyzed by 15% SDS-PAGE under reducing and non-reducing conditions.

### **II.3.2.10 Western blotting**

The protein was loaded on a 15% SDS-PAGE under reducing conditions and then transferred onto a PVDF membrane using Trans Blot SD semi-dry (Bio-Rad), according to the manufacturer's recommendations. After protein transfer, the membrane was blocked with 5% NFDM in TTBS (20 mM Tris-HCl, 0.9% NaCl, 0.05 % Tween 20, pH 7.5 buffer) for 1 h at R.T. After three washes with TTBS, the filter was incubated with the His-probe-HRP conjugated diluted 1:1000 in TTBS/0.5% BSA for 1 h at R.T. Detection was carried out using an Opti-4CN goat anti-mouse detection Kit according to the manufacturer's protocol.

### **II.3.2.11 Vinyl pyridine reaction**

To assess the presence of disulfide bridges, 50 µg of purified refolded His6x-D2 domain (at 1 mg/mL) was denatured in 50 µL solution containing 250 mM Tris-HCl, 1 mM EDTA, and 6 M guanidine chloride pH 8.5 buffer, for 30 min. at 45°C without reducing agents. The protein was then alkylated by incubating the sample mix in the presence of 0.12 M 4-vinyl-pyridine at 25°C for 60 min. The reaction was stopped by cooling the sample at 4°C.

### **II.3.2.12 Gel Filtration analysis**

The oligomeric state of His6x-D2 domain was investigated by gel filtration chromatography. To this purpose, 100 µg of His6x-D2 domain and 200 µg of the same protein opportunely reduced with DTT, were loaded on a Superdex 75 10/300 GL column equilibrated with 30 mM Tris-HCl, 500 mM NaCl, pH 8.0 buffer at 0.4 mL/min. The eluate was monitored at 280 nm.

### **II.3.13 Protein characterization by LC-MS**

LC-MS analyses were performed to estimate the protein purity and assess the molecular weight. For this analysis, 0.5 µg of His6x-D2 domain were loaded on a 300 Å narrow bore 250x2mm C4 Jupiter column (Phenomenex, Torrance, CA) coupled to the LC-MS system previously described. A gradient of solvent B (0.05% TFA in CH<sub>3</sub>CN) from solvent A (0.08% TFA in H<sub>2</sub>O) of 30% to 70% was applied over 40 min. Mass spectra were recorded continuously in the mass interval 400-2000 amu, in

positive mode (LC-MS, condition 1). Multicharge spectra were then deconvoluted using the BioMass program implemented in the Bioworks 3.1 package provided by the manufacturer's instruction. Mass calibration was performed automatically by means of selected multiple charged ions, in the presence of a calibrant agent (UltraMark; ThermoElectron, Milan). All mass values are reported as average.

### II.3.2.14 Circular Dichroism analyses

CD spectra of His6x-D2 domain were acquired in 20 mM phosphate buffer pH 8.0 solutions with  $C = 8 \times 10^{-6}$ , as determined by Bradford measurements [48], at room temperature. CD spectra of IgE-TRAP polypeptides were acquired in aqueous solutions with  $C_{\text{pep}} = 3.85 \times 10^{-5}$ , calculated by UV measurements using a molar extinction coefficient at 280 nm of  $31345 \text{ M}^{-1}\text{cm}^{-1}$  for IgE-TRAP ox and  $31220 \text{ M}^{-1}\text{cm}^{-1}$  for IgE-TRAP red, at room temperature. Spectra were recorded using a 0.1-mm path length quartz cuvette. Data were collected at 0.2-nm intervals with a  $20 \text{ nm min}^{-1}$  scan speed, a 2 nm bandwidth, and a 16 s response, within the spectral range of 260 to 190 nm. The recorded spectra were then signal-averaged over at least three scans, and the baseline was corrected by subtracting the spectrum of the buffer. Spectra were then transformed in molar ellipticity/mean residue  $[\theta]$ , expressed in  $\text{deg}\cdot\text{cm}^2\cdot\text{dmol}^{-1}$  and calculated using the following equation:

$$[\theta] = [\theta]_{\text{obs}} \cdot \text{mrw} / 10 \cdot l \cdot C$$

where  $[\theta]_{\text{obs}}$  is the ellipticity measured in millidegrees, mrw is the average MW of protein residues, C is the protein concentration in  $\text{g}\cdot\text{L}^{-1}$ , and l is the optical path length of the cell used, expressed in cm.

### II.3.2.15 Polypeptides synthesis, purification and characterization

All peptides were synthesized in batch by solid phase peptide synthesis as C-terminally amidated and N-terminally acetylated derivatives following standard Fmoc chemistry protocol [49]. A Rink-amide MBHA resin (substitution 0.53 or 1.12 mmol/g) and amino acid derivatives with standard protections were used in all syntheses. A 4-fold excess of amino acids, preactivated with PyBOP/DIEA (1:2), was used throughout the synthesis. Coupling and deprotection times were kept at 25 min. and 15 min., respectively. Standard side-chain protection groups for Fmoc chemistry were used for all residues except lysine (Lys133), introduced as 4-methyl-trityl (Mtt) derivative; succinic anhydride and ethylenediamine were not preactivated. The selective deprotection of Lys(Mtt)-containing peptidyl resins were performed by treatment with a dichloromethane (DCM)/trifluoroacetic acid (TFA)/tri-isopropylsilane (TIS) (94:1:5, v/v/v) mixture for 2 min. at R.T. several times. Succinic acid was introduced by resin treatment with a 10-fold excess of succinic anhydride mixed with DIPEA (1:2) and the reaction was kept at room temperature for 20 minutes. A 2-fold excess of ethylenediamine was instead introduced using ethylenediamine/DIPEA (1:1) after on resin pre-activation with conventional reagents and the reaction was left at room temperature for 20 minutes. Total cleavage from the solid support was performed by treatment with a trifluoroacetic acid (TFA)/tri-isopropylsilane (TIS)/water (90:5:5, v/v/v) mixture for 90 minutes at R.T. Crude peptides were precipitated in cold diethyl-ether, dissolved in a water/acetonitrile (1:1, v/v) mixture and lyophilized. IgE-TRAP and 2<sup>nd</sup> Loop cysteine oxidation were performed in 100 mM carbonate buffer pH 8.0 for 16 h at R.T.

Peptide purification was carried out by RP-HPLC using a C18 Jupiter 250x22mm ID column (15  $\mu\text{m}$ , 300  $\text{\AA}$ ) applying a linear gradient of acetonitrile in 0.1% TFA from 10% to 70% in 50 min. at 20 mL/min. Detection was achieved at 210 nm. Peptide purity and integrity were confirmed by LC-MS as previously described.

### II.3.2.16 Immunoglobulin coating on sensor surface

Binding assays were performed using the SPR technique at 25°C on a BIACORE 3000 instrument (Pharmacia Biosensor). A specific binding surface was prepared by coupling the immunoglobulins to a CM5 sensor chip using the amine coupling kit according to the manufacturer's instructions. The sensor chip was activated using a 1:1 volume mixture of an NHS solution (50 mM N-hydroxysuccinimide in water) and an EDC solution (200 mM N-ethyl-N'-(dimethylaminopropyl) carbodiimide in water), to give a reactive N-hydroxy-succinimide ester. The immobilization was efficiently performed in 10 mM NaAc pH 5.5 buffer at a flow rate of 30  $\mu\text{L}/\text{min}$ . Any residue unreacted surface groups was inactivated by injecting a solution of ethanolamine 1M, pH 8.0.

All three types of immunoglobulins IgE, IgG and IgA (Sigma-Aldrich) were efficiently immobilized.

### II.3.2.17 SPR data fitting and analysis

Data were analyzed using the BIAevaluation analysis package (version 4.1, Pharmacia Biosensor). Non specific binding was subtracted from the specific binding prior to analysis. A binding data fitting was carried out using a monophasic or biphasic model and evaluating the goodness of fitting by analysis of residual [19,32]. For the monophasic model the dissociation rate constant ( $kd$ ) was obtained by fitting the dissociation phase data to the following equation:

$$R=R_0*\exp(-kd*(t-t_0))$$

where  $R_0$  is the response at the start of the dissociation,  $t-t_0$  is the time function for the dissociation phase.

The association rate constant ( $ka$ ) was obtained by fitting the association phase data to the following equation:

$$R=ka*Conc*Rmax/(ka*Conc+kd)*(1-\exp(-(ka*Conc+kd)*(t-t_0)))+Rl$$

where  $Rmax$  is the maximum analyte binding capacity (RU),  $ka$  is the association rate constant,  $C$  is the molar concentration of the ligand,  $kd$  is the dissociation rate constant, and  $t-t_0$  is the time function for the association phase.

For the biphasic model the dissociation rate constants were obtained by fitting the dissociation phase data to the following equation:

$$R=R1*\exp(-kd_1*(t-t_0))+(R_0-R1)*\exp(-kd_2*(t-t_0))+Offset$$

where  $R_0$  is the total response at the start of dissociation,  $R_1$  is the contribution to  $R_0$  from component 1 and  $R_0-R_1$  is the contribution to  $R_0$  from component 2,  $t-t_0$  is the

time function for the dissociation phase, and  $kd_1$  and  $kd_2$  are the dissociation rate constants for the two components.

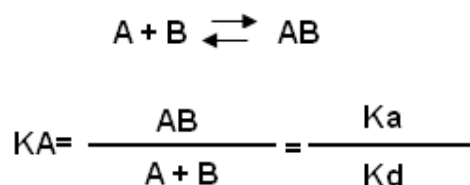
The association rate constants were obtained by fitting the association phase data to the following equation:

$$R = ka_1 \cdot Conc \cdot Rmax / (ka_1 \cdot Conc + kd_1) \cdot (1 - \exp(-(ka_1 \cdot Conc^{n1} + kd_1) \cdot (t - t_0))) + ka_2 \cdot Conc \cdot Rmax / (ka_2 \cdot Conc + kd_2) \cdot (1 - \exp(-(ka_2 \cdot Conc^{n2} + kd_2) \cdot (t - t_0)))$$

where  $Rmax$  is the maximum analyte binding capacity,  $ka_1$  and  $ka_2$  are the association rate constants for components 1 and 2,  $C$  is the molar concentration of the ligand,  $t-t_0$  is the time function for the association phase, and  $n1$  and  $n2$  are the steric interference factors for the two components, which are set at 1 when the binding of one component does not inhibit the binding at another ligand site. Biphasic dissociation may occur for the complex with a stoichiometry 1:1 when re-association of the release ligand takes place.

The ability of the models to describe the experimental data was determined by examination of the residual plots, which were calculated by subtracting the experimental data points from the fitted curve. The residuals should be small and randomly distributed around zero for a good fit.

The affinity constant can either be measured directly by equilibrium binding analysis or calculated. The affinity constant  $KA$  (or association constant) is simply the ratio of the kinetic constants for the interaction :



Data fitting and Scatchard analysis were carried out by non-linear regression and programs implemented within the GraphPad Prism, vers. 4.0 software.

### II.3.2.18 ELISA assay

An ELISA assay was set up to check the binding between IgE and His6x-D2 domain [50]. IgE at fixed concentrations in PBS buffer (10 mM  $Na_2HPO_4$ , 2 mM  $KH_2PO_4$ , 137 mM NaCl, 2.7 mM KCl pH 7.4 buffer) was dispensed into 96-well microtiter plates (Nunc, Milan, Italy). Some wells were filled with buffer alone and were used as blank. After 16h incubation at 4°C, plates were washed three times with PBS-T buffer (PBS containing 0.04% Tween-20). The wells were filled to the top with 250  $\mu$ L BSA 1% in PBS buffer and plates were incubated for 2 h at 37°C. After washing, increasing concentrations of His6x-D2 domain in the appropriate buffer were added and the plate was incubated for 1 h at 37°C. After washing, wells were filled with 100  $\mu$ L anti-His6x-probe conjugated with HRP, diluted 1:1000 in PBS, and incubated for 1 h at 37°C. After washing, 100  $\mu$ L of chromogenic substrate *o*-phenyldiamine 0.4 mg/mL in 50 mM sodium-phosphate-citrate buffer pH 5.0, containing 0.4 mg/mL hydrogen peroxide, were added to each well. The reaction was stopped by adding 50  $\mu$ L of 2.5

M H<sub>2</sub>SO<sub>4</sub> in each well. The absorbance was measured at 490 nm using a Synergy 4 multi-wavelength reader (BIOTEK Instruments, Inc. Highland Park, VT, USA). For the competition experiment, IgE at 2 µg/mL in coating and His6x-D2 domain at 5 µM was chosen as the pre-saturation condition based on previous experiments. In dose-dependent competition assays, increasing concentrations of peptide competitors (IgE-TRAP red, 1<sup>st</sup> Loop and 2<sup>nd</sup> MiniLoop), ranging from 0 to 500 µM were pre-incubated with His6x-D2 domain solution at 5 µM for 30 min. at R.T. before addition to each well. The subsequent steps were carried out as previously described. Data fitting and analysis were carried out by non-linear regression using the GraphPad Prism software, vers. 4.0.

## II.4 RESULTS AND DISCUSSION

### II.4.1 Molecular design of FcεRI receptor mimicking polypeptides

In a first attempt at obtaining peptides binding IgE, we designed a set of peptides from the known crystal structure of the Fc-IgE-αFcεRI complex.

The crystal structure of the Fc-IgE-αFcεRI complex, deposited in the Protein Data Bank (1F6A), has been used to design a polypeptide mimicking the receptor binding sites. As extensively described in the introduction, the residue Y131, located in the C'-E region of the receptor D2 domain in binding site 1, resides in a shallow pocket formed by residues from one IgE chain (R334, V336, D362, A364, and H424).

Binding Site 2 is dominated by interactions occurring between surface-exposed tryptophans (W87, W110, W113, W156) from the D1-D2 linker region (W87) and from the D2 domain (W110, W113, W156) of αFcεRI. In particular, the two conserved tryptophan residues (W87 and W110) form a pocket for the IgE residue P426, giving rise to a "proline sandwich" and the two non-conserved tryptophans (W113, W156), in binding Site 2, form a platform interacting with the IgE-Cε2-Cε3 linker. The antibody binding specificity is due to the non-conserved residues. In the following Fig. 6, the patch of tryptophans (yellow) and the region around the Tyr131 (green) are evidenced as "surface". Also the two distinct D1 and D2 domains are clearly visible.

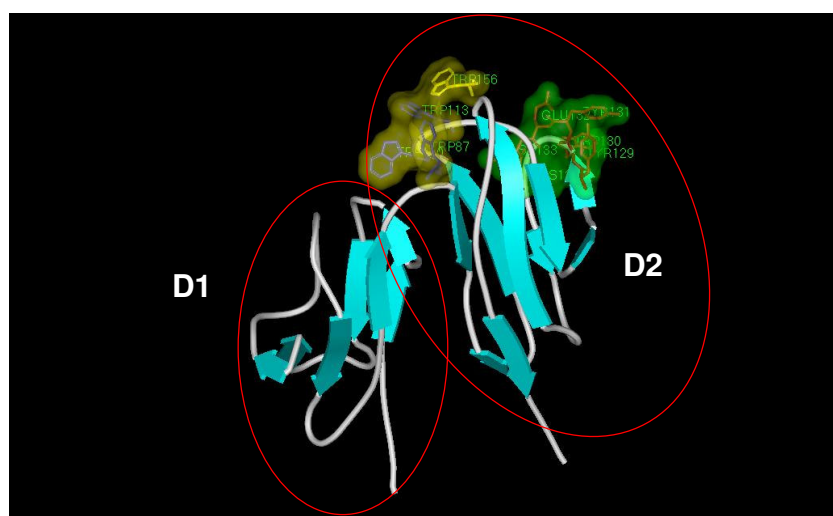


**Figure 6:** 3D representation of αFcεRI receptor. D1 and D2 domains are ringed in red; the binding pocket residues for site 1 and site 2 are highlighted in yellow and in green, respectively. The model was built using the programs Insight II and WebLab Pro.

Four regions belonging to the αFcεRI were selected as potential recognition surfaces for the construction of the IgE-binding peptide and these being from site 1 and site 2. It must be underlined here that only residues from the D2 domain are essentially needed to bind to the immunoglobulin. The polypeptide structure, named IgE-TRAP is reported in Fig.7. It can be seen that it recapitulates both sites which are shared by two distinct loop regions, named 1<sup>st</sup> Loop and 2<sup>nd</sup> Loop. Site 1, which is entirely within the 1<sup>st</sup> Loop (boxed), contains residues from the C'-E loop of the receptor (129-134, YWYEKH). The Asn133 is mutated to Lys in order to exploit its side chain as a linker

to join the residues WRNW (from 110 to 113), connecting the NH<sub>2</sub>ε of the Lys side chain and the N-terminus of Trp113 (distance about 10.7 Å). On the N-terminus of the Trp110, a new Trp, putatively mimicking the Trp87, was joined using a βAla as a linker (about 5Å). To join residues corresponding to the region Cys151-Ser162, a linker composed of a succinic acid and an ethylenediamine was designed (accounting for about 10 Å). This last portion of the molecule was designed as a cyclic peptide in order to mimic the turn around the central Trp156-Gln157 peptide diade and to reduce the conformational flexibility. For this purpose, a cysteine replaced the isosteric residue Ser162.

In summary, the molecule contained three recognition elements from site 1 and site 2, ideally encased within two loops, 1<sup>st</sup> Loop and 2<sup>nd</sup> Loop (Fig.8). The two elements forming the 1<sup>st</sup> Loop were named 1<sup>st</sup> miniLoop [residues 129-134] and 2<sup>nd</sup> miniLoop [residues 87, βAla, 110-113]. The aim of this design was to try to preserve these regions stabilizing the overall structure with the introduction of mutations and suitable linkers to ensure the appropriate distance between the two sites. To increase the polypeptide stability, both N-terminal and C-terminal ends were acetylated and amidated respectively.

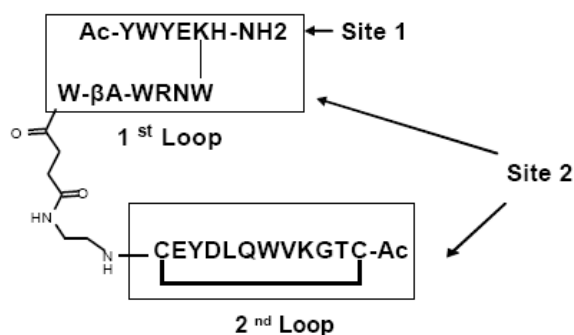


**Figure 7:** Schematic representation of IgE-TRAP polypeptide in the oxidized form.

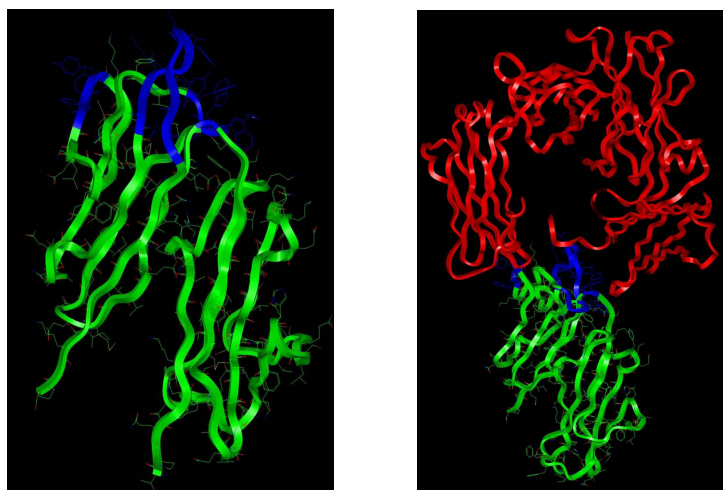


**Figure 8:** 3D representation of receptor regions utilized to design the IgE-TRAP (in blue). The same structure is reported within the complex with the Fc-IgE. The model was built using programs Insight II and WebLab Pro.

In order to improve the affinity of the designed polypeptide and to understand a possible correlation between structure and activity, a set of peptides corresponding to the IgE-TRAP polypeptide subregions, reported in the following table IV, were tested.

129 130 131 132 133 134 85 110 111 112 113		
Ac-Tyr-Trp-Tyr-Glu-Lys(HisAc)-Trp-βAla-Trp-Arg-Asn-Trp-Ac		
	<b>1<sup>st</sup> Loop [129-134, 85, βAla, 110-113]</b>	<b>M.W.1909.12</b>
129 130 131 132 133 134		
Ac-Tyr-Trp-Tyr-Glu-Lys-His-NH <sub>2</sub>		
	<b>1<sup>st</sup> miniLoop [129-134]</b>	<b>M .W. 1009.12</b>
85 110 111 112 113		
Ac-Gly-Trp-βAla-Trp-Arg-Asn-Trp-NH <sub>2</sub>		
	<b>2<sup>st</sup> miniLoop [85, βAla, 110-113]</b>	<b>M.W.1016.14</b>
110 111 112 113		
Ac-Gly-Trp-Arg-Asn-Trp-NH <sub>2</sub>		
	<b>Peptide S [110-113]</b>	<b>M.W. 758.84</b>
151 152 153 154 155 156 157 158 159 160 161 162		
Ac-Cys-Thr-Gly-Lys-Val-Trp-Gln-Leu-Asp-Tyr-Glu-Cys-NH <sub>2</sub>		
	<b>2<sup>nd</sup> Loop [151-162]</b>	<b>MW.1484.70</b>

**Table IV:** Peptides corresponding to the IgE-TRAP subregions: 1<sup>st</sup> Loop [residues 129-134, 85, βAla, 110-113]; 1<sup>st</sup> miniLoop [residues 129-134]; 2<sup>nd</sup> miniLoop [residues 85, βAla, 110-113], Peptide S [residues 110-113] and 2<sup>nd</sup> Loop [residues 151-162].

#### II.4.1.2 Synthesis, purification and characterization of polypeptides

All peptides were synthesized and purified by RP-HPLC as described in the section II.3.2.15 of methods. The polypeptides IgE-TRAP and 2<sup>nd</sup> Loop were cyclized by spontaneous oxidation in 100 mM carbonate buffer, pH 8.0. To obtain the same product in the reduced form, 100 mM DTT was added before purification. All final products were characterized by LC-MS. Deconvoluted mass spectra of active peptides are reported in Fig.9.

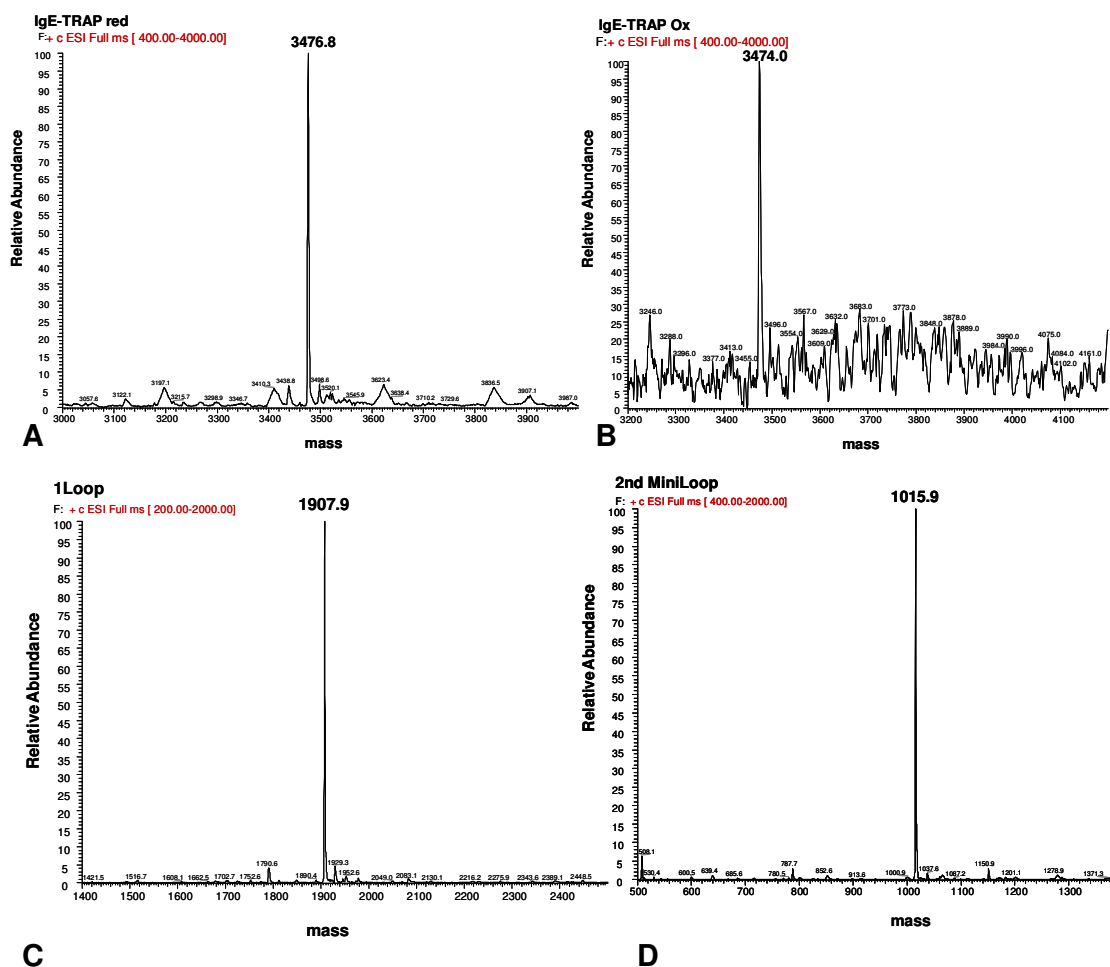


**Figure 9:** Mass spectra of: **A)** IgE-TRAP before ( $MW_{exp}/MW_{theor.}: 3476.8/3476.1 \text{ amu}$ .) and **B)** after oxidation ( $MW_{exp}/MW_{theor.}: 3474.2/3474.0 \text{ amu}$ ); **C)** 1<sup>st</sup> Loop ( $MW_{exp}/MW_{theor.}: 1907.9/1909.12 \text{ amu}$ ); **D)** 2<sup>nd</sup> miniLoop, ( $MW_{exp}/MW_{theor.}: 1015.9/1016.14 \text{ amu}$ ).

The polypeptides IgE-TRAP, in their oxidized and reduced form, were characterized in solution by far-UV circular dichroism (190-260 nm) to investigate their conformational behaviour. The far UV-CD spectra were acquired in aqueous solution and at room temperature, using a concentration of  $3.85 \times 10^{-5} \text{ M}$  for both polypeptides. The CD spectra showed no canonical spectral features (Fig.10). The spectrum obtained for the polypeptide IgE-TRAP ox shows a random coil conformation, with a negative band at 200 nm and no positive band in the wavelength region between 190 nm and 200 nm. On the other hand, the positive signal at 190 nm and the negative band between 200 nm and 210 nm, observed in the IgE-TRAP red spectrum, is more indicative of a  $\beta$ -sheet structure. In both spectra the positive signal at 230 nm may reflect contributions from the high density of surface exposed aromatic residues [51]. However, an analysis of CD spectra indicates that the IgE-TRAP red possesses a higher contribution from the structured form (positive band at 195 nm) respected to IgE-TRAP ox.

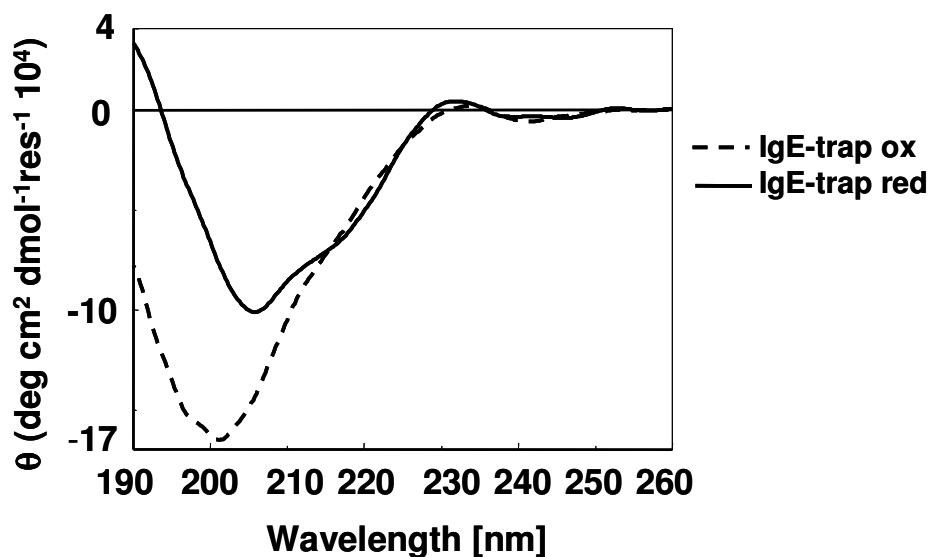


**Figure 10:** Far-UV CD spectrum of the IgE-TRAP ox and red polypeptides. CD spectra are reported in molar ellipticity  $[\theta]$ .

### II.4.1.3 Equilibrium affinity measurements between Immunoglobulins E and the receptor mimicking polypeptides by SPR assay.

The interaction between the designed polypeptides and IgE was assessed by SPR using a BIACORE 3000 system. Immunoglobulins E were efficiently immobilized on a CM5 sensor chip, obtaining a signal of about 54700 RU.

The IgE-TRAP polypeptides (IgE-TRAP red and IgE-TRAP ox, reduced and oxidized variant, respectively) were dissolved in a water:acetonitrile buffer (90:10) and injected at 20  $\mu\text{L}/\text{min}$  flow rate, after proper dilution in HBS (100 mM Hepes, 150mM NaCl, 5mM EDTA) buffer pH 7.4. Dose-dependent binding curves were observed with increasing concentrations between 2.5  $\mu\text{M}$  and 40  $\mu\text{M}$  of the oxidized and reduced forms, reaching binding saturation at 30  $\mu\text{M}$ , as shown in Fig.11 and 14. The saturating condition at 40  $\mu\text{M}$  is not shown. The association and dissociation phases of the response curves were fitted to a biphasic model assuming a 1:1 (Langmuir) binding. The ability of the model to describe the experimental data was evaluated by examination of the residual plots, which were calculated by subtracting the experimental data points from the fitted curve. The residual values are considerably small thus suggesting an acceptable fitting with the biphasic model. The analysis of SPR data for IgE-TRAP ox and red are reported in Fig.12 and Fig.15, respectively.

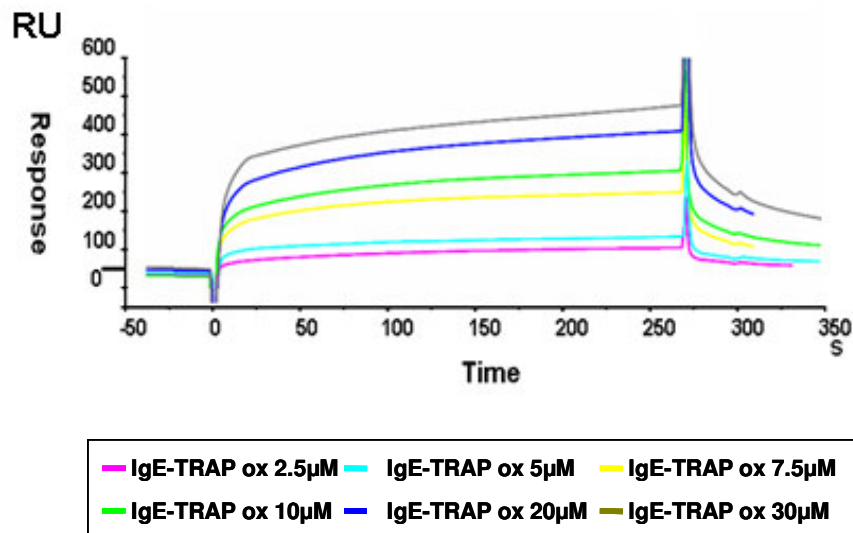


**Figure 11:** Overlapping sensorgrams for the interaction of IgE with IgE-TRAP ox. The interactions were monitored at seven IgE-TRAP ox concentrations (2.5  $\mu\text{M}$ , 5  $\mu\text{M}$ , 7.5  $\mu\text{M}$ , 10  $\mu\text{M}$ , 20  $\mu\text{M}$ , 30  $\mu\text{M}$  and 40  $\mu\text{M}$ ).

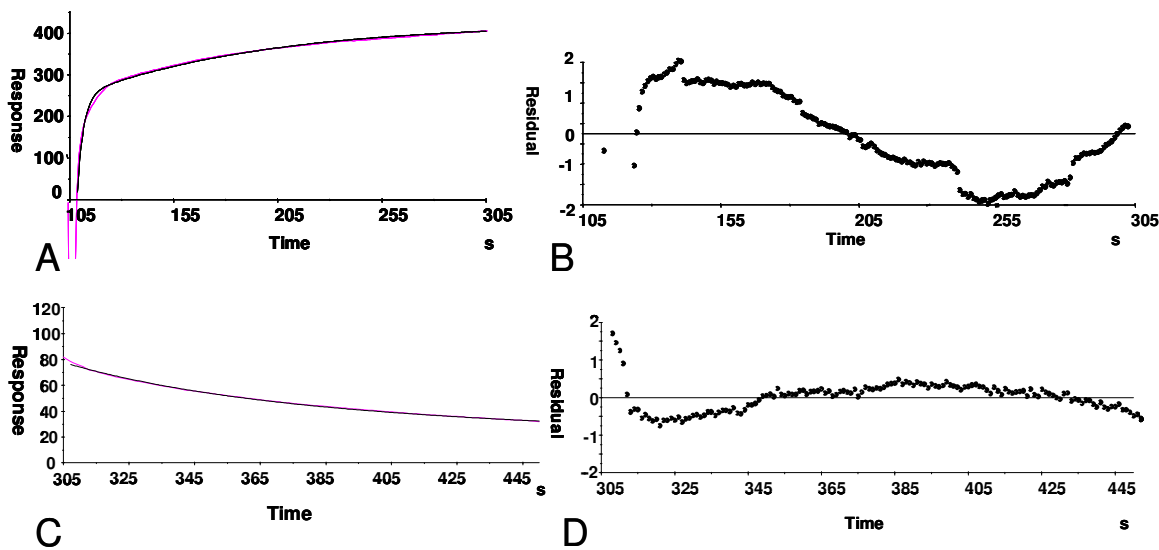


**Figure 12:** Analysis of SPR data for the binding of IgE-TRAP ox at 2.5  $\mu\text{M}$  to immobilized IgE. The fitted lines (black) are overlaid with the experimental curves (fuchsia) for the association phase (**A**) and the dissociation phase (**B**). The corresponding residual plots are shown (**C** and **D**, respectively). Curves from all other experiments were similarly fitted.

The biphasic fit is characterized by two association rates and two dissociation rates and these value yield an affinity constant for each phase of the interaction. A summary of association and dissociation rate constants obtained by data fitting, as well as the calculated affinity constants, are reported in table V.

The rate constants  $k_{d1}$  ( $1.06 \pm 0.15 \times 10^{-2} \text{ s}^{-1}$ ),  $k_{d2}$  ( $3.69 \pm 0.62 \times 10^{-1} \text{ s}^{-1}$ ),  $k_{a1}$  ( $1.63 \pm 0.19 \times 10^2 \text{ M}^{-1} \text{ s}^{-1}$ ) and  $k_{a2}$  ( $6.14 \pm 0.70 \times 10^3 \text{ M}^{-1} \text{ s}^{-1}$ ) were extrapolated and averaged

over all experiments, and used to calculate the two equilibrium constants  $KD_1 = 65 \pm 0.8 \mu\text{M}$  and  $KD_2 = 60 \pm 0.9 \mu\text{M}$ .

Analyte Concentration IgE-TRAP ox	Association rate ( $\text{M}^{-1} \text{s}^{-1}$ ) $K_{a1}$	Dissociation rate ( $\text{s}^{-1}$ ) $K_{d1}$	Association rate ( $\text{M}^{-1} \text{s}^{-1}$ ) $K_{a2}$	Dissociation rate ( $\text{s}^{-1}$ ) $K_{d2}$
2.5 $\mu\text{M}$	$3.09 \times 10^2$	$8.79 \times 10^{-3}$	$7.52 \times 10^3$	$3.40 \times 10^{-1}$
5 $\mu\text{M}$	$1.34 \times 10^2$	$1.07 \times 10^{-2}$	$8.16 \times 10^3$	$4.70 \times 10^{-1}$
7.5 $\mu\text{M}$	$2.30 \times 10^2$	$1.43 \times 10^{-2}$	$7.93 \times 10^3$	$3.90 \times 10^{-1}$
10 $\mu\text{M}$	$1.11 \times 10^2$	$1.29 \times 10^{-2}$	$5.26 \times 10^3$	$5.12 \times 10^{-1}$
20 $\mu\text{M}$	$1.37 \times 10^2$	$8.69 \times 10^{-3}$	$5.36 \times 10^3$	$2.61 \times 10^{-1}$
30 $\mu\text{M}$	$5.88 \times 10^1$	$8.41 \times 10^{-3}$	$2.58 \times 10^3$	$2.36 \times 10^{-1}$
MEAN	$1.63 \times 10^2$	$1.06 \times 10^{-2}$	$6.14 \times 10^3$	$3.69 \times 10^{-1}$
	$KD_1 = 65 \times 10^{-6} \text{ M}$		$KD_2 = 60 \times 10^{-6} \text{ M}$	

**Table V:** Table of kinetic and thermodynamic constants extrapolated for the binding of IgE-TRAP ox by the equilibrium affinity measurements by SPR. All data fit optimally with a biphasic association and dissociation.

Binding constants were further analyzed by plotting the RUmax value against the polypeptide concentrations and calculated by data fitting using both a non-linear regression and a Scatchard analysis (Fig.13). Data were consistent with  $KD$  of  $16 \pm 4 \mu\text{M}$ , which is a measure of a macroscopic apparent association constant resulting from the two distinct association-dissociation events.

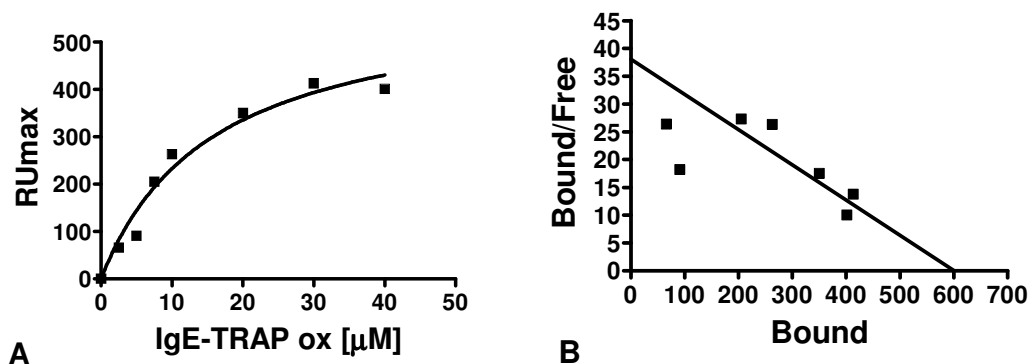


**Figure 13:** Plot of the RUmax vs IgE-TRAP ox concentrations fitted by non-linear regression (A) and the corresponding Scatchard analysis (B).

For IgE-TRAP red, a similar analysis was carried out, obtaining the following average kinetic parameters:  $k_{d1}$  ( $6.43 \pm 0.03 \times 10^{-1} \text{ s}^{-1}$ ),  $k_{d2}$  ( $1.05 \pm 0.08 \times 10^{-2} \text{ s}^{-1}$ ),  $k_{a1}$  ( $3.30 \pm 0.4 \times 10^4 \text{ M}^{-1} \text{ s}^{-1}$ ) and  $k_{a2}$  ( $2.87 \pm 0.82 \times 10^2 \text{ M}^{-1} \text{ s}^{-1}$ ). The thermodynamic KD extrapolated by these data were:  $KD1 = 19 \mu\text{M} \pm 0.1$  and  $KD2 = 37 \mu\text{M} \pm 0.9$  (table VI).

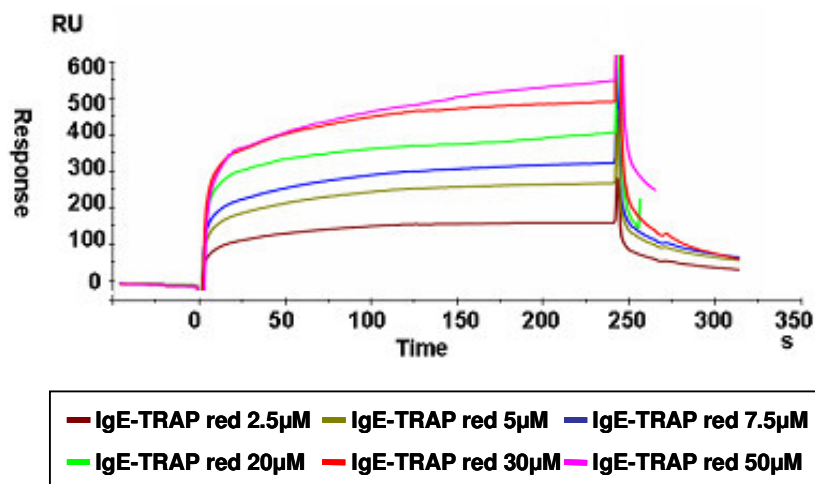


**Figure 14:** Overlapping sensorgrams for IgE interacting with IgE-TRAP red. The interaction were monitored at six IgE-TRAP red concentrations (2.5  $\mu\text{M}$ , 5  $\mu\text{M}$ , 7.5  $\mu\text{M}$ , 20  $\mu\text{M}$ , 30  $\mu\text{M}$ , and 50  $\mu\text{M}$ ) injected in HBS buffer pH 7.4 at 25°C, at flow rate of 20  $\mu\text{L}/\text{min}$ .

Analyte Concentration IgE-TRAP red	Association rate ( $\text{M}^{-1} \text{ s}^{-1}$ ) $K_{a1}$	Dissociation rate ( $\text{s}^{-1}$ ) $K_{d1}$	Association rate ( $\text{M}^{-1} \text{ s}^{-1}$ ) $K_{a2}$	Dissociation rate ( $\text{s}^{-1}$ ) $K_{d2}$
2.5 $\mu\text{M}$	$1.40 \times 10^4$	$7.25 \times 10^{-1}$	$3.53 \times 10^2$	$1.88 \times 10^{-2}$
5 $\mu\text{M}$	$1.92 \times 10^4$	$6.29 \times 10^{-1}$	$3.69 \times 10^2$	$1.45 \times 10^{-2}$
7.5 $\mu\text{M}$	$7.02 \times 10^4$	$0.18 \times 10^{-1}$	$2.95 \times 10^2$	$1.26 \times 10^{-2}$
20 $\mu\text{M}$	$2.44 \times 10^4$	$2.12 \times 10^{-1}$	$3.31 \times 10^2$	$6.73 \times 10^{-3}$
30 $\mu\text{M}$	$6.20 \times 10^4$	$4.18 \times 10^{-1}$	$2.20 \times 10^2$	$8.18 \times 10^{-3}$
50 $\mu\text{M}$	$7.99 \times 10^3$	$4.96 \times 10^{-2}$	$1.58 \times 10^2$	$2.55 \times 10^{-3}$
MEAN	$3.30 \times 10^4$	$6.43 \times 10^{-1}$	$2.87 \times 10^2$	$1.05 \times 10^{-2}$
	$KD_1 = 19 \times 10^{-6} \text{ M}$		$KD_2 = 37 \times 10^{-6} \text{ M}$	

**Table VI:** Table of kinetic and thermodynamic constants for the binding of IgE-TRAP red to IgE extrapolated to the equilibrium affinity measurements by SPR. All data fit optimally with a biphasic association and dissociation.

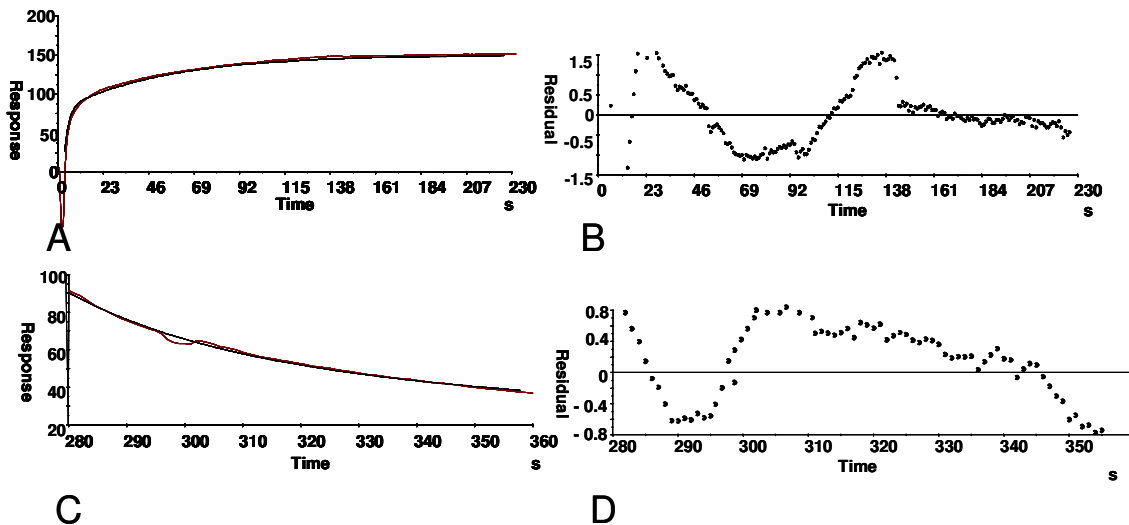


**Figure 15:** Analysis of SPR data for binding IgE-TRAP red at 2.5  $\mu\text{M}$  to immobilized IgE. The fitted lines (black) are overlaid with the experimental curves (brown) for the association (A) and dissociation phases (B). The corresponding residual plots are shown (C and D, respectively). Curves from all other experiments were similarly fitted.

By data fitting using a non-linear regression and Scatchard analysis, reported in Fig.16, a  $K_D$  of  $6.2 \pm 0.7 \mu\text{M}$  was extrapolated as a global apparent binding constant.

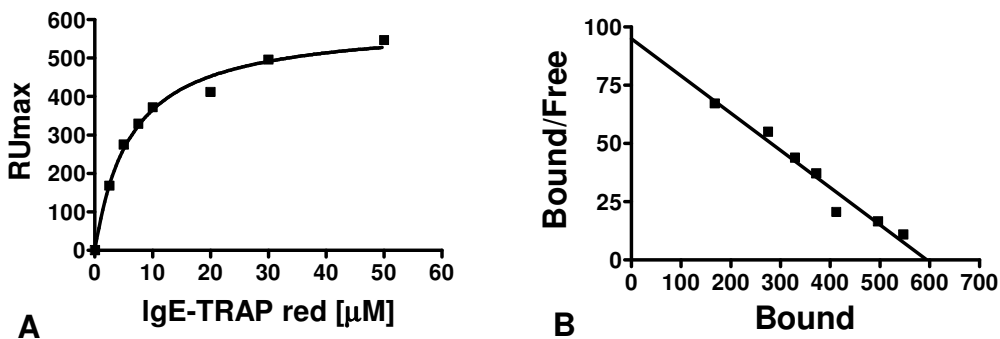


**Figure 16:** A plot of the RUmax vs the concentration of the protein fitted by a non-linear regression (A) and the corresponding Scatchard analysis (B).

Importantly, for both the IgE-TRAP polypeptides, the global affinity constant ( $K_D$ ) is lower than the two separate equilibrium constants, supporting the existence of a two phase event and suggesting a cooperative mechanism between the two sites. However the macroscopic affinity constants are much lower than the overall receptor affinity ( $K_D = 10^{-9} - 10^{-10} \text{M}$ ). Interestingly, the value of affinity for IgE of the IgE-TRAP red is 2.5 times stronger than the cyclized variant and this increase of affinity is arises from the absence of the disulfide bridge between Cys151 and the newly created Cys162. This result, is probably due to a greater conformational flexibility of the polypeptide than can more easily adapt to the immunoglobulin surface.

Strictly, the stronger affinity of the reduced molecule in solution is also reflected by the two separate  $K_D$  for the two binding sites. Indeed,  $K_{D1}$  and  $K_{D2}$  for the two

molecules are 19  $\mu\text{M}$  and 37  $\mu\text{M}$  (reduced form) versus 65  $\mu\text{M}$  and 60  $\mu\text{M}$  (oxidized form), respectively. On the basis of these data, the binding difference between the two polypeptides could essentially be ascribed to an improved recognition of the first site which is dependent on the presence/absence of the disulfide bridge and which seemingly corresponds to the peptide 1<sup>st</sup> Loop that resume partially 2 site also. Correspondingly, also the KD2 of IgE-TRAP red is lower (1.5 times) than that of oxidized form (37  $\mu\text{M}$  compared with 60  $\mu\text{M}$ ) thus suggesting a better recognition also for site 2. Overall, results indicate that the reduced form shares many of the bound structural features or that it must overcome a lower energy barrier to adopt a binding conformation. In order to improve the affinity of the designed polypeptide and to understand a possible correlation between structure and activity, a set of peptidic fragments of the IgE-TRAP was prepared and studied by SPR. Sub-domains reproducing the two separate binding sites, previously reported in table IV, were designed, chemically synthesized and characterized. Remarkably, only the so-called 1<sup>st</sup> Loop bound in a dose-dependent way to the IgE (Fig.17) and we again found, on the basis of fitting residuals, that an optimal fit was obtained with bi-phasic curves (Fig.18). For the 1<sup>st</sup> Loop, the rate constants  $k_{d1}$  ( $8.73 \pm 0.38 \times 10^{-1} \text{ s}^{-1}$ ),  $k_{d2}$  ( $2.54 \pm 0.29 \times 10^{-2} \text{ s}^{-1}$ ),  $k_{a1}$  ( $1.35 \pm 0.17 \times 10^4 \text{ M}^{-1} \text{ s}^{-1}$ ) and  $k_{a2}$  ( $1.33 \pm 0.17 \times 10^2 \text{ M}^{-1} \text{ s}^{-1}$ ) were extrapolated by averaging data from all experiments (table VII) and  $\text{KD1} = 65 \pm 0.2 \mu\text{M}$  and  $\text{KD2} = 19 \pm 0.2 \times 10^{-5} \text{ M}$  were calculated as the two equilibrium constants.

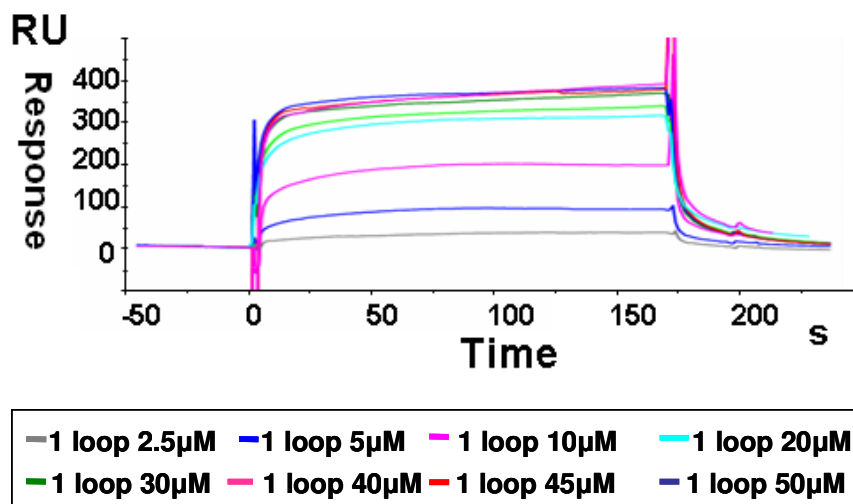


**Figure 17:** Overlapping sensorgrams for IgE interacting with 1<sup>st</sup> Loop. Interactions were monitored at eight concentrations (2.5  $\mu\text{M}$ , 5  $\mu\text{M}$ , 10  $\mu\text{M}$ , 20  $\mu\text{M}$ , 30  $\mu\text{M}$ , 40  $\mu\text{M}$ , 45  $\mu\text{M}$ , 50  $\mu\text{M}$ ) injected in HBS buffer pH 7.4 at 25°C, at flow rate of 20  $\mu\text{L}/\text{min}$ .

Analyte Concentration 1 <sup>st</sup> LOOP	Association rate (M <sup>-1</sup> s <sup>-1</sup> ) K <sub>a1</sub>	Dissociated rate (s <sup>-1</sup> ) K <sub>d1</sub>	Association rate (M <sup>-1</sup> s <sup>-1</sup> ) K <sub>a2</sub>	Dissociated rate (s <sup>-1</sup> ) K <sub>d2</sub>
2.5 μM	2.25 x 10 <sup>4</sup>	0.23 x 10 <sup>-1</sup>	2.26 x 10 <sup>2</sup>	1.82 x 10 <sup>-2</sup>
10 μM	1.31 x 10 <sup>4</sup>	0.23 x 10 <sup>-1</sup>	2.21 x 10 <sup>2</sup>	3.63 x 10 <sup>-2</sup>
20 μM	7.19 x 10 <sup>4</sup>	9.22 x 10 <sup>-1</sup>	1.18 x 10 <sup>2</sup>	3.94 x 10 <sup>-2</sup>
30 μM	1.21 x 10 <sup>4</sup>	3.48 x 10 <sup>-1</sup>	1.20 x 10 <sup>2</sup>	2.59 x 10 <sup>-2</sup>
40 μM	1.20 x 10 <sup>4</sup>	4.31 x 10 <sup>-1</sup>	1.02 x 10 <sup>2</sup>	2.79 x 10 <sup>-2</sup>
45 μM	9.18 x 10 <sup>3</sup>	5.33 x 10 <sup>-1</sup>	4.31 x 10 <sup>2</sup>	1.91 x 10 <sup>-2</sup>
50 μM	1.81 x 10 <sup>4</sup>	1.97 x 10 <sup>-2</sup>	1.03 x 10 <sup>2</sup>	1.14 x 10 <sup>-2</sup>
MEAN	1.35 x 10 <sup>4</sup>	8.73 x 10 <sup>-1</sup>	1.33 x 10 <sup>2</sup>	2.54 x 10 <sup>-2</sup>
	KD1= 65 x 10 <sup>-6</sup> M		KD2= 19 x 10 <sup>-5</sup> M	

**Table VII:** Table of kinetic and thermodynamic constants for the binding of 1<sup>st</sup>Loop to IgE extrapolated by the equilibrium affinity measurements by SPR. All data fit optimally with a biphasic association and dissociation.

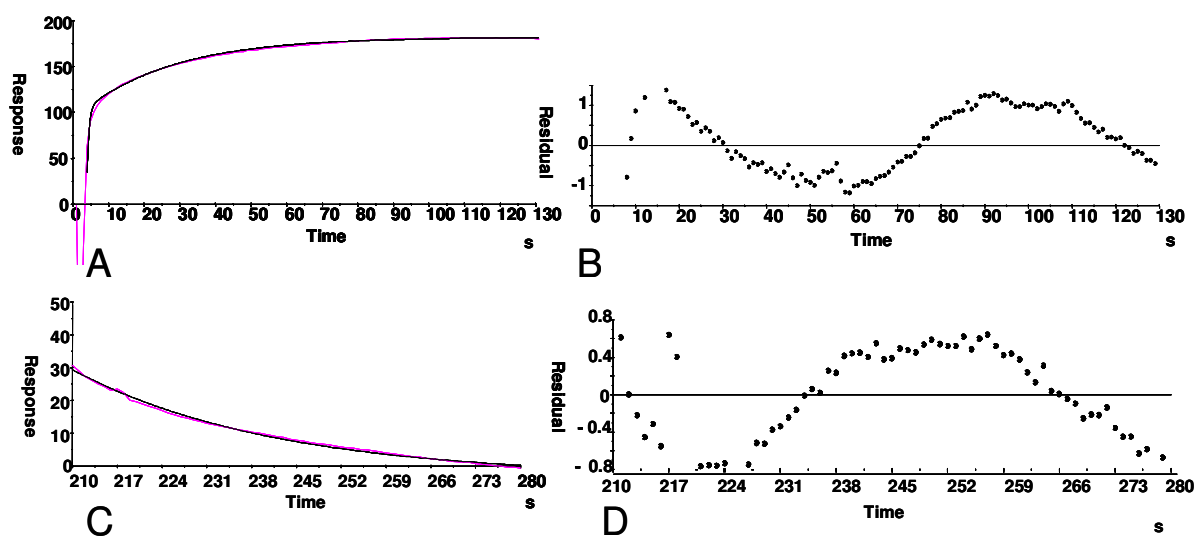


**Figure 18:** Analysis of SPR data for binding 1<sup>st</sup> Loop 10 μM to immobilized IgE. The fitted lines (black) are overlaid with the experimental curves (fuchsia) for association phase (A) and dissociation phase (B) with corresponding residual plots are shown (C and D, respectively).

To obtain the macroscopic KD for the binding of this peptide, we again carried out a non-linear regression and Scatchard analysis of RUmax versus concentration data (Fig.19). A KD of  $19 \pm 4 \mu\text{M}$  was extrapolated as a global apparent binding constant, which also in this case, was lower than the two single KD. This result confirms that a biphasic event occurs also for the binding of the 1<sup>st</sup> Loop to IgE and that a cooperative mechanism underlines the binding.

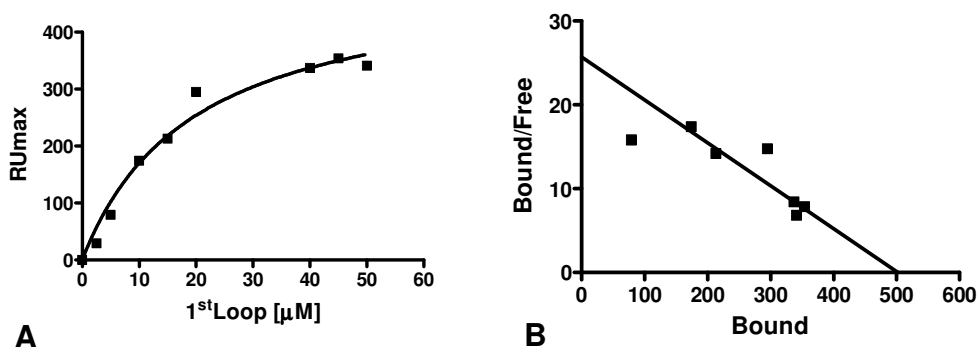


**Figure 19:** Plot of the RUmax vs the concentration of the protein fitted by a non-linear regression (A) and the corresponding Scatchard analysis (B).

We next analyzed the synthetic 2<sup>nd</sup> Loop, and found that both the reduced and oxidized variants showed no binding to immobilized IgE. This outcome, though unexpected on the basis of the different activity of the oxidized and reduced IgE-TRAP, can be explained by a very poor association rate of this peptide for IgE, which instead is greatly enhanced in the presence of the first loop. The 1<sup>st</sup> Loop therefore presumably acts as an anchor, favouring the subsequent interaction of the 2<sup>nd</sup> Loop. On the basis of the binding affinities between the different peptides (Summarized in the following table VIII), we can conclude that:

The overall affinity of the originally designed peptide IgE-TRAP ox, about  $16 \mu\text{M}$  is higher than the respective KDs for the two distinct binding sites, which are very similar each other.

Reduction of the disulfide bridge produces a 3-fold increase of affinity, mostly due to an effect on the site 1 (the KD1 decreases from  $65 \mu\text{M}$  to  $19 \mu\text{M}$ ) and a partial effect on the site 2. This effect can be explained by a contribution from the 2<sup>nd</sup> Loop, which, when not cyclized can probably more rapidly adopt a conformation useful for binding. However, the 2<sup>nd</sup> Loop, when separated from the 1<sup>st</sup> Loop is ineffective probably because of a very poor association rate. The cooperative effect of the 2<sup>nd</sup> Loop is higher on site 1 than on site 2, indeed when it is removed the KD1 is restored ( $65 \mu\text{M}$ ); at the same time, the presence of the 2<sup>nd</sup> Loop (in both the reduced or the cyclized form) seems to increase the recognition on site 2, as a 3-4 fold decreased of affinity is measured when it is absent.

Molecule	KD1( $\mu\text{M}$ )	KD2( $\mu\text{M}$ )	KD( $\mu\text{M}$ )	Fold affinity increase relative to IgE-TRAPox
IgE-TRAP ox	65	60	16	--
IgE-TRAP red	19	37	6.2	3
1 <sup>st</sup> Loop	65	190	19	--
2 <sup>nd</sup> Loop	--	--	--	--

**Table VIII:** Summary of binding affinities between the different molecules and immobilized IgE, as obtained by SPR.

We next investigated the separated effects of 1<sup>st</sup> miniLoop; 2<sup>nd</sup> miniLoop and the so-called Peptide S (table IV). Remarkably, the 1<sup>st</sup> miniLoop and Peptide S were incapable of binding to IgE while the 2<sup>nd</sup> miniLoop, assayed at concentration up to 75  $\mu\text{M}$  (at higher concentration it was insoluble), bound very weakly the immobilized immunoglobulins (Fig. 20-21-23 and table IX). As shown, the binding was dose-dependent, but we only observed a linear dependence between the two variables without any saturation up to 75  $\mu\text{M}$ . This outcome confirmed the very weak interaction ( $KD = 8.3 \pm 0.5 \times 10^{-4}$  M) of this fragment.

The data obtained with 1<sup>st</sup> miniLoop; 2<sup>nd</sup> miniLoop clearly show that a high cooperation occurs between these two peptide fragments when they are covalently interconnected, while they essentially appear inactive when assayed separately.

Altogether, the comparative analyses of binding affinities of this set of peptides derived from the Fc $\epsilon$ RI recognition site, indicates that, despite the relative low affinity (all in the  $\mu\text{M}$  range), a strong cooperativity occurs between the different peptide blocks present at the interface with the immunoglobulin.

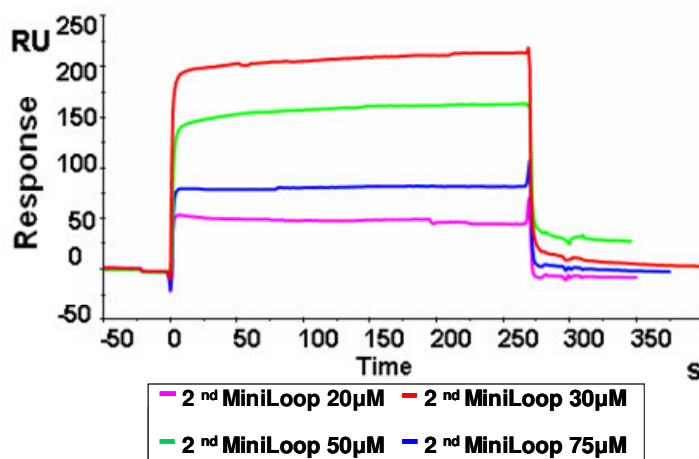


**Figure 20:** Overlapping sensorgrams for the interaction of immobilized IgE with 2<sup>nd</sup> miniLoop. The interaction was monitored at four concentrations (20  $\mu\text{M}$ , 30  $\mu\text{M}$ , 50  $\mu\text{M}$ , 75  $\mu\text{M}$ ) injected in HBS buffer pH 7.4 at 25°C, at a flow rate of 20  $\mu\text{L}/\text{min}$ . According to the hypothesis that 2<sup>nd</sup> miniLoop reproduced only one site of the  $\alpha\text{Fc}\epsilon\text{RI}$ , binding and dissociation curves fit better with a monophasic model, assuming a 1:1 stoichiometry.

Analyte Concentration 2 <sup>nd</sup> miniLoop	Association rate (M <sup>-1</sup> s <sup>-1</sup> ) K <sub>a</sub>	Dissociated rate (s <sup>-1</sup> ) K <sub>d</sub>
20 μM	2.47 x 10 <sup>2</sup>	5.47 x 10 <sup>-1</sup>
30 μM	2.16 x 10 <sup>3</sup>	3.87 x 10 <sup>-2</sup>
50 μM	3.38 x 10 <sup>2</sup>	3.85 x 10 <sup>-3</sup>
75 μM	1.18 x 10 <sup>2</sup>	2.07 x 10 <sup>-2</sup>
Mean	K <sub>D</sub> = 8.3 x 10 <sup>-4</sup>	

**Table IX:** Table of kinetic and thermodynamic constants for the binding of 2<sup>nd</sup> miniLoop to IgE extrapolated by the equilibrium affinity measurements by SPR.

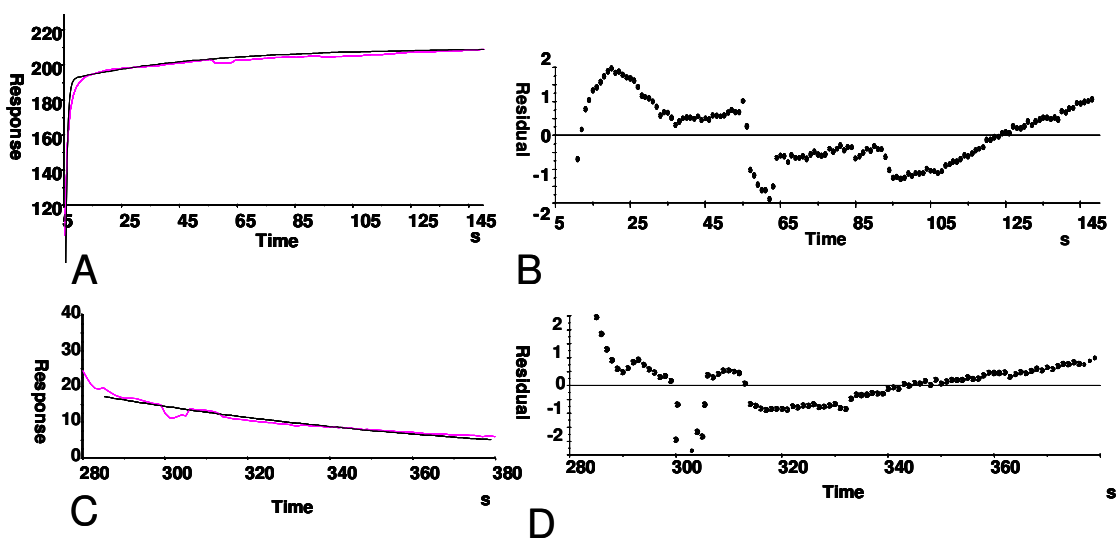


**Figure 21:** Analysis of SPR data for binding 2<sup>nd</sup> miniLoop to immobilized IgE at 20 μM. The fitted lines (black) are overlaid with the experimental curves (fuchsia) for association phase (A) and dissociation phase (B), corresponding residual plots are shown (C and D, respectively). Data fit optimally with a single phase association and dissociation.

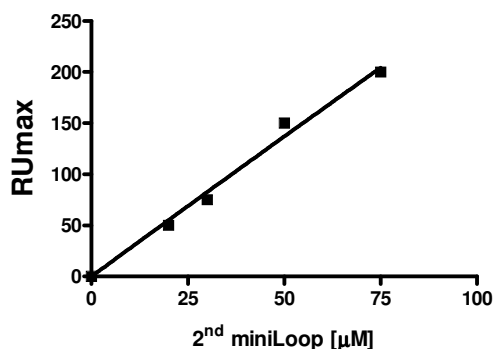


**Figure 22:** Plot of RU<sub>max</sub> vs concentration for the binding of 2<sup>nd</sup> miniLoop to the Immobilized IgE. Data points were fitted with a non linear regression algorithm. The binding was dose-dependent, but not saturable within this concentrations range.

## II.4.1.4 Selectivity affinity measurements between Immunoglobulins–receptor mimicking polypeptides by SPR assay

The specificity of the designed peptides for Immunoglobulins E was tested again by SPR. For this purpose, IgG and IgA were chosen as controls, since they represent the most abundant immunoglobulins circulating within plasma and show the highest structure similarity to IgE. A multiple alignment between IgE, IgG, IgM and IgA is reported in the following Fig.23.

```

CLUSTAL W (1.82) multiple sequence alignment

sp|P01876|IGHA1_HUMAN      CPVPSTPPTPSPSTPPTP-----
tr|Q9BU10|IGHM_HUMAN      PVIAELPPKVSVFVPPRDGFFGNPRKSKLICQATGFSPRQIQVSWLREGK
sp|P01857|IGHG1_HUMAN      EPKSCDKHTCPPCPA-----
tr|Q6P6C4|IGHG2_HUMAN      ERKCCVECPPCP-----
sp|P01854|IGHE_HUMAN       CADSNPRGVS-----

                                334

sp|P01876|IGHA1_HUMAN      -----
tr|Q9BU10|IGHM_HUMAN      QVGSQVTTDQVQAEAKESGPTTYKVTSTLTIKESDWLSQSMFTCRVDHRG
sp|P01857|IGHG1_HUMAN      -----
tr|Q6P6C4|IGHG2_HUMAN      -----
sp|P01854|IGHE_HUMAN       -----

sp|P01876|IGHA1_HUMAN      -----SPSCCHP-----RLSLHRPALEDLLLGSEANLTCLTIGLRDAS
tr|Q9BU10|IGHM_HUMAN      LTFQQNASSMCPVDQDTAIRVFAIPPSFASIFLTKSTKLTCLVTLDTTYD
sp|P01857|IGHG1_HUMAN      -----PELLGGPS-----VFLFPPKPKDTLMISRTPEVTCVVDVSHED
tr|Q6P6C4|IGHG2_HUMAN      -----APPVAGPS-----VFLFPPKPKDTLMISRTPEVTCVVDVSHED
sp|P01854|IGHE_HUMAN       -----AYLSRPSPFDFLIRKSPITITCLVVDLAFSK
                                .   .:: .   .:** 361 .

sp|P01876|IGHA1_HUMAN      G-VFTFTWTPSSGKSAVQGP--PERDLCCGYSSVSVLPGCAEPWNHGKFTFT
tr|Q9BU10|IGHM_HUMAN      S-VTISWTRQNGEAVKTHTNISESHPNATFSAVGEASICEDDWNSSGERFT
sp|P01857|IGHG1_HUMAN      PEVKFNWYVDGVEVHNAKTKPREEQYNSTYRVVSVLTVLHQDWLNGKEYK
tr|Q6P6C4|IGHG2_HUMAN      PEVQFNWYVDGVEVHNAKTKPREEQFNSTFRVSVLTVVHQDWLNGKEYK
sp|P01854|IGHE_HUMAN       GTVNLWTSRASGKPNHSTRKEEKQRNGTLTVTSTLTPVGTDRWIEGETYQ
                                *  .:* . : . * 392 . . . *  ** :

sp|P01876|IGHA1_HUMAN      CTAAYPESKTPLTATLS--KSGNTFRPEVHLLPPPSEELALNELVTLTCL
tr|Q9BU10|IGHM_HUMAN      CTVTHTDLPSPKQTI SRPKGVALHRPDVYLLPPAREQLNLRESATITCL
sp|P01857|IGHG1_HUMAN      CKVSNKALPAPIEKTISKAKG-QPREPQVYTLPPSRDELTKNQVS-LTCL
tr|Q6P6C4|IGHG2_HUMAN      CKVSNKGLPAPIEKTISKTKG-QPREPQVYTLPPSRDEEMTKNQVS-LTCL
sp|P01854|IGHE_HUMAN       CRVTHPHLPRALMRSTTKTSG-PRAAPEVYAFATP-EWPGSRDKRTLACL
                                *  .: 424 . : : : . . *:*: . . . : . : : **

```

**Figure 23:** Multiple alignment of the human heavy chains of IgA, IgM, IgG1, IgG2 and IgE. Highlighted are the region of complementarity with the IgE receptor. Alignments were performed using BLAST on the Expasy server (<http://www.expasy.org/cgi-bin/blast.pl>). Numbers in red refer to human IgE numbering. The highest regions of similarity are between IgGs and IgE, whereas the sequences of IgM and IgA are highly divergent throughout this sequences.

IgG and IgA were efficiently immobilized on the CM5 sensor chips, following the same procedure utilized for IgE, achieving a similar extent of immobilization (about 50000 RU).

All active peptides were then injected on the sensor chip at fixed concentrations. As can be seen, IgE-TRAP ox (30  $\mu$ M), 1<sup>st</sup> loop (50  $\mu$ M) and 2<sup>nd</sup> miniLoop (25  $\mu$ M) were tested and, as expected, no binding was detected on IgG and IgA (Fig.24 A-B-C). This is a result suggestive of high specificity of the designed peptides for binding E-type antibodies

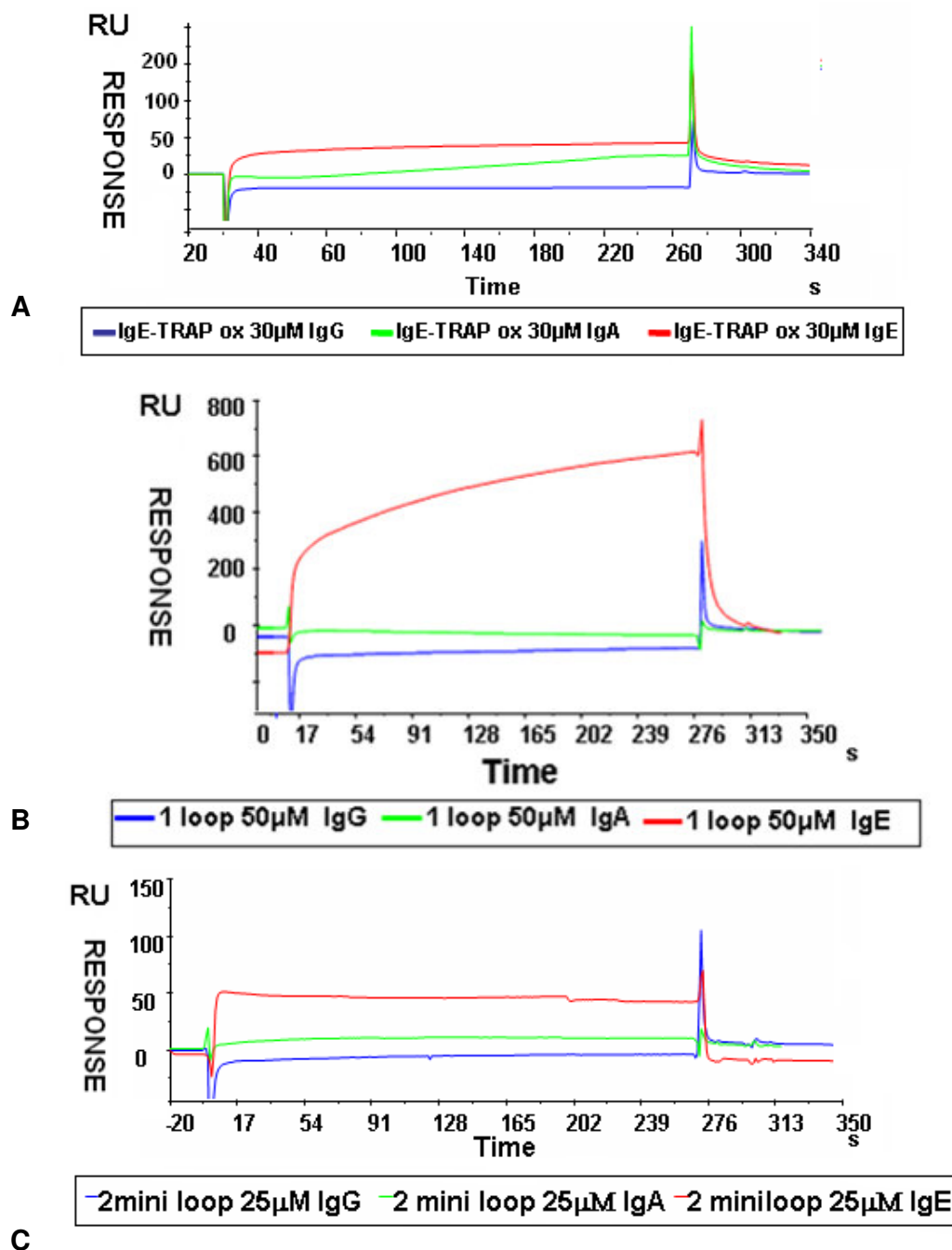


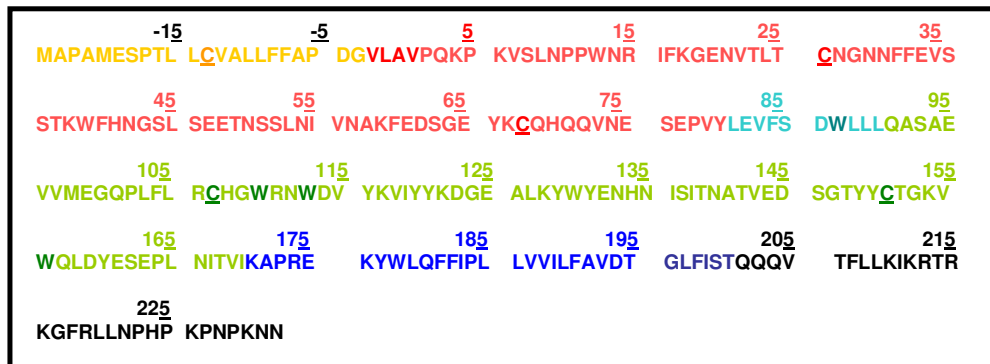
**Figure 24:** SPR binding assay to IgE, IgG and IgA. **A)** Sensorgrams of IgE-TRAPox at 30  $\mu$ M; **B)** Sensorgrams of 1<sup>st</sup> Loop at 50  $\mu$ M; **C)** Sensorgrams of 2<sup>nd</sup> miniLoop at 25  $\mu$ M. No interaction was detected for three peptides with IgG and IgA.

## II.4.2 Expression of human FcεRI αchain as recombinant protein

The expression of the extra-cellular portion of the human FcεRI alpha subunit in alternative systems has been already described, including the expression in insect cells [16], bacteria [17-19], yeast [20] and mammalian cells [21]. The reported expression in bacteria present several problems associated with the refolding of the protein, the yield and overall activity. Nevertheless, in order to try to obtain large amounts of αFcεRI to be evaluated as an optimal soluble antagonist of the circulating IgE and to have a source of protein for the set up of assays to be used in the screening of inhibitors, *E.coli* prokaryotic strains has been identified as an easy, quick and economic expression system. As outlined in the Introduction, all binding residues are located in the D2 domain and the linker between the D1 and the D2 domain, however in a first attempt of stabilizing the entire receptor structure, the preparation of the human full length FcεRI alpha subunit (Fig.24A) and the D1-D2 domain from ECD were pursued (Fig. 24B). Subsequently the D2 domain from ECD was chosen as the final target protein (Fig. 24B).

C-TERMINALE	DOMINIO D1	DOMINIO D2	SEGMENTO TRANSMEMBRANARIO	N-TERMINALE	αFcεRI
1-22	23-110	111-205	206-226	226-257	[1-257]

A



B

**Figure 24:** **A)** Schematic representation of the human full-length FcεRI receptor α-chain [1-257]. **B)** Amino acid sequence of the receptor α-chain, positively numerated beginning from EDC (extra-cellular domain). The N-terminal part is yellow; the D1 domain is in red; the linker between D1-D2 is sky blue; the D2 domain is green, the transmembrane part is blue and the C-terminal part in black. The 5 cysteines are underscored: Cys13 is free instead Cys26-Cys68 and Cys107-Cys151 are involved in two disulfide bridges within the two distinct Ig-like domains.

### II.4.2.1 Expression and purification of full length hFcεRI αchain

The full-length (FL) α-chain (residues 1-257) was amplified by PCR from the cDNA of the human αFcεRI using suitable primers, allowing its cloning in pET and pGEX expression vectors. The FL α-chain protein was cloned and expressed both cytoplasmatic and periplasmatic recombinant protein. The addition of "tags" during the cloning is a successful and useful method to

simplify the purification process of recombinant proteins. Therefore, the optimal expression conditions (vector, *E.coli* strain, time, temperature and inducing agent concentration) were selected for each recombinant protein and are reported in table X. Each recombinant protein was purified according to the specific tag properties.

	vector	N-terminal TAG	<i>E.coli</i> strain	Optimal Expression conditions
Cytoplasmatic expression	pETM11	His6x	BI21 (DE3)	0.2mM IPTG 16h 22°C
	pGEX6P	GST	BI21 (DE3)trxB	0.1mM IPTG 16h 22°C
	pETM40	MBP	BI21 (DE3)	0.1mM IPTG 16h 22°C
Periplasmatic expression	pET22b	His6x	Origami (DE3)	0.2mM IPTG 16h 22°C
	pEM50	Dsb-His6x	BI21 (DE3)	0.5mM IPTG 16h 22°C

**TABLE X:** A summary of the expression conditions attempted to try to obtain the recombinant  $\alpha$ -chain of the IgE receptor.

One of the most commonly used tag consists of six consecutive histidine residues (His6x) added to either the N- or C-terminal part of the protein of interest.

The purification of His6x-tagged fusion proteins is facilitated by the immobilized metal affinity chromatography (IMAC), a powerful and versatile system.

The His6x  $\alpha$ -chain FL (Theoretical M.W. 32708.2 Da) is a protein very rich in hydrophobic aminoacids and contains 5 cysteines. This protein was soluble in 30 mM Tris-HCl, 500 mM NaCl, 1 mM DTT and 6 M urea pH 8.0. The total cell protein fraction, the soluble fraction (supernatant of cell lysate) and the affinity purified fraction were analyzed by SDS-PAGE (Fig.25), observing protein bands of the expected size. The purified protein was thus dialyzed gradually decreasing the urea concentration to 2 M. Further attempts to reduce the urea concentration were unsuccessful because of immediate precipitation of the protein. The final product in 2 M urea, obtained with about 60% purity was again submitted to a step of anionic exchange chromatography, but the material, under these conditions (30 mM Tris-HCl, 150 mM NaCl, 1mM DTT and 2 M urea pH 8.0), though quite pure, was not active and unable to recognize IgE in ELISA binding assay.

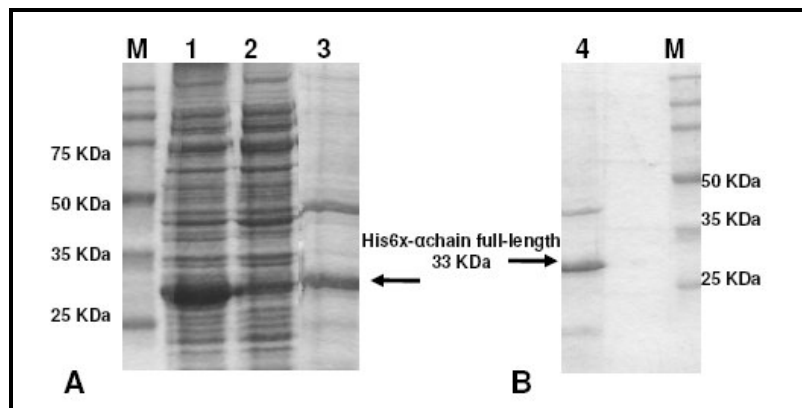


**Figure 25:** 10% SDS-PAGE analysis: **A)** His-Trap purification of the His6x- $\alpha$ -chain FL receptor: lane M, Perfect Protein Marker 15-150 KDa (Novagen); lane 1, total fraction; lane 2, soluble fraction; lane 3, purified fraction; **B)** a protein sample after Mono Q purification (lane 4).

To improve solubility, the same protein was expressed as a recombinant protein with GST (Glutathione-S-Transferase) and with the MBP (Maltose Binding Protein) fusion proteins. The GST- $\alpha$ -chain FL (Theoretical M.W 56332.9 Da), purified in batch using a GST-trap resin, and the MBP- $\alpha$ -chain FL receptor (Theoretical M.W 72533.2 Da), purified in batch using an amylose resin, were soluble in 30 mM Tris-HCl, 150 mM NaCl pH 8.0 buffer, without added urea. For both constructs, the total cell protein fraction, the soluble fraction (supernatant of cell lysate) and purified fractions were analyzed by SDS-PAGE (Fig.26). The yield achieved for the two recombinant proteins was different. Higher expression levels were obtained for MBP than for the GST-fused protein. From a 50 mL bacterial culture, 2 mg of MBP- $\alpha$ -chain FL receptor were obtained, which was about 3-fold more than the GST- $\alpha$ -chain FL receptor. However, in both cases, after digestion with the specific proteases (TEV for the MBP-protein and PreScission protease for the GST-fused), the protein resulted largely insoluble. Importantly, both fusion proteins, resulted as being incorrectly folded, as demonstrated by the lack of binding to IgE in ELISA as well as SPR assays.

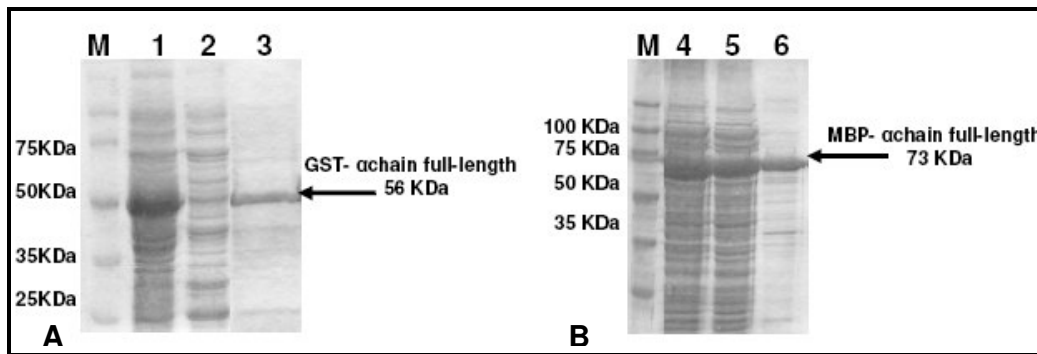


**Figure 26:** **A)** 12% SDS-PAGE analysis of the GST- $\alpha$ -chain FL receptor purification: lane M, Perfect Protein Marker 15-150 KDa (Novagen); lane 1, total fraction; lane 2, soluble fraction; lane 3, purified fraction under reducing condition; **B)** 15% SDS-PAGE analysis of the MBP- $\alpha$ -chain FL receptor fraction during the purification on amylose resin. Lane 4, total fraction; lane 5, soluble fraction; lane 6, purified fraction under reducing condition. The tag-fused proteins were recovered with a purity higher than 85%, but resulted inactive in the binding assay.

A further attempt to obtain a correctly folded recombinant protein was made by using periplasmatic expression. Although the levels of periplasmatic expression are lower than in cytoplasm, the slightly oxidizing environment of the periplasmatic space can allow the formation of correctly formed disulfide bonds. Therefore the His6x- $\alpha$ -chain and the Dsb-His6x- $\alpha$ -chain (Dsb, Disulfide bond protein) FL receptor were expressed in the periplasm. The periplasmatic His6x- $\alpha$ -chain and the Dsb-His6x- $\alpha$ -chain proteins (Theoretical M.W. 30660.9 Da and M.W 55963.8 Da, respectively), after purification on a His-trap column, were soluble in 30 mM Tris-HCl, 500 mM NaCl, 1 mM DTT and 4 M urea pH 8.0. Both recombinant proteins were then dialyzed, decreasing the urea concentration slowly, to 1 M and removing the DTT (buffer 30 mM Tris-HCl, 150 mM NaCl, pH 8.0). The periplasmatic FL His6x- $\alpha$ -chain protein was obtained with 90% purity after anion exchange chromatography. The purified fractions were analyzed by SDS-PAGE (Fig.27).

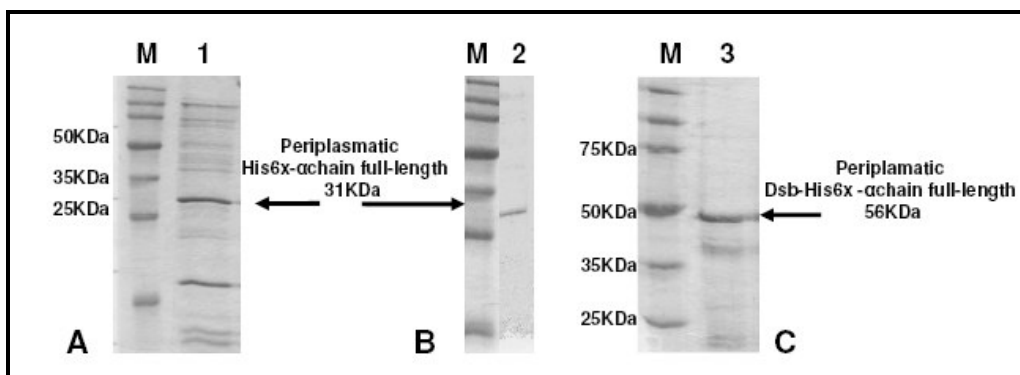


**Figure 27:** 15% SDS-PAGE: **A)** His-trap purification of periplasmic His6x- $\alpha$ chain full-length: lane M, Perfect Protein Marker 15-150 KDa (Novagen); lane 1, purified fraction; **B)** after Mono Q: lane 2, purified fraction; **C)** His-trap purification of periplasmic Dsb-His6x- $\alpha$ chain full-length: lane 3, purified fraction.

The pure proteins, obtained very pure after the two chromatographic steps but in low yield, show no activity in ELISA and SPR binding assays.

From all these experiments, we conclude that the expression and refolding difficulties persists also under the conditions we have explored, as low yields and lack of activity are consistent with previous reports. These difficulties may arise from the presence of the unpaired cysteines and the hydrophobic transmembrane region, therefore the new D1-D2 domain from ECD of hFc $\epsilon$ R1, containing only residues 1-170 (Fig.24B) was designed and produced as a recombinant protein.

#### II.4.2.2 Expression and purification of the D1-D2 domain

The D1-D2 domain was amplified by PCR from the cDNA of the  $\alpha$ -chain of the Fc $\epsilon$ R1 using suitable primers, allowing its cloning in pETM11 vector. The His6x-D1-D2 domain (residues 1-170 from ECD) (Theoretical M.W. 23274.9 Da) recombinant protein was expressed in BI21(DE3) 1 mM IPTG 4h 37°C and was retrieved only from inclusion bodies. From 250 mL pellet, 0.1 g of inclusion bodies were obtained and solubilized in 50 mM Tris-HCl, 100 mM NaCl, 10 mM EDTA, 2 mM DTT, pH 8.0 buffer, containing 6 M guanidine chloride. The residual insoluble fraction was removed by centrifugation while the soluble fraction was analyzed by SDS-PAGE (Fig.28). The denatured protein His6x-D1-D2 domain was used for subsequent refolding experiments. Several refolding strategies [52-56] were tested in order to obtain the recombinant protein with the correct arrangement of disulphide bonds, but they all failed, leading invariably to an inactive, though pure protein. The His6x-D1-D2 domain recombinant protein was stable in 30 mM Tris-HCl, 150 mM NaCl pH 8.0 buffer but SDS-PAGE analysis shows that, under non-reducing conditions, it possess a strong tendency to form aggregate.

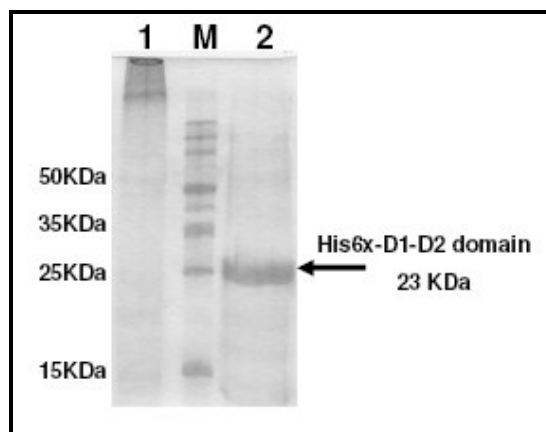


**Figure 28:** 15% SDS-PAGE analysis of the His6x-D1-D2 domain recovered from the inclusion bodies after *E.coli* expression. Lane 1, purified His6x-D1-D2 domain under non reducing conditions; lane M, Perfect Protein Marker 15-150 KDa (Novagen); lane 2, purified His6x-D1-D2 domain under reducing conditions.

Since the expression of the D1-D2 domain as active and soluble recombinant protein was unsuccessful, the expression of D2 domain only was considered.

### II.3.2.3 Expression and purification of D2 domain

D2 domain (residues 84-170 from ECD) was amplified by PCR from the cDNA of the human  $\alpha$ Fc $\epsilon$ RI using suitable primers allowing its cloning in two pET expression vectors. Optimal expression conditions were selected for both recombinant proteins, as reported in table XI.

	<i>Vector</i>	<i>N-terminal TAG</i>	<i>E.Coli strain</i>	<i>Optimal Expression conditions</i>
<i>Cytoplasmatic expression</i>	pETM40	MBP	BI21(DE3)	0.1 mM IPTG 16h 22°C
	pETMA11	His6x	BI21(DE3)trxB	0.2 mM IPTG 16h 22°C

**TABLE XI:** A summary of the optimal expression conditions for the recombinant D2 domain of  $\alpha$ Fc $\epsilon$ RI.

The D2 domain was initially expressed as a recombinant protein with MBP (Maltose Binding Protein) fused at the N-terminal part. The protein, named MBP-D2, was isolated as a soluble and stable product after an affinity step on an amylose derivatized resin in 30 mM Tris-HCl, 150 mM NaCl pH 8.0 buffer. The total cell protein fraction, the soluble fraction (supernatant of cell lysate) of cytoplasmatic fraction and the purified fraction were analyzed by SDS-PAGE (Fig.29). After digestion with TEV protease, the D2 domain alone resulted highly unstable and poorly soluble. However the residual protein in solution was assayed by ELISA and SPR for binding to immobilized IgE, but resulted essentially inactive.

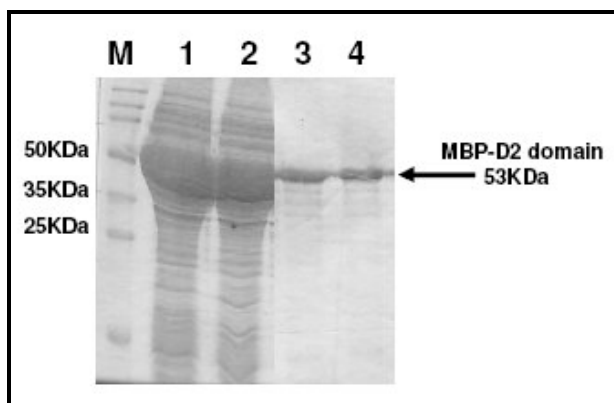


**Figure 29:** 15% SDS-PAGE analysis of MBP-D2 domain purification: lane M, Perfect Protein Marker 15-150 KDa (Novagen); lane 1, total fraction; lane 2, soluble fraction; lanes 3-4, purified fractions under reducing condition.

#### II.4.2.4 Expression, purification and characterization of His6x-D2 domain

##### II.3.2.4a His6x-D2 domain expression and purification

The amino acid sequence His6x-D2 domain expressed is reported in Fig.30:

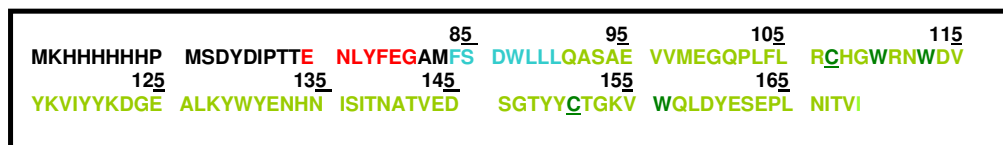


**Figure 30:** Amino acid sequence of N terminal His6x tag (in black); TEV site (in red); linker D1-D2 (in sky blue); D2 domain (in green) C-terminal part. Two cysteines are underscore: Cys107-Cys151 are involved in disulfide bridge to form Ig-like domain.

The His6x-D2 domain (Theoretical M.W. 13548.1 Da), was recovered within the soluble fraction buffered with 30 mM Tris-HCl, 500 mM NaCl and 3 M Urea, pH 8.0. The total cell protein fraction, the soluble fraction (supernatant of cell lysate) and the purified fractions were analyzed by SDS-PAGE to assess purity (Fig.31A). The same fraction was also analyzed by western blot analysis using an anti-His6x antibody conjugated with HRP to assess the protein identity (Fig.31B).

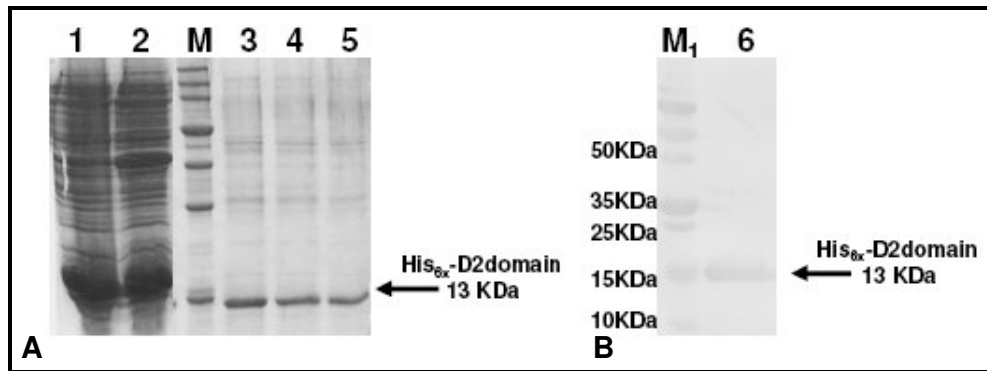


**Figure 31:** **A)** 15% SDS-PAGE analysis of the His<sub>6x</sub>-D2 domain purification. Lane M, Perfect Protein Marker 15-150 KDa (Novagen); lane 1, total fraction; lane 2, soluble fraction; lanes 3-4-5, purified fractions under denaturing condition. **B)** Western blot analysis using an anti-His<sub>6x</sub> antibody HRP-conjugated: lane M<sub>1</sub>. Marker Precision Plus Protein 10-250 KDa (Biorad); lane 6, His<sub>6x</sub>-D2 domain purified fraction. The M.W. is consistent with the protein sequence.

#### II.4.2.4b Refolding of His<sub>6x</sub>-D2 domain

The His<sub>6x</sub>-D2 domain was refolded by gradually removing the urea from the refolding buffer by dialysis. Finally, the protein resulted soluble in 30 mM Tris-HCl, 150 mM NaCl, 2 M urea pH 8.0 buffer. The final step of dialysis was performed at 4°C overnight against 30 mM Tris-HCl, 150 mM NaCl, 5 mM reduced glutathione, 0.5 mM oxidized glutathione at pH 8.0. The precipitate that formed during the refolding procedure was removed by centrifugation and the recovered His<sub>6x</sub>-D2 was analyzed by SDS-PAGE under reducing and non-reducing conditions (Fig.32). The reduced His<sub>6x</sub>-D2 domain under reducing conditions migrated much slower on SDS-PAGE compared to the refolded protein, and this was likely due to the more compact structure of the disulfide bonded protein.

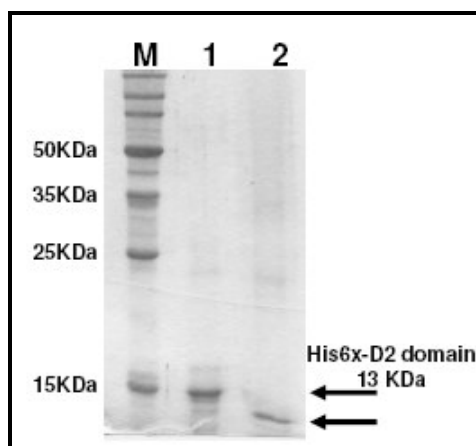


**Figure 32:** 15% SDS-PAGE analysis after refolding procedure: lane M, Perfect Protein Marker 15-150 KDa (Novagen); lane 1, His<sub>6x</sub>-D2 domain under reducing conditions; lane 2, His<sub>6x</sub>-D2 domain under no reducing conditions.

### II.4.2.4c His6x-D2 domain characterization

The formation of the single disulfide bond was assessed by alkylating the protein and verifying cysteine derivatization by mass spectrometry. The reaction was performed using 4-vinylpyridine (4-VP) on the refolded His6x-D2 domain. The protein was unaffected by this reaction, indicating the absence of free thiols. Importantly, LC-MS analysis of the domain under reducing and non-reducing conditions reproducibly indicated the difference of only 2 amu between the two mass values. (Fig.33A and 33B). The resulting value of molecular weight are 13546 amu for reduced His6x-D2 domain and 13542 amu for His6x-D2 domain in agreement with that calculated respectively ( $MW_{\text{exp}}/MW_{\text{theor.}}:13546 \pm 2/13548$  amu and  $MW_{\text{exp}}/MW_{\text{theor.}}:13542 \pm 4/13546$  amu ).

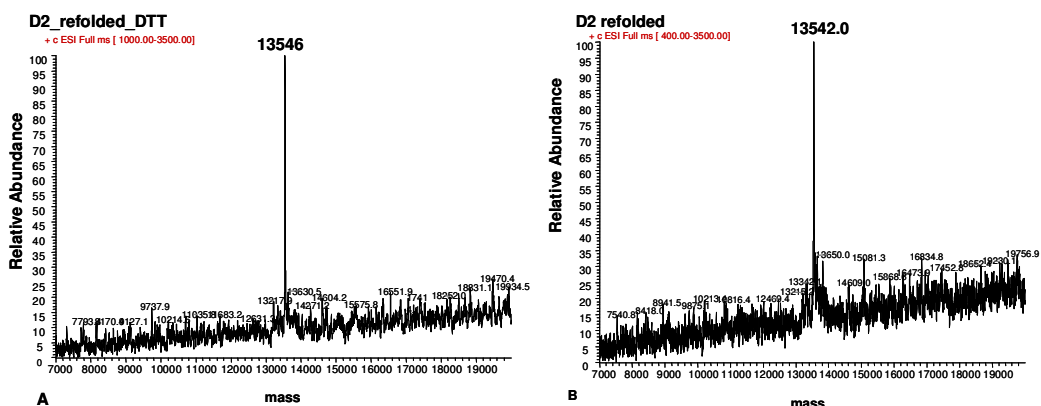


**Figure 33:** **A)** Deconvoluted mass spectrum of the DTT-reduced recombinant His6x-D2 domain and **B)** spectrum of the same protein before reduction.

The His6x-D2 domain was dialyzed over night at 4 °C against 20 mM phosphate pH 8.0 buffer and analysed by CD to assess the protein conformation in solution. The spectrum shown in Fig.34, as expected, showed a predominance of  $\beta$ -sheet structures, with a minimum at 215 nm and a positive band at about 195 nm. CD spectra are reported in molar ellipticity [ $\theta$ ].

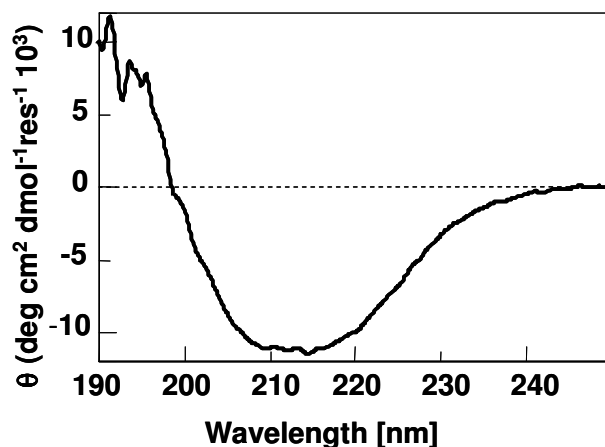


**Figure 34:** CD spectrum of the recombinant refolded His6x-D2 domain. The protein exhibits a spectrum with a large content of  $\beta$ -structures.

All attempts to obtain the D2 domain without the polyhistidine tag using TEV protease, were unsuccessful. Indeed, despite the correct formation of the disulfide bridge, the protein has a very strong tendency to form non covalent oligomers, as demonstrated by gel filtration. The protein analyzed under both reducing and non reducing conditions eluted at a volume consistent with an aggregate of molecular size greater than about 80 kDa (Fig.35), thereby suggesting the occurrence of non covalent oligomers. Addition of different salt concentrations to increase the ionic strength and detergents to disrupt hydrophobic unspecific interactions lead invariably to the same result.

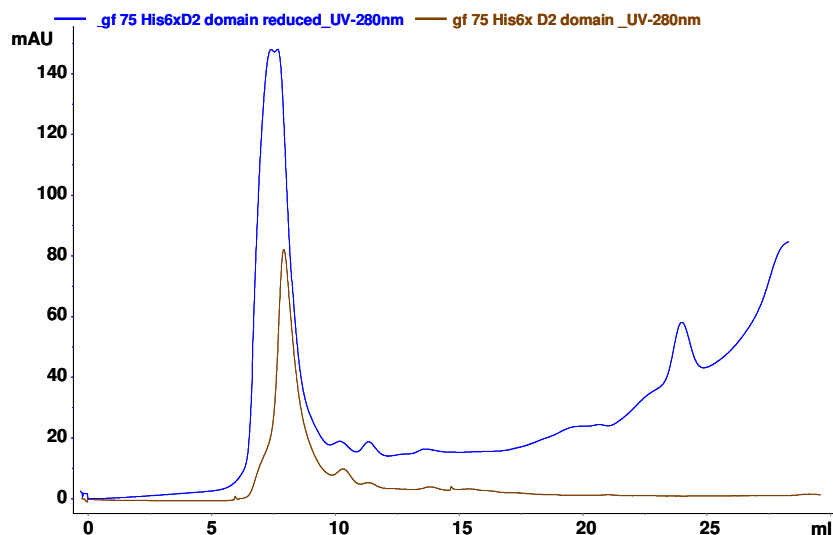


**Figure 35:** Gel filtration analysis on a Superdex75 10/300 GL column of the refolded His6x-D2 domain (brown line) and reduced His6x-D2 domain (blue line). Both proteins were eluted at the void volume, suggesting the presence of large aggregates.

#### II.4.4.5 His6x-D2 domain–Immunoglobulins E binding assay

The refolded His6x-D2 domain, despite its oligomeric form, was tested for binding to IgE by ELISA and SPR assays. In a first ELISA assay, IgE were immobilized at 2  $\mu\text{g/mL}$  (10 nM) on the surface of the microtiter plate and the refolded receptor domain was assayed at concentrations ranging between 0.15  $\mu\text{M}$  to 40  $\mu\text{M}$ . 30 mM Tris-HCl, 150 mM NaCl, pH 8.0 was used as buffer. Detection was achieved using an anti-polyhistidine antibody conjugated to HRP (Methods section II.3.2.18). Data obtained are reported in Fig.36, where a dose-dependent and saturable binding is observable. By data analysis and fitting using a non-linear regression algorithm, a  $K_D$  of  $2.29 \pm 0.06 \mu\text{M}$  was estimated.

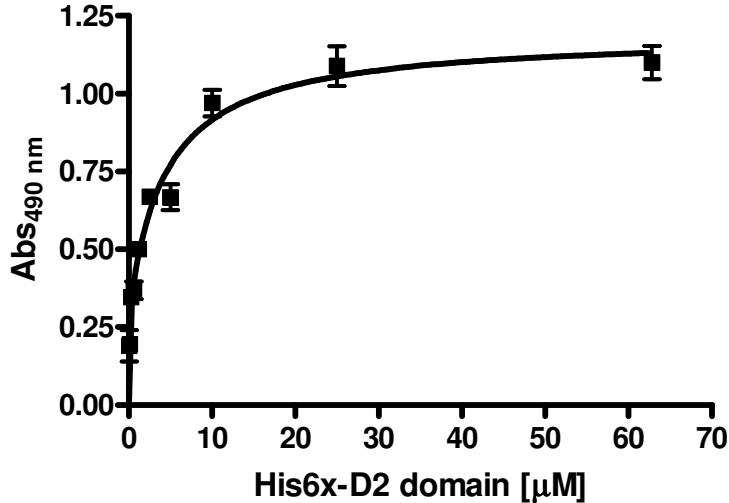


**Figure 36:** Dose-dependent ELISA binding assay between coated IgE (10 nM) and the refolded His6x-D2 domain of the IgE receptor.

The binding was further confirmed by SPR assays. In this instance, solutions of the receptor domain at increasing concentration were injected at 20  $\mu\text{L}/\text{min}$  on the IgE-activated chip. Fig.37 A-E show the recombinant protein bound in a dose-dependent manner to the immobilized IgE.

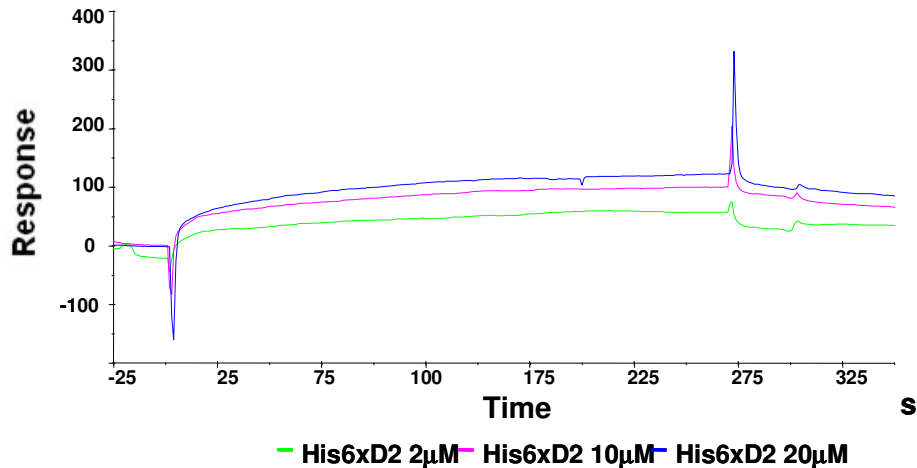


**Figure 37 A:** Overlapping sensorgrams relative to the binding between His6xD2 domain and IgE. Curves refer to the concentration of 2  $\mu\text{M}$ , 10  $\mu\text{M}$  and 20  $\mu\text{M}$ .

The association and dissociation phases of the response curves, as previously shown for the synthetic peptides, were fitted to biphasic models assuming a 1:1 stoichiometry.

The ability of the model to describe the experimental data was evaluated by examination of the residual plots, which were calculated by subtracting the experimental data points from the fitted curve. Also in this case, residual values were considerably small as compared to the monophasic fitting and largely scattered throughout the data points, thus suggesting a better fitting.

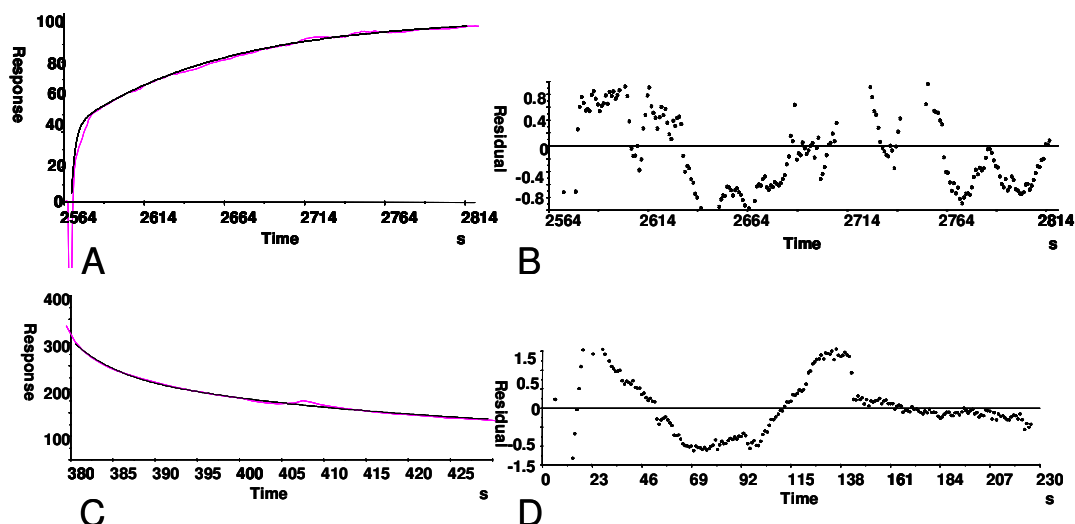


**Figure 37 B-E :** Analysis of SPR data for the binding of His6xD2 domain at a concentration of 10  $\mu\text{M}$  to immobilized IgE. The fitted lines (black) are overlaid with the experimental curves (fuchsia) for the association (B) and dissociation phases (D). The corresponding residual plots are shown (C and E respectively).

The biphasic fitting is characterized by two association rates and two dissociation rates which yield an affinity constant for each phase of the interaction. A summary of association rate and dissociation rate constants obtained by fitting the data, as well as the affinity constants are reported in the following Table XII.

The rate constant  $k_{d1}$  ( $5.82 \pm 0.73 \times 10^{-3} \text{ s}^{-1}$ ),  $k_{d2}$  ( $3.44 \pm 0.19 \times 10^{-1} \text{ s}^{-1}$ ),  $k_{a1}$  ( $6.99 \pm 0.16 \times 10^2 \text{ M}^{-1} \text{ s}^{-1}$ ) and  $k_{a2}$  ( $3.10 \pm 0.32 \times 10^4 \text{ M}^{-1} \text{ s}^{-1}$ ) were extrapolated and obtained by averaging all experiments. The thermodynamic equilibrium constants are:  $KD1 = 8.3 \mu\text{M}$  and  $KD2 = 11.1 \mu\text{M}$ , which are both higher than that obtained by the ELISA assay.

Analyte Concentration His6x-D2 domain	Association rate ( $\text{M}^{-1} \text{ s}^{-1}$ ) $K_{a1}$	Dissociated rate ( $\text{s}^{-1}$ ) $K_{d1}$	Association rate ( $\text{M}^{-1} \text{ s}^{-1}$ ) $K_{a2}$	Dissociated rate ( $\text{s}^{-1}$ ) $K_{d2}$
2 $\mu\text{M}$	$8.91 \times 10^2$	$6.81 \times 10^{-3}$	$1.69 \times 10^4$	$3.02 \times 10^{-1}$
10 $\mu\text{M}$	$1.02 \times 10^3$	$2.44 \times 10^{-4}$	$2.01 \times 10^4$	$9.70 \times 10^{-2}$
20 $\mu\text{M}$	$1.85 \times 10^2$	$1.04 \times 10^{-2}$	$5.59 \times 10^4$	$6.33 \times 10^{-1}$
MEAN	$6.99 \times 10^2$	$5.82 \times 10^{-3}$	$3.10 \times 10^4$	$3.44 \times 10^{-1}$
	<b><math>KD1 = 8.33 \times 10^{-6} \text{ M}</math></b>		<b><math>KD2 = 11.1 \times 10^{-6} \text{ M}</math></b>	

**Table XII:** Kinetic and thermodynamic parameters for association of the D2 domain to immobilized IgE. Data refer to the indicated concentrations. Association and dissociation rate constants were averaged and used to calculate the thermodynamic dissociation constants for the two association sites. All data fit optimally with a biphasic association and dissociation.

To obtain a macroscopic dissociation constant that takes into account both binding sites, we plotted (as for the synthetic peptides) the RUmax for all concentrations explored versus the concentration and then fitting the data by a non-linear regression algorithm followed by a Scatchard analysis (Fig.38A-B). By this approach we could measure a  $K_D$  of  $1.8 \pm 0.9 \mu\text{M}$  that was in very good agreement with that obtained by the ELISA assay. Again, as experienced with the synthetic peptides, the global apparent  $K_D$  was lower (stronger affinity) than that referred to the single constants, confirming the two-site association and the cooperative mechanism between them.

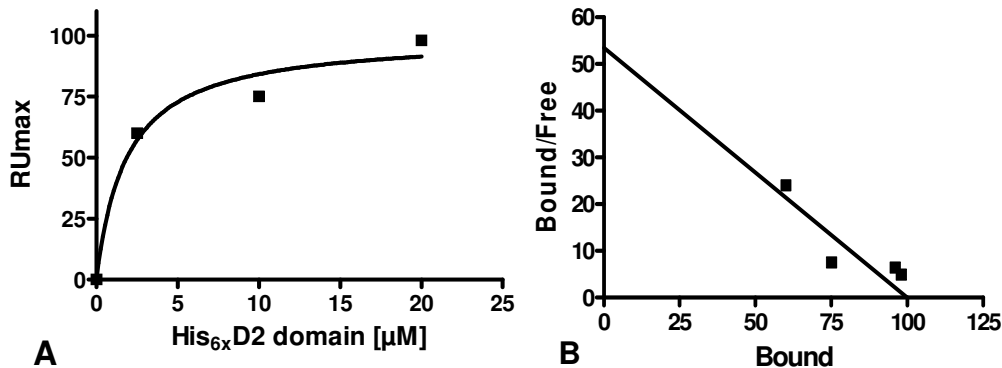


**Figure 38:** Plot of the RUmax vs His<sub>6x</sub>-D2 domain concentration fitted by a non-linear regression (A) and corresponding Scatchard analysis (B).

The His<sub>6x</sub>-D2 recombinant protein shows reduced affinity for IgE compared to the native receptor, exhibiting a  $K_D$  in the very low  $\mu\text{M}$  range. As reported in the literature, the D1 domain is required for optimal binding with the IgE. Although D1 domain is not directly involved in the binding, it structurally contribute to the high affinity maintenance [10]. The linker region between the D1 and D2 (residues 85-89), at the membrane distal portion of the interface, is reported to affect the display of the two domains and the ligand-binding region, therefore could have a critical supportive role in the maintenance of the D1-D2 interface (overall complex organization). In addition, the low affinity displayed by this single domain, could suffer the occurrence of the oligomeric structure leading to a reduced exposure of contact sites. This behaviour could also be attributed to the presence of the polyhistidine tag which is indeed inaccessible to the TEV protease and could therefore contribute to the aggregation. If the protein aggregates to greater extent at the N-terminus, this could also make the linker residues (belonging to the binding site 2) poorly accessible for binding to the immunoglobulin. To try to optimize the binding conditions, the effects of the ionic strength, the presence of detergents and various pH values were evaluated. This screening was carried by ELISA assay using IgE immobilized at  $2 \mu\text{g/mL}$  ( $10 \text{ nM}$ ) and the His<sub>6x</sub>-D2 domain at  $5 \mu\text{M}$ . The binding was carried out using 4 different buffers, reported in Table XIII, which accounted for the indicated conditions. As shown in Fig.39, the binding between IgE and the His<sub>6x</sub>-D2 domain, diluted in Buffer 4, was 1.5 fold higher than that in Buffer 1.

Buffer	
1	Tris-HCl 30mM pH 8.0 NaCl 0.15M
2	Tris-HCl 30mM pH 8.0 NaCl 0.5M
3	Tris-HCl 30mM pH 8.0 Triton 0.02%
4	Bis-Tris 25 mM pH 6.5 NaCl 0.15M

**TABLE XIII:** summary of conditions explored for binding of the receptor D2 domain to IgE.

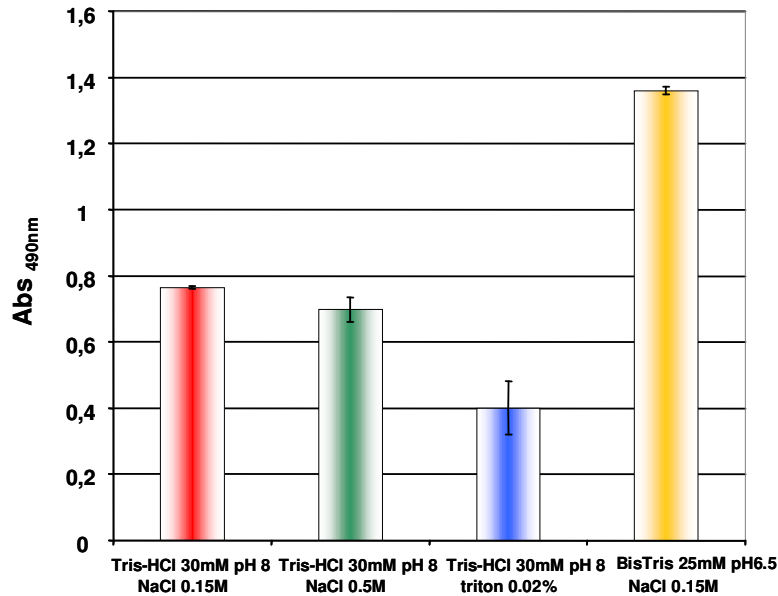
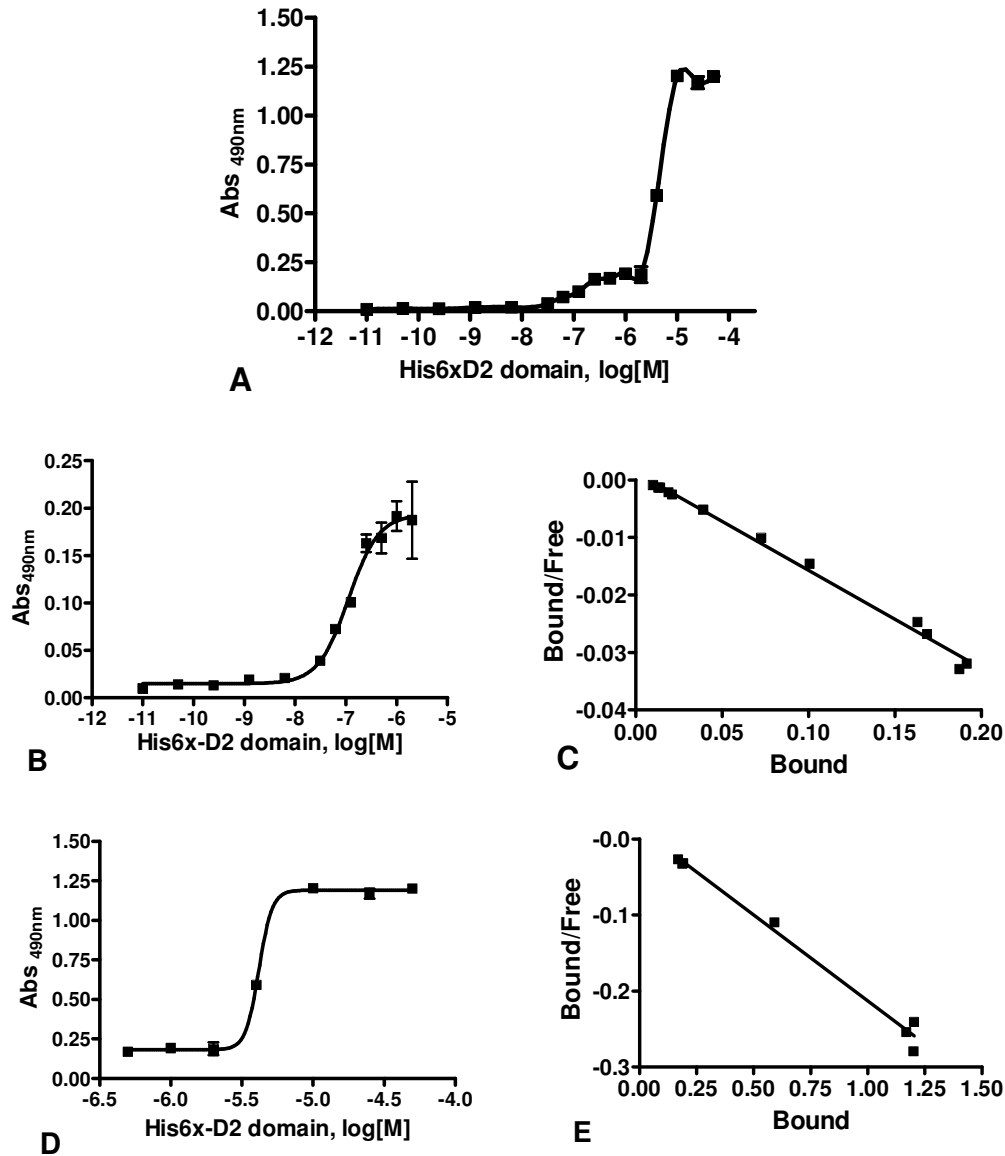


**Figure 39:** ELISA test of binding between the recombinant His6x- D2 domain and IgE to monitor the effects of salts detergents and buffer. As shown the binding seems to be optimal at pH 6.5 in the presence of a low concentration of buffering salt.

On the basis of these results, we have assumed that slightly acidic conditions could influence the N-terminal His6x-tag by introducing positive charges on the histidine side chains. These conditions were utilized in all subsequent binding experiments.

New dose-dependent binding assays were then carried out by ELISA immobilizing IgE at 5 µg/mL (25 nM) and the His6x-D2 domain at progressively increasing concentrations [0.05 - 20 µM] in 25 mM Bis-Tris, 150 mM NaCl pH 6.5 buffer. Analysis of these data by non-linear regression and by Scatchard plot, showed that clearly two independently saturable sites are present (Fig.40 A). One is saturated for concentrations up to about 1 µM (Fig.40 B-C) and has a binding affinity of  $112 \pm 0.04$  nM, while the second (site 2) is saturated only for concentrations between 1 µM and 20 µM and displays a much higher KD  $4.1 \pm 0.06$  µM (Fig.40 D-E).



domain and IgE. In a preliminary experiment the pre-saturation conditions were set up and identified using 10 nM IgE (2 µg/mL) and 5 µM His6x-D2 domain. At this receptor concentration both binding sites are saturated. For the dose-dependent competition assay, we explored peptide:receptor molar ratios between 1 and 100. Competitor concentrations therefore ranged between 5 µM and 500 µM. Results reported in the following Fig.41 A-C are the average of triplicate experiments and are reported as  $(B/B_0)*100$ , where B stands for the average Abs from triplicate data points for a given analyte and  $B_0$  is the average Abs determined without competitor.

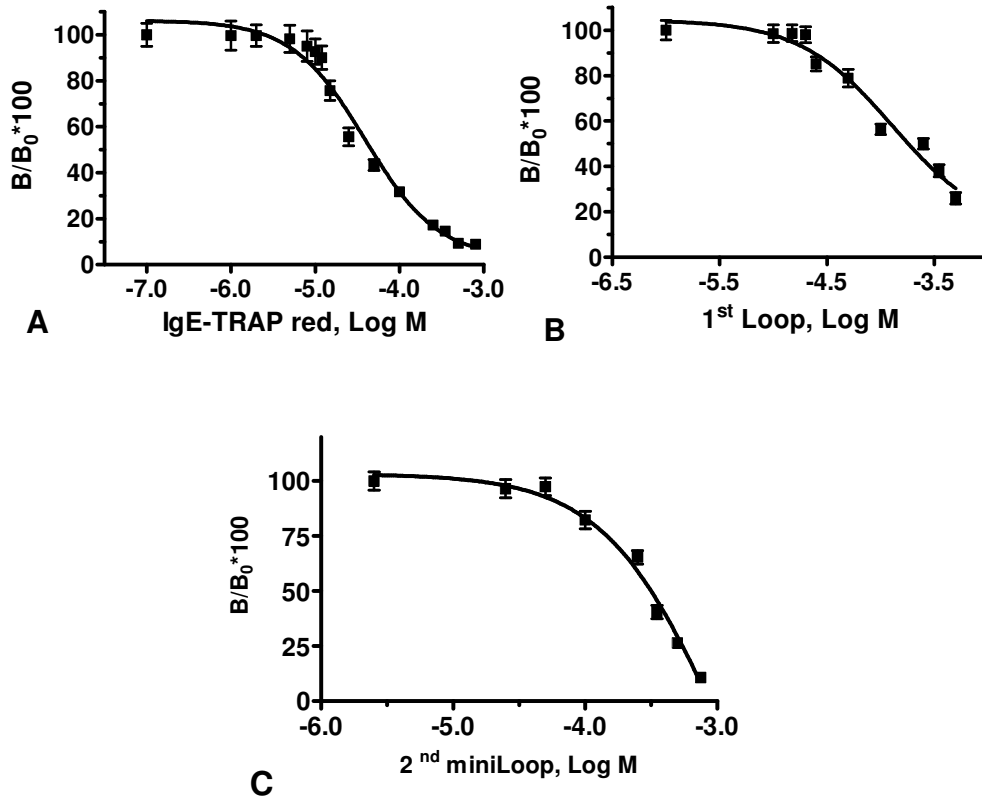


**Figure 41.** Dose-dependent binding competition ELISA assays carried out using the recombinant His6XD2 domain of the IgE receptor and commercial IgE. The peptides used were: IgE-TRAP red (A), 1<sup>st</sup> Loop (B) and 2<sup>nd</sup> miniLoop (C). By data fitting and analysis using non-linear regression the following  $IC_{50}$  were estimated: IgE-TRAP red:  $36.0 \pm 0.1 \mu\text{M}$ ; 1<sup>st</sup> Loop:  $103.0 \pm 0.2 \mu\text{M}$ ; 2<sup>nd</sup> miniLoop:  $864.0 \pm 0.2 \mu\text{M}$ .

Data show that all three peptides efficiently block the interaction between IgE and the receptor D2 domain, confirming the view that the peptides actually mimic the receptor binding sites, though with a reduced affinity. Noticeably,  $IC_{50}$  values determined by this approach, are consistent with the relative binding affinities of the 3 bioactive peptides. In particular, IgE-TRAP red has an  $IC_{50}$  of 36 µM, while the 1<sup>st</sup> Loop and 2<sup>nd</sup> miniLoop show  $IC_{50}$  of 103 and 864 µM, respectively.

## II.5 CONCLUSIONS AND PERSPECTIVES

One of the major challenges for the comprehension of physiological and pathological functions regulating the cellular processes, is the elucidation of molecular mechanisms underlining protein–protein interactions.

Protein–protein interactions, indeed, play a key role in a variety of biological processes and are therefore important targets for the design of novel therapeutics. Unlike the design of enzyme inhibitors, the disruption of protein–protein interactions is far more challenging, due to large interfacial areas involved in protein recognition and to the relatively flat topologies of these surfaces. Nevertheless, in spite of such difficulties, there has been considerable progress in the recent years.

In the first part of PhD thesis we have studied small peptides that act as modulators of protein–protein interactions playing a crucial role in allergic reactions.

The binding of IgE to its high affinity receptor FcεRI is a critical step in the allergic reaction and the knowledge at atomic level of the interaction interface between the two proteins has paved the way to the design of effective drugs blocking the receptor signalling and thus to new opportunities for molecular therapeutic intervention. The exact three-dimensional structure of the IgE-FcεRI complex, elucidated by X-ray crystallography, is indeed the ideal starting scaffold for the design of specific inhibitors that bind the receptor or the immunoglobulin as well. While binding the receptor binding site could easily lead to agonistic activities, the blocking of circulating IgE by soluble factors is an approach validated by the demonstrated efficacy of the rhu-Mab 25, a humanized recombinant monoclonal anti-IgE antibody, known as Omalizumab, which has recently entered the clinical phase IV and is therefore already on the market as a unique non-symptomatic treatment of allergic asthma.

Under these premises, on the basis of the receptor structure, we have designed small polypeptides that mimic the receptor binding interface and specifically bind IgE. The receptor-mimicking polypeptides, named IgE-TRAP, have been designed to reproduce the two distinct receptor binding sites unveiled by the crystallographic structure.

Although the polypeptides show a relatively low binding capacity (low micromolar range) compared to the full length receptor ( $KD = 10^{-9} - 10^{-10}M$ ), they exhibit a very high selectivity for IgE, being incapable to recognize the conserved IgG and IgA. Furthermore they clearly show a two-site mechanism of binding, demonstrating the efficiency of the design and suggesting a high specificity of recognition on the two distinct sites. Worthy of note, peptides, also exhibit a cooperative mechanism of interaction, as demonstrated by an average increase in affinity of 2-3 times of macroscopic KD compared to single-site KDs.

The soluble and functional D2 domain of hαFcεRI has been prepared as recombinant protein, in order to verify the ability of the selected peptides to inhibit its binding to IgE and to validate the hypothesized binding site. As expected, the active peptides efficiently block the interaction between IgE and the receptor D2 domain in competition ELISA assays, therefore confirming that the peptides mimic the receptor binding sites, though with a reduced affinity. Noticeably,  $IC_{50}$  values determined are consistent with the relative binding affinities of the 3 bioactive peptides.

Despite the lower affinity of these new molecules compared to that of the full receptor, these peptides are very promising in terms of selectivity as they appear to target with high specificity the binding site on the IgE.

Given the small molecular size (especially the 1<sup>st</sup> Loop), they also do not show

immunogenic properties and can be used in in vivo experiments at high doses and without modifications.

## II.6 REFERENCES

1. Cookson W. The alliance of gene and environmental in asthma and allergy. *Nature* (1999) 402 (supp b): 5-11
2. Meltzer E.O. and J.A. Grant Impact of cetirizine on the burden of allergic rhinitis. *Ann. Allergy Asthma Immunol.* (1999) 83(5):455-63
3. Radaev S. and P.D. Sun Recognition of IgG by Fc-gamma receptor. The role of Fc glycosylation and the binding of peptide inhibitors. *J. Biol. Chem.* (2001) 11;276(19):16478-83
4. Metzger H., Alcaraz G., Hohman R., Kinet J.P., Pribluda V. and R. Quarto The receptor with high affinity for immunoglobulin E. *Annu. Rev. Immunol.* (1986) 4:419-470
5. Saini S.S., MacGlashan D.W., Jr. S.A, Sterbinsky A., Togias D.C, Adelman L.M., Lichtenstein S. and B.S. Bochner Down-regulation of human basophil IgE and FcεRI surface densities and mediator release by anti-IgE-infusions is reversible in vitro and in vivo. *J. Immunol.* (1999) 162:5624–5630
6. Chang T.W. The pharmacological basis of anti-IgE therapy. *Nat. Biotechnol.* (2000) 18:157–162
7. Presta L.G., Lahr S.J., Shields R.L., Porter J.P., Gorman C.M., Fendly B.M. and P.M. Jardieu Humanization of an antibody directed against IgE. *J. Immunol.* (1993) 1;151(5):2623-32
8. Bousquet J., Wenzel S., Holgate S., Lumry W., Freeman P. and H. Fox Predicting response to omalizumab, an anti-IgE antibody, in patients with allergic asthma. *Chest.* (2004) 125(4):1378-86
9. Milgrom R.B. Fick, Jr., Su J.Q., Reimann J.D., Bush R.K., Watrous M.L. and W.J. Metzger Treatment of allergic asthma with monoclonal anti-IgE antibody. rhuMAb-E25. Study Group. *N. Engl. J. Med.* (1999) 341:1966–1973
10. Kraft S. and J.P. Kinet New developments in FcεRI regulation, function and inhibition. *Nat. Rev. Immunol.* (2007) 7(5):365-78
11. Garman S.C., Wurzburg B.A., Tarchevskaya S.S., Kinet J.P. and T.S. Jardetzky Structure of the Fc fragment of human IgE bound to its high-affinity receptor FcεRI. *Nature* (2000) 406:259–266
12. Nakamura G.R., Reynolds M.E., Chen Y.M., Starovasnik M.A. and H.B. Lowman Stable "zeta" peptides that act as potent antagonists of the high-affinity IgE receptor. *Proc. Natl. Acad. Sci. U.S.A.* (2002) 5;99(3):1303-8
13. Buku A., Keselman I., Lupyan D., Mezei M. and J.A. Price Effective Mast Cell Degranulating Peptide Inhibitors of the IgE/FcεRI Receptor Interaction. *Chem. Biol. Drug Des.* (2008) 72(2):133-9
14. Yagi S., Yanagida M., Tanida I., Hasegawa A., Okumura K. and C. Ra High-level expression of the truncated alpha chain of human high-affinity receptor for IgE as a soluble form by baculovirus-infected insect cells. Biochemical characterization of the recombinant product. *Eur. J. Biochem.* (1994) 1;220(2):593-8
15. Robertson M.W. Phage and Escherichia coli expression of the human high affinity immunoglobulin E receptor alpha-subunit ectodomain. Domain localization of the IgE-binding site. *J. Biol. Chem.* (1993) 15;268(17):12736-43
16. Takai T., Okumura K. and Ra C. Direct expression of the extracellular portion of human FcεRI chain as inclusion bodies in Escherichia Coli. *Biosci. Biotechnol. Biochem.* (2001) 65:79-85
17. Iwasaki A., Doi T., Umetani M., Watanabe M., Suda M., Hattori Y. and T. Nagoya Affinity improvement of the high-affinity immunoglobulin E receptor by phage display.

- Biochem. Biophys. Res. Commun.* (2002) 26;293(1):542-8
18. Rigby L.J., Trist H., Snider J., Hulett M.D., Hogarth P.M., Rigby L.J. and V.C.Epa Monoclonal antibodies and synthetic peptides define the active site of FcεRI and a potential receptor antagonist. *Allergy*. (2000) 55(7):609-19
  19. Cook, J.P.D., Henry A.J., McDonnell J.M., Owens R. J., Sutton B. J. and H. J. Gould Identification of contact residues in the IgE binding site of human FcεRIα. *Biochemistry* (1997) 36:155799-46
  20. Kochan J., Pettine L.F., Hakimi, J., Kishi, K. and J.P. Kinet Isolation of the gene coding for the alpha subunit of the human high affinity IgE receptor. *Nucleic Acids Res.* (1998) 16:3584
  21. Kinet J.P. The high affinity IgE receptor (FcεRI): from physiology to pathology. *Annu. Rev. Immunol.* (1999) 17:931-72
  22. Sutton B.J and H.J. The human IgE network. *Nature* (1993) 366:421-28
  23. Letourneur O., Sechi S., Willette-Brown J., Robertson M.W and J.P. Kinet Glycosylation of human truncated FcεRI αchain is necessary for efficient folding in the endoplasmic reticulum. *J.Biol.Chem.* (1995) 270:8249-8256
  24. Wedemeyer J., Tsai M. and S.J. Galli Roles of mast cells and basophils in innate and acquired immunity. *Curr. Opin. Immunol.* (2000) 12:624–631
  25. Galli S.J., Maurer M. and C.S. Lantz Mast cells as sentinels of innate immunity. *Curr. Opin. Immunol.* (1999) 11:53–59
  26. Asai K., Kitaura J., Kawakami Y., Yamagata N., Tsai M., Carbone D.P., Liu F.T., Galli S.J. and T. Kawakami Regulation of mast cell survival by IgE. *Immunity* (2001) 14:791–800
  27. Kalesnikoff J., Huber M., Lam V., Damen J.E., Zhang J., Siraganian R.P. and G. Krystal Monomeric IgE stimulates signaling pathways in mast cells that lead to cytokine production and cell survival. *Immunity* (2001) 14:801–811
  28. Rivera J. and A.M. Gilfillan Molecular regulation of mast cell activation. *J. Allergy Clin. Immunol.* (2006) 117:1214–1225
  29. Gilfillan A.M. and C. Tkaczyk Integrated signalling pathways for mast-cell activation. *Nature Rev. Immunol.* (2006) 6:218–230
  30. Hulett M.D., Brinkworth R.I., McKenzie I.F. and P.M. Hogarth Fine structure analysis of interaction of FcεRI with IgE. *J. Biol. Chem.* (1999) 274(19):13345-52
  31. Basu M., Hakimi J., Dharm E., Kondas J.A., Tsien W.H., Pilson R.S., Lin P., Gilfillan A., Haring P. and E.H. Braswell Purification and characterization of human recombinant IgE-Fc fragments that bind to the human high affinity IgE receptor. *J. Biol. Chem.* (1993) 268(18):13118-27
  32. Henry A.J., Cook J.P., McDonnell J.M., Mackay G.A., Shi J., Sutton B.J. and H.J. Gould Participation of the N-terminal region of Cε3 in the binding of human IgE to its high-affinity receptor FcεRI. *Biochemistry* (1997) 36:15568–15578
  33. Sechi S, Roller PP, Willette-Brown J, Kinet JP. A conformational rearrangement upon binding of IgE to its high affinity receptor. *J Biol Chem.* 1996;271:19256–19263.
  34. Maxwell K. F., Powell M.S., Hulett M.D., Barton P.A., McKenzie I.F., Garrett T.P. and P.M. Hogarth Crystal structure of the human leukocyte Fc receptor, FcγRIIa. *Nature Struct. Biol.* (1999) 6:437–442
  35. Sondermann P., Huber R. and U. Jacob Crystal structure of the soluble form of the human FcγRIIIb: a new member of the immunoglobulin superfamily at 1.7 Å resolution. *EMBO J.* (1999) 18:1095–1103
  36. Sondermann P., Jacob U., Kutscher C. and J. Frey Characterization and crystallization of soluble human FcγRII (CD32) isoforms produced in insect cells. *Biochemistry* (1999) 38,469– 8477

37. Hulett M. D., Brinkworth R.I. , McKenzie I.F. and P.M. Hogarth Fine structure analysis of interaction of FcεRI with IgE. *J. Biol. Chem.* (1999) 274:13345–13352
38. Garman S.C., Sechi S., Kinet J.P. and T.S. Jardetzky The analysis of the human high affinity IgE receptor FcεRI alpha from multiple crystal forms. *J. Mol. Biol.* (2001) 31;311(5):1049-62
39. Wurzburg B.A. and T.S. Jardetzky Structural insights into the interactions between human IgE and its high affinity receptor FcεRI. *Mol. Immunol.* (2002) 38(14):1063-72
40. Nissim A., Jouvin M. H. and Z. Eshhar Mapping of the high affinity Fcε-receptor binding site to the third constant region domain of IgE. *EMBO J.* (1991) 10:101–107
41. Presta L., Shields R., O'Connell L., Lahr S., Porter J., Garman C., and P. Jardieu The binding site on human immunoglobulin E for its high affinity receptor. *J. Biol. Chem.* (1994) 269:26368–26373
42. Mallamaci M.A. *et al.* Identification of sites on the human FcεRI α-subunit which are involved in binding human and rat IgE. *J. Biol. Chem.* (1993) 268:22076–22083
43. Wurzburg B.A., Garman S.C. and T.S. Jardetzky Structure of the human IgE-Fc Cε3-Cε4 reveals conformational flexibility in the antibody effector domains. *Immunity* (2000) 13:375-385
44. [www.emble-heidelberg.de](http://www.emble-heidelberg.de)
45. Harper S., Speicher D.W. Expression and purification of GST fusion proteins. *Curr Protoc Protein Sci.* (2008) Chapter 6:Unit 6.6.
46. Korf U., Kohl T., Van der Zandt H., Zahn R., Schleegeer S., Ueberle B., Wandschneider S., Bechtel S., Schnölzer M., Otleben H., Wiemann S. and A. Poustka Large-scale protein expression for proteome research. *Proteomics.* (2005) 5(14):3571-80.
47. Inaba K. Protein disulfide bond generation in Escherichia coli DsbB-DsbA. *J. Synchrotron Radiat.* (2008) 15(Pt 3):199-201.
48. Bradford M. A rapid and sensitive method for the quantitation of microgram quantities of protein utilizing the principle of protein-dye binding. *Anal. Biochem.* (1976) 72:248
49. Fields G.B, Noble R.L. Solid phase peptide synthesis utilizing 9-fluorenylmethoxy-carbonil amino acids. *Int. J. Pept. Protein Res.* (1990) 35:161-214
50. Crowther J.R. The ELISA guidebook. *Methods Mol Biol.* (2000) 149:III–IV; 1–413:III-413 (2005) 6:195-205
51. Kahn P.C *Methods Enzimol.* (2002) 961:335-378
52. Tsumoto K., Ejima D, Kumagai I. and T. Arakawa Practical considerations in refolding proteins from inclusion bodies. *Protein Expr Purif.* (2003) 28(1):1-8.
53. Tsumoto K., Umetsu M, Yamada H, Ito T, Misawa S and I. Kumagai Immobilized oxido-reductase as an additive for refolding inclusion bodies: application to antibody fragments. *Protein Eng.* (2003) 16(7):535-41
54. Tsumoto K., Umetsu M., Kumagai I., Ejima D., Philo J.S. and T. Arakawa Role of arginine in protein refolding, solubilization, and purification. *Biotechnol. Prog.* (2004) 20(5):1301-8
55. Matsumoto M., Misawa S., Tsumoto K., Kumagai I., Hayashi H. and Y. Kobayashi On-column refolding and characterization of soluble human interleukin-15 receptor alpha-chain produced in Escherichia coli. *Protein Expr Purif.* (2003) 31(1):64-71
56. Zhang G., Xi J., Wang X., Zhang H., He L., and Y. Zhu Efficient recovery of a functional extracellular domain of bovine IgG2 Fc receptor from inclusion bodies by a rapid dilution refolding system. *J. Immunol. Methods.* (2008) 20;334(1-2):21-8

## **CHAPTER III**

### **III. IDENTIFICATION OF A BCL10 INHIBITORY PEPTIDE**

#### **III.1 INTRODUCTION**

Modular protein interaction domains play an important role in signal transduction by the assembly of components into specific signalling complexes.

The interchange of protein modules between signalling molecules has enabled the elucidation of new signal transduction pathways due to specific stress and developmental stimuli.

The cytoplasmatic proteins, transporting information from cell surface receptors to their intracellular targets, are commonly constructed of modular domains that either have a catalytic function (such as protein or lipid kinase activity), or mediate the interactions of proteins with one another, or with phospholipids, nucleic acids or small molecule second messengers. These interacting domains play a critical role in the selective activation of signalling pathways, through their ability to recruit target proteins to activated receptors, and to regulate the subsequent formation of signalling complexes.

An intriguing challenge is to understand how interacting domains cooperate to establish the complex signalling networks, controlling events as fundamental and complex as cell development, maintenance of homeostasis and immune system function.

The cellular life-cycle is actually governed by one of the most important regulated processes: the apoptotic cascade pathway [1].

Apoptosis is a conserved, gene-directed mechanism essential for the elimination of unnecessary or dangerous cells and for maintaining cellular homeostasis [2].

Dysregulation in apoptosis mechanisms may contribute to a variety of human diseases such as autoimmune syndromes, lymphomas and solid tumours.

Apoptosis results in a complex cascade of events and signalling pathways involving a large variety of receptors and factors, such as the so called "Death Domain" superfamily, composed of the "death domain" (DD), the "death effector domain" (DED) and the "caspase recruitment domain" (CARD) proteins. These proteins regulate apoptosis signalling through specific interactions necessary for transducing a "death signal" in the vital process of normal cell development and maintenance of homeostasis [3,4].

Over the past few years, a number of adaptor molecules containing the CARD domain have been identified [5].

CARD was originally described as a protein-binding motif that interacts with specific caspases through a CARD-CARD homophilic interaction. However, CARD has also been found in many adaptor proteins that do not interact with caspases, but rather mediate assembly of proteins involved in apoptosis and/or the control of the activation state of NF- $\kappa$ B transcription factor [4]. Thus, it is now well established that CARD-containing proteins play important roles in the assembly and activation of apoptotic and inflammatory complexes, which are mediated by homotypic interactions between CARD domains [5].

BCL10 is a CARD-containing protein that several groups have independently identified as a regulator of apoptosis and as an activator of NF- $\kappa$ B factor [6,9,34,35]. Several studies report that BCL10 oligomerizes through its N-terminal CARD domain thus promoting the inappropriate activation of the transcriptional factor NF- $\kappa$ B [4,6].

### III.1.2 The family of CARD containing proteins

Homotypic interactions between proteins containing CARDS, DEDs or DDs have been found in divergent signalling pathways resulting in caspase activation and apoptosis. A classic example is the CD95 (Fas/APO-1) pathway. After interaction with its ligand, the CD95 receptor recruits the adaptor Fas-associated protein with death domain (FADD) via DD motifs present in both proteins [7]. In turn, FADD recruits caspase-8 to the receptor complex via a single DED motif present in the former, and two tandemly arranged DED motifs present in the latter. This interaction leads to caspase-8 activation and propagation of the death signal through a cascade of further proteolytic events.

Notably, CARD–CARD interactions between Apaf-1 and caspase-9 are critical for the assembly of a protein complex (called the apoptosome) that promotes caspase-9 activation during apoptosis [8].

Certain CARD-containing caspases have also been implicated in proteolytic processing of cytokines (caspase-1 is required for maturation of IL-1 $\beta$  and IL-18) that are involved in the inflammatory response.

However, in the past years, the family of CARD-containing proteins has been extensively investigated and it has recently been confirmed that CARD-containing proteins do not only promote the caspase activation. Rather, accumulating evidence suggest that many CARD proteins participate in NF- $\kappa$ B signalling pathways associated with apoptosis and immune responses [9].

Proteins containing CARD domains can be divided into subfamilies based on their overall domains structures: nuclear binding CARD domains (NBD-CARDS), coiled-coiled CARD domains (CC-CARDS), bipartite-CARDS and CARD-only proteins [9].

The NBD-CARDS contain a nucleotide-binding domain in addition to a CARD module and most also contain repeats, such as leucine-rich, within their C-terminal. The NBD module most likely acts as an oligomerisation surface and the repeat region as a sensory domain that regulates oligomerisation.

The CC-CARD proteins are structurally similar to the NBD-CARDS but the central NBD is replaced by a coiled-coil motif acting as an oligomerisation surface.

The bipartite-CARDS contain a CARD domain plus an other motif such as a kinase domain, a DD motif or a protease domain. After recruitment by the NBD-CARDS or the CC-CARDS they either become active in the process or to recruit additional effector molecules to the complex, such as the I $\kappa$ B kinase subunit (IKK $\gamma$ /NEMO).

The CARD-only proteins may act as positive or negative regulators of the multi-domain CARDS (NBD-CARDS and CC-CARDS) by regulating recruitment between protein. Alternatively, the CARD-only proteins may compete with the bipartite CARDS for binding to their targets.

Although all CARDS possess a remarkably similar secondary structure and often a discrete sequence identity, the members of each group act in related signalling pathways.

CARD domains are 10-15 kDa, located at the N-terminal end, and consist of anti-parallel six-helices bundles in the Greek key topology that form highly specific homophilic interactions between signalling partners [10,11].

There are, at least, three major pathways in which CARD proteins act: the regulation of caspase activation in the context of apoptosis; the regulation of caspase activation in the context of inflammation; the regulation of NF- $\kappa$ B activation in the context of innate or adaptive immune responses.

All CARD proteins described so far have been implicated in one way or other in host defense against infection, environmental stress, or cellular damage. Clearly, there is significant cross-talk between the pathways that result in NF- $\kappa$ B activation and those that lead to caspase-mediated inflammation or apoptosis. Thus, it is not much of a surprise to find that similar protein modules are found repeatedly in proteins from all pathways.

### **III.1.3 BCL10 protein: a modular protein**

BCL10 (B-cell lymphoma 10) belongs to a family of proteins containing caspase recruitment domains (CARD). It has a bipartite structure consisting of an N-terminal CARD and a C-terminal domain that is rich in serine and threonine residues which undergo multiple phosphorylations and are therefore structural elements with a regulative role.

Although the BCL10 pathway is still to be clarified, several studies have been focused on its homophilic interactions with other protein partners mediated by its CARD domain. These include interactions with RIP2 [14], CARMA1 (also known as CARD11 or Bimp2) [14-16], CARMA2 (also known as CARD14 or Bimp3) [14], CARMA3 (also known as CARD10 or Bimp1) [17,18] and CARD9 [19].

These three CARMA proteins share similar structural motifs, with an N-terminal CARD domain, followed by a coiled-coil domain, a PDZ domain (acronym combining the first letters of three proteins: Psd95 (post synaptic density protein 95), DlgA (Drosophila disc large tumor suppressor), and Zo-1 (zonula occludens-1 protein)), a SH3 domain, and a C-terminal GUK domain (guanylate kinase-like domain). Their expression and diversification in signalling pathways depends on their cellular localization [14-19]. Functionally, CARMA proteins are supposed to function as molecular scaffolds that assist recruitment and assembly of signal transduction molecules.

Several studies report that BCL10 acts at a convergence point between the T- and B-cell receptor-driven NF- $\kappa$ B signalling pathways [12,13,20,21].

In the TCR (T cell receptor) signalling pathway (Fig.1), phosphorylated CARMA1 recruits BCL10, MALT1, and TRAF6 [19-22]. MALT1 and TRAF6 then functions as E2 ligase to further induce K63-linked poly-ubiquitination of NEMO, leading to phosphorylation and activation of the IKK complex [23-25].

Thus, in lymphocytes, the N-terminal CARD domain of BCL10 binds to the CARD domain of CARMA1, and this interaction is required for the correct transduction of the NF- $\kappa$ B activating signal [26].

Targeted mutation of the gene encoding either proteins results in severe impairment of T cell and B cell proliferative responses to antigen stimulation, due to the failure to activate NF- $\kappa$ B [15,19-21,25-27]. Additionally, cytogenetic studies have revealed that, whereas BCL10 translocation is associated with mucosa associated lymphatic tissue (MALT) B cell lymphomas, missense mutations in the CC-domain of CARMA1 are frequently detected in diffuse large B cell lymphomas [28,29].

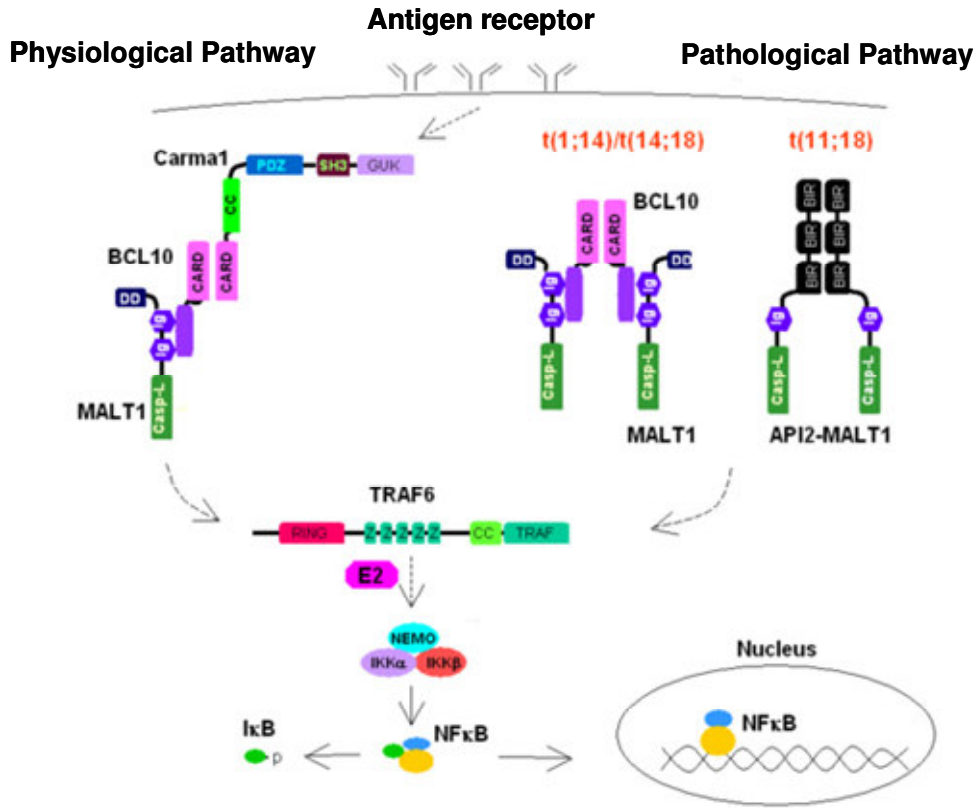


**Figure 1:** Physiological (A) and pathological (B) BCL10 signalling in T-cell receptor-mediated activation

Instead, the complex of proteins that comprises CARMA3, BCL10 and MALT1, appears to play an important role in cells outside of the immune system. In fact, recent studies indicate that CARMA3 and BCL10 are implicated in the signal transduction pathways elicited by G protein-coupled receptors, a large family of cell surface receptors that regulate cell migration, differentiation, proliferation, and survival [30-32]. Specifically, it appears that NF- $\kappa$ B activation induced by G protein-coupled receptors utilize a pathway dependent on the molecular complex containing CARMA3 and BCL10 [33].

Altogether, these data indicate that BCL10 is a cytosolic signalling intermediate in the pathway connecting antigen receptors to activation of the NF- $\kappa$ B transcription factor [34,35] and is likely to play a significant role in the etiology and/or pathogenesis of MALT lymphoma [36,37]. It therefore represents the molecular target for the treatment of pathologic conditions associated with inappropriate NF- $\kappa$ B activation, ranging from the MALT B cell lymphomas with t(1;14)(p22;q32), to the inflammatory disorders involving G protein-coupled receptors, such as chronic liver injury, atherosclerosis and cardiac hypertrophy [33].

Several studies have reported that the BCL10-CARD oligomerization event assist the formation of cytoplasmatic filaments that serve as scaffold for recruitment of NF- $\kappa$ B-activating signal transduction elements [6] and these filaments seem to be responsible for the inappropriate NF- $\kappa$ B activation which induces cell proliferation and tumorigenesis, as in the Lymphomas of Malt.

## III.2 PROJECT AIMS

The emerging importance of BCL10 as a target for modulating the NF- $\kappa$ B mediated inflammation and tumorigenesis and the involvement of an oligomerization process in these mechanisms, has lead us to investigate the self-association regions of the BCL10 CARD domain and the possibility of inhibiting the BCL10-mediated functions by peptides able to interfere with protein oligomerization process. While it is widely accepted that BCL10 oligomerizes through its N-terminal CARD domain [4,6] the structural basis for this interaction remains to be defined. Following a simple and effective methodology based on the use of fragments derived by limited proteolysis of the protein, we have selected a peptide that mimics the self-recognition interface and disrupts the interaction at nM concentrations. By this method, coupled to the use of synthetic peptides, we have been able to identify single residues involved in CARD-CARD contacts and to demonstrate that by interfering with the protein oligomerization, NF- $\kappa$ B activation is also strongly impaired.

## III.3 EXPERIMENTAL PROCEDURES

### III.3.1 Materials

N-protected Fmoc-amino acid derivatives and coupling reagents for peptidic synthesis were from Inbios (Pozzuoli, Napoli). HPLC-grade solvents and trifluoroacetic acid (TFA) are from LabScan (Stillorgan, Dublin, Ireland).

Trypsin treated with L-(tosylamido-2-phenyl) ethyl chloromethyl ketone (TPCK-trypsin), streptavidin horseradish peroxidase conjugated (STR-HRP), o-phenyldiamine (OPD) table sets, Rink amide p-Methylbenzhydrylamine (MBHA) resin, tri-isopropyl-silane (TIS), Fluorescein isothiocyanate (FITC), Phorbol12-myristate13-acetate (PMA) and ionomycin are from Sigma-Aldrich (Milan, Italy).

Enhanced Chemiluminiscent (ECL) substrate and EZ Link NHS-LC biotin reagent (succinimidyl-6-(biotinamido) hexanoate) is from Pierce (Milano, Italy).

TransBlot SD semi-dry, blotting grade blocker Non-Fat Dry Milk (NFDM) are from Biorad.

Anti-BCL10 antibodies were provided by Dr. P. Vito, Università del Sannio [6]. Horseradish peroxidase (HRP) conjugated secondary antibodies, luciferase assay Kit are from Promega.

All molecular biology kits are from Qiagen (Milano, Italy) except Quik Change Site-Directed Mutagenesis Kit that is from Stratagene. All plasmids and expression vectors used in this study were generated by standard procedures and confirmed by sequencing.

Dulbecco's Modified Eagle's Medium (DMEM), Fetal calf serum (FCS), and Trypsin are from GIBCO (Milan, Italy).

Solid-phase peptide synthesis was carried out on a fully automated peptide synthesizer AAPTECH 348 W, Advanced Chemtech (Louisville, KY).

Preparative RP-HPLC was carried out on a Shimadzu LC-8A system, equipped with a SPD-M10 AV detector.

LC-MS analyses were carried out on an LCQ DCA XP Ion Trap mass spectrometer (ThermoElectron, Milan, Italy) equipped with an OPTON ESI source, operating at 4.2 kV needle voltage and 320°C and with a complete Surveyor HPLC system. LC-MS columns were from ThermoElectron.

CD spectra were recorded using a Jasco J-810 spectropolarimeter (JASCO Corp) equipped with a Peltier-type temperature control system

Other reagents and chemical suppliers are indicated in the section of methods.

### III.3.2 Methods

#### III.3.2.1 BCL10-CARD domain cloning, expression and purification

The doubly mutated Cys29Ser-Cys57Ser N-terminal region of BCL10, comprising residues 1-107, named BCL10-CARD, was recombinantly expressed in *E.Coli* as a His6x-tagged fusion protein. Mutations, designed to minimize the possible protein aggregation due to disulfide formation, were introduced by site-directed mutagenesis of the wild-type gene using Quik Change Site-Directed Mutagenesis Kit following manufacturer's instructions. The mutated sequence was cloned in the pET28 vector to obtain the fusion-His6x protein with a  $\Delta$ -link of 36 residues (poly-histidine tag included). Protein expression was carried out in BL21 (DE3) at 37°C and inducing overnight with 1 mM IPTG before lysing the pellets in PBS buffer (137 mM NaCl, 2.7

mM KCl, 10 mM Na<sub>2</sub>HPO<sub>4</sub>, 2 mM KH<sub>2</sub>PO<sub>4</sub> pH 7.4) containing 8 M urea. Fractions of purified protein were obtained by affinity chromatography purification on Ni-NTA columns equilibrated in 100 mM phosphate, 10 mM Tris-HCl, 8 M urea pH 8.0 buffer. The protein was eluted by gradually lowering the pH from pH 8.0 to pH 4.5, then the pooled fractions were further purified by gel filtration on a Sephadex G150 column in a 50 mM Tris pH 4.0 buffer and finally dialyzed against a 100 mM sodium acetate buffer at pH 4.0. This buffer was used throughout all the experiments as the protein displayed a strong tendency to precipitate at pH values comprised between 5.0 and 8.0. About 5 mg of protein from 100 g of pellets were recovered in typical preparations. The recombinant protein was prepared at the Dipartimento di Biologia e Patologia Cellulare e Molecolare, Università Federico II, Napoli.

### III.3.2.2 Circular Dichroism analysis

CD spectra of BCL10-CARD was acquired in sodium acetate 1x10<sup>-6</sup>M buffer solution at pH 4.5, calculated by Bradford measurements [43], and at room temperature.

CD spectra of BCL10 peptides were acquired in 10 mM phosphate pH 7.0 buffer with C<sub>pep</sub> = 20 x 10<sup>-6</sup> M, calculated by UV measurements, and R.T.

Spectra were recorded using a 0.1 mm path length quartz cuvette. Data were collected at 0.2 nm intervals with a 20 nm min<sup>-1</sup> scan speed, a 2 nm bandwidth, and a 16 s response, from 260 to 190 nm, under constant N<sub>2</sub> flow. The recorded spectra were then signal-averaged over at least three scans, and the baseline was corrected by subtracting the spectrum of the buffer. Spectra were then transformed in molar ellipticity/mean residue [θ], expressed in deg·cm<sup>2</sup>·dmol<sup>-1</sup>.

### III.3.2.3 Biotinylation of BCL10-CARD domain

Aliquots of the recombinant BCL10-CARD domain were biotinylated using the EZ Link NHS-LC biotin reagent according to the manufacturer's instructions. A freshly prepared solution of NHS-LC-biotin (10 mM in DMSO:water 1:9 v/v) was added to a protein at a 20:1 mol/mol ratio; the pH was then adjusted to 8.0 with NaOH and the solution incubated for 30 minutes at R.T. Biotinylated samples were dialyzed against 50 mM sodium acetate pH 4.0 buffer in order to remove the excess free biotin. The biotinylated BCL10-CARD domain solution was sterilized by passing the solution through a 0.22 μm filter and stored in working aliquots at -80°C. Protein biotinylation was confirmed by LC-MS analysis as determined by the MW increase of 340 amu due to the biotin moiety.

### III.3.2.4 Protein digestion with trypsin and peptide fractionation

An aliquot of BCL10-CARD domain (1.0 mg; 62 nmoles) was dissolved in 1.0 mL of 50 mM Tris-HCl, 20 mM CaCl<sub>2</sub> pH 8.0 buffer, 10% acetonitrile was then added to enhance peptide solubility. TPCK-treated trypsin was then added at a final 1:100 enzyme-substrate ratio (w/w) and the reaction was left at 37°C under gentle agitation for 16 hours. A protein sample (0.1 mg) was analyzed by LC-MS/MS to assess protein digestion and to identify the fragments obtained. For this analysis a C18 BioBasic 30x2 mm ID column (ThermoElectron), equilibrated at 0.2 mL/min with 5% CH<sub>3</sub>CN, 0.05% TFA, was utilized and applying a gradient from 5% to 55% in CH<sub>3</sub>CN, 0.05% TFA over 65 minutes. Tryptic products were fractionated by RP-HPLC using a C18 250x4.6 mm ID column equilibrated at 1.5 mL/min flow rate with 5% CH<sub>3</sub>CN,

0.1% TFA, and applying a gradient of the same solvent from 5% to 70% in 50 minutes. Ten fractions, 1F to 10F, were collected and subsequently analyzed by analytical LC-MS/MS to obtain their relative composition. Fractions 1-3, putatively containing highly hydrophilic fragments, were analysed with a gradient of CH<sub>3</sub>CN, 0.05% TFA from 1% to 30% over 30 minutes, while the remaining were analyzed under the same analytical conditions reported above. Lyophilized fractions were stored at -80°C until use.

For the identification of the tryptic fragments the program MS-Digest for trypsin digestion cleavage was used on the web page <http://www.expasy.org/tools>.

### **III.3.2.5 BCL10-CARD domain self-association and binding competition ELISA assays**

To monitor BCL10-CARD domain self-association, we set up an ELISA-like assay where the protein was adsorbed on the plate surface at different concentrations, whereas the biotinylated variant was utilized to detect the binding [44]. Adsorption was performed in a 96-well plate (Nunc, Falcon) in sodium acetate 50 mM pH 4.0 buffer (AcNa buffer) at protein concentrations of 0.12 μM, 0.31 μM and 0.62 μM overnight at 4°C (100 μL/well). Some wells were filled with buffer alone and were used as blank. After washing 3 times with the same buffer, the wells were filled with 200 μL of 1% w/v BSA in PBS (137 mM NaCl, 2.7 mM KCl, 10 mM Na<sub>2</sub>HPO<sub>4</sub>, 2 mM KH<sub>2</sub>PO<sub>4</sub> pH 7.4 buffer) and incubated for 2 h at 37°C. The plate was washed again with PBS-T (137 mM NaCl, 2.7 mM KCl, 10 mM Na<sub>2</sub>HPO<sub>4</sub>, 2 mM KH<sub>2</sub>PO<sub>4</sub> pH 7.4 with 0.004% w/v Tween 20), then solutions of biotinylated protein in AcNa buffer were added to wells at concentrations ranging between 0.18 μM and 3.1 μM (0.18 μM, 0.36 μM, 0.75 μM, 1.6 μM, 3.1 μM; 100 μL/well) and incubated for 1 h at R.T. After washing 3 times with AcNa-T buffer (AcNa buffer with 0.004% Tween), the wells were filled with 100 μL HRP-conjugated streptavidin (STRV-HRP) at 1:10000 dilution in PBS, and incubated for 1 h at 37°C. After washing, detection was achieved using *o*-phenyldiamine (OPD) at 0.4 mg/mL in 50 mM Phosphate citrate buffer pH 5.0, containing urea-hydrogen peroxide 0.4 mg/mL. The reaction was stopped by adding 50 μL of 2.5 M H<sub>2</sub>SO<sub>4</sub> and the adsorbance was measured at 490 nm using a Synergy 4 multi-wavelength reader (BIOTEK Instruments, Inc. Highland Park, VT, USA).

For the binding competition experiment unlabelled BCL10-CARD domain at 0.12 μM in coating and soluble biotinylated protein at 0.80 μM (1:7 mol/mol ratio) was fixed as pre-saturation condition by previous experiments. In the screening competition assay peptides contained in the 11 RP-HPLC fractions, obtained by tryptic digestion, were used at a nominal concentration of 0.80 μM (1:1 ratio with the biotinylated protein) and 8.0 μM (10:1 ratio with the biotinylated protein). Peptide concentration was calculated assuming a 100% trypsin cleavage and a 50% recovery from the RP-HPLC fractionation. In dose-dependent competition assay with the synthetic fragments, peptide concentrations ranging from 0.03 μM to 15 μM were used and pre-incubated with biotinylated BCL10-CARD domain 0.8 μM for 45 min. at R.T. before addition to each well. The subsequent steps were carried out as described. All assays were carried out at least twice.

Competition results were reported as  $(B/B_0)*100$ , where B stands for the average OD from triplicate data points for a given analyte and B<sub>0</sub> is the average OD determined without competitor. Data fitting and analysis was carried out by non-linear regression using GraphPad Prism, vers. 4.00 for Windows, GraphPad Software, San Diego California, USA.

### III.3.2.6 Peptide synthesis, purification and characterization

All peptides were prepared by solid phase synthesis as C-terminally amidated and N-terminally acetylated derivatives following standard Fmoc chemistry protocols [45]. A Rink-amide MBHA resin (substitution 1.1 mmol/g) and amino acid derivatives with standard protections were used in all syntheses. Cleavage from the solid support was performed by treatment with a trifluoroacetic acid (TFA)/tri-isopropylsilane (TIS) /water (90:5:5, v/v/v) mixture for 90 min. at R.T., then crude peptides were precipitated in cold ether, dissolved in a water/acetonitrile (1:1, v/v) mixture and lyophilized. Products were purified by RP-HPLC applying a linear gradient of 0.1% TFA/CH<sub>3</sub>CN in 0.1% TFA water from 5% to 70% over 50 min. using a semi-preparative 2.2x5 cm C18 column at a flow rate of 20 mL/min. Peptide purity and identity were confirmed by LC-MS analyses using a LCQ DCA XP Ion Trap mass spectrometer, previously described. The peptides BCL10[91-98] and BCL10[91-98]T91A,Q92A, utilized for cellular assays, were also prepared fused to the basic region of the HIV Tat protein (fragment 48-60) [43]. Aliquots of peptides VIII and IX were also prepared with N-terminal fluorescein labelling to monitor cell delivery. FITC (fluorescein isothiocyanate) was linked to an N-terminal-β-alanine. A solution of FITC (1.1 equivalents) dissolved in DMF/DCM/DIEA (12:7:5) was added to the resin and left over night under agitation.

Peptide purity and integrity were confirmed by LC-MS on a LCQ DCA XP Ion Trap mass spectrometer (Thermo Electron, Milan, Italy), as previously described.

### III.3.2.7 Size Exclusion Chromatography analysis

SEC analysis was carried out on a Biosep/SEC/S 2000 at 1.0 mL/min. Both peptides I and II were loaded onto the SEC column, opportunely equilibrated in phosphate 50 mM pH 6.8 buffer, at increasing concentrations (5 μM, 10 μM, 50 μM, 100 μM, 400 μM). A calibration curve was used to determine the MWs. Specific molecular mass markers were run on the column under the same conditions in duplicate for calibration. The selected calibrants were: Trypsinogen, 23.0 kDa; Myoglobin, 17.0 kDa; Cytochrome C, 12.4 kDa; Angiotensin II, 1.0 kDa; an unrelated synthetic Peptide I, 3.5 kDa; an unrelated synthetic Peptide II, 1.67 kDa. All measurements were done at least twice. Elution volumes and partition coefficients of the standards and samples were calculated according to manufacturer's protocol.

### III.3.2.8 Serum stability

The TAT-fused Peptides VIII and IX were dissolved in H<sub>2</sub>O at a 10 mg/mL. The samples, serially diluted in PBS pH 7.4 buffer containing 10% FCS in order to obtain 100 μg/mL solutions, were incubated at 37°C for 24 h. 10 μL aliquots (1.0 μg total peptide) were removed at 0, 4 h, 8 h, 12 h, 16 h and 20 h. After centrifugation, the recovered samples were analyzed by RP-HPLC applying a linear gradient of 0.1% TFA/CH<sub>3</sub>CN in 0.1% TFA/H<sub>2</sub>O from 5% to 70% over 50 minutes using a semi-preparative 2.2x5 cm C18 column at a flow rate of 20 mL/min. A reference curve was obtained by analyzing different amounts of the pure compounds under the same conditions. The reference curve was used to exclude effects of sample subtraction by non-specific binding to albumin or other serum proteins that were pelleted during centrifugation. Experiments were carried out twice and data were reported as a plot of peak area (%) versus time.

### **III.3.2.9 Cell culture**

All experiments with cells were carried out in the laboratory of Prof. P. Vito, Università del Sannio, Benevento.

HEK293 (Human Embryonic Kidney cells) cells (ATCC, Manassas, VA, USA) were grown in complete DMEM supplemented with 10% FCS and 100 µg/mL penicillin / streptomycin, and maintained at 37°C with 5% CO<sub>2</sub>.

### **III.3.2.10 Immunoblot analysis and co-immunoprecipitation**

HEK293 cells transfected, with plasmids encoding for two tagged versions of BCL10 (1-127) bearing the HA and the FLAG epitopes by calcium phosphate precipitation, were prepared by Dipartimento di Biologia Molecolare, II Policlinico, Napoli.

HEK293 cells co-transfected with HA-BCL10 (1-127) and FLAG-BCL10 (1-127) were resuspended in lysis buffer (150 mM NaCl, 20 mM Hepes pH 7.4, 1% Triton X-100, 10% glycerol, and a mixture of protease inhibitors). Proteins were resolved by 10% SDS-PAGE, and gels were transferred to nitrocellulose membrane using Trans Blot SD semi-dry (Bio-Rad). The membranes were then blocked for 1 h at R.T. in PBS containing 0.05% Tween 20 and 5% NFDM. After washing 3 times for 10 min., the filter was incubated with the primary antibody overnight at 4°C in blocking buffer (PBS containing 0.05% Tween 20 and 2.5% NFDM). After washing 5 times for 10 min., the filter was incubated with the HRP-conjugated secondary antibody for 1 h at R.T. in blocking buffer. Detection was achieved using the ECL system following manufacturing's protocol. For the co-immunoprecipitation experiments, cells were resuspended in lysis buffer and immunocomplexes were bound to protein A/G, resolved by SDS-PAGE and analyzed by immunoblot assay as already described.

### **III.3.2.11 Fluorescence peptide assay**

Peptide entry tests were carried out using fluorescently labelled molecules. HEK293 cells transfected were grown onto glass coverslips in 6 wells multi-dishes. After 24 h the cells were washed with PBS (137 mM NaCl, 2.7 mM KCl, 10 mM Na<sub>2</sub>HPO<sub>4</sub>, 2 mM KH<sub>2</sub>PO<sub>4</sub>, pH 7.4) and fixed with 3% paraformaldehyde. After additional washes with PBS, the cells were treated for 5 h at R.T. with FITC and TAT-conjugated Peptides VIII and Peptide IX (used as a control) at 100 µM, 200 µM and 300 µM. Samples were then analyzed by fluorescence microscopy (Axiovert, Carl Zeiss).

### **III.3.2.12 NFκB luciferase reporter gene assays**

The inhibition of NF-κB activation induced by BCL10 (1-127) over-expression in HEK293 cells and PKC activation was determined by luciferase activity measurement. HEK293 cells transiently co-transfected with an expression vector encoding for BCL10 (HA-BCL10 (1-127) or FLAG-BCL10 (1-127)) together with an NF-κB-luciferase and β-galactosidase reporter vectors were used.

The total amount of transfected plasmidic DNA was maintained constant by adding the empty vector. 16 h after transfection, the cells were treated with FITC and TAT-conjugated Peptides VIII and Peptide IX (used as a control) at different concentrations for 5 h at R.T. Cells were lysed and assayed using the Luciferase Assay System (Promega) according to the manufacturer's instructions using a luminometer (Berthold Analytical Instruments, Nashua, NH, USA). Luciferase activity

was normalized against  $\beta$ -galactosidase activity and the data are representative of six independent experiments done in triplicate.

HEK293 cells were transfected with an NF- $\kappa$ B-luciferase reporter plasmid. 24 h after trasfection, the cells were untreated or treated with 40 ng/mL PMA and 1  $\mu$ M ionomycin together with TAT-Peptide VIII or TAT-ctr (Peptide IX) for 5 h. The cells were harvested, and the luciferase activity was measured as already described. A dose and time dependent assay were carried out. Data are representative of five independent experiments.

## III.4 RESULTS AND DISCUSSION

### III.4.1 Expression, purification and characterization of the BCL10-CARD domain

Expression of the N-terminal region of BCL10 (the CARD domain, M.W.16238 Da) doubly mutated on Cys29 and Cys57 to Serines, was carried out in BL21(DE3). The sequence of recombinant domain carried an N-terminal linker used for the affinity purification is reported in Fig.1

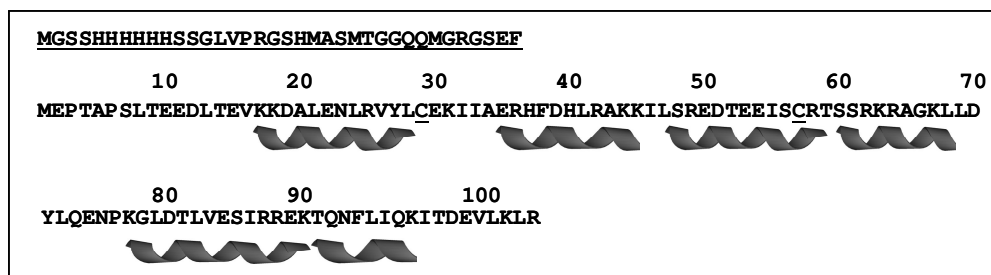


**Figure 1:** Amino acidic sequence of the BCL-10 CARD domain used in this study. The two mutated cysteines and the linker (without numbering) are underlined.

The purified protein, soluble in 100 mM sodium acetate pH 4.5 buffer, was analyzed by SDS-PAGE (Fig.2A). Furthermore, to assess the proper folding, an analysis by far-UV circular dichroism was performed. Spectra were acquired in sodium acetate  $1 \times 10^{-6}$  M buffer solution at pH 4.5 at room temperature. The final CD spectrum, reported in Fig.2B, shows one negative band centred at 208 nm with a shoulder at 222 nm and a positive band at 196 nm. These values are typical for  $\alpha$ -helical structures.

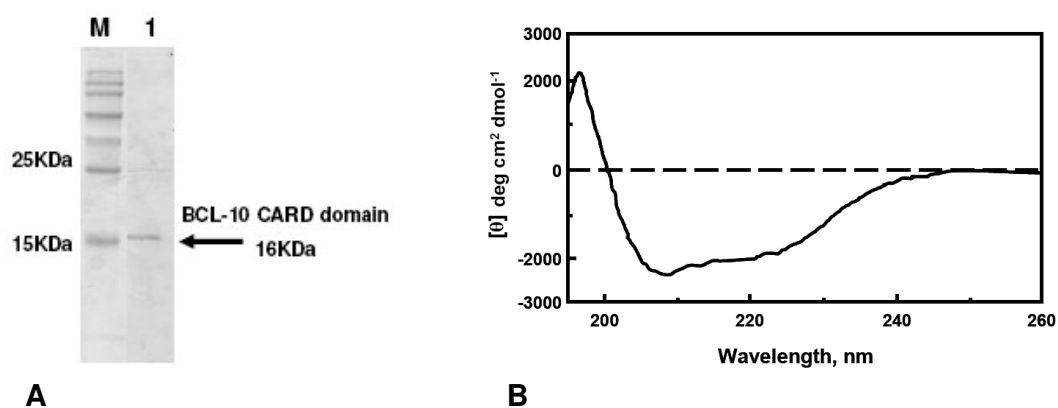


**Figure 2:** **A)** 15% SDS-PAGE analysis of the recombinant CARD domain of BCL10. Lane M, Perfect Protein Marker 15-150 KDa (Novagen); lane 1, purified BCL-10 CARD domain **B)** BCL10-CARD domain CD spectrum.

### III.4.2 Identification of BCL10-CARD regions involved in self-association

To identify the specific regions involved in BCL10-CARD domain self-association a simple and effective approach was followed [38,39].

An ELISA assay was set up to monitor the binding, measure the affinity and select the pre-saturation concentrations needed to carry out competition assays. The protein was enzymatically fragmented and the resulting peptides were fractionated by RP-HPLC and then used as competitors in the binding competition assay, identifying those able to disrupt the binding [40].

#### III.4.2.1 BCL10–CARD domain self association assay

Preliminary ELISA-like assay experiments were performed immobilizing the BCL10-CARD domain on the microtiter plate and verifying its binding to the biotin-labelled BCL10-CARD domain, using the biotin-streptavidin system to detect association. Increasing concentrations of biotinylated BCL10-CARD domain (0.2  $\mu\text{M}$ , 0.4  $\mu\text{M}$ , 0.8  $\mu\text{M}$ , 1.3  $\mu\text{M}$ , 2.6  $\mu\text{M}$ ) were applied to the unlabelled BCL10-CARD domain coated at three different concentrations (0.12  $\mu\text{M}$ , 0.30  $\mu\text{M}$  and 0.6  $\mu\text{M}$ ). Detection was achieved using the STR-HRP conjugate and the absorbance was measured at 490 nm. Binding was saturable for concentrations of soluble protein higher than about 1.5  $\mu\text{M}$ , suggesting that several BCL10-CARD molecule can bind to one coated polypeptide. In Fig. 3, the plot of curves relative to these bindings at different protein concentrations is reported.  $K_D$  values were obtained by averaging the  $K_D$  on the three curves derived by non-linear regression fitting of data and was estimated to be  $1.33 \pm 0.16 \mu\text{M}$ .

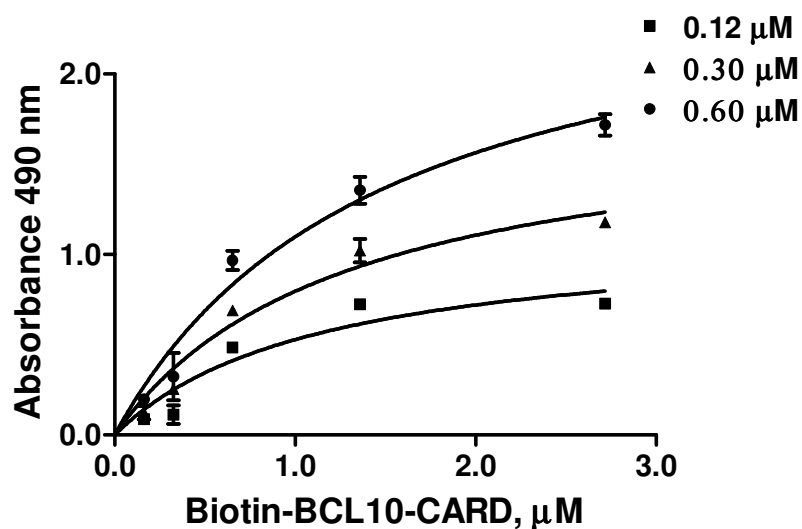


**Figure 3:** Dose-dependent binding curves of biotinylated BCL10-CARD domain to the unlabelled protein.

For the binding competition assay, BCL-CARD was coated at 0.12  $\mu\text{M}$  and the biotinylated variant was used at 0.80  $\mu\text{M}$ .

### III.4.2.2 Protein digestion with trypsin and peptide fractionation

Proteolytic digestion with trypsin was carried out on the BCL10-CARD domain as reported in the section III.3.2.4 of Methods.

The tryptic digestion mixture was separated by RP-HPLC and 11 fractions, 1F to 11F, were collected. The lyophilized fractions were reconstituted in water, properly diluted with buffer and subsequently assayed as competitors in the BCL10-CARD domain self-association test.

### III.4.2.3 Protein fragments characterization and screening competition assay

Competitors were used at a nominal 5-fold excess over the soluble protein. Peptide fragments concentration was deduced by assuming an initial quantitative protein cleavage by trypsin and a subsequent recovery of 50% by RP-HPLC fractionation.

Tryptic peptides were identified by LC-MS/MS analysis (Fig.4). An LC-MS analysis of single fractions also allowed the determination of fragments distribution and composition as described in Table I. Relative distribution of fragments, in column 3, were calculated by comparing area integration of extracted ion peaks from a given fragment taken from the different fractions. The relative composition within each fraction was derived by comparing area integrations of extracted ion peaks of all fraction components. As can be seen, fractions F1 and F2 contained no peptides, whereas fractions F3-F8 and fraction F10 contained more than one fragment. Fraction F9 contained only the L68-K77 fragment. In spite of the prolonged reaction times and of the high temperature (37°C), many fragments contained uncleaved lysines and arginines peptide bonds, suggesting the presence of poorly accessible cleavage site. Several other fragments, such as the N-terminal M1-K17 bearing the linker tetrapeptide GSEF (see Fig.1) and H38-K45 and T59-K67 peptides were only poorly detected and thus not considered further.

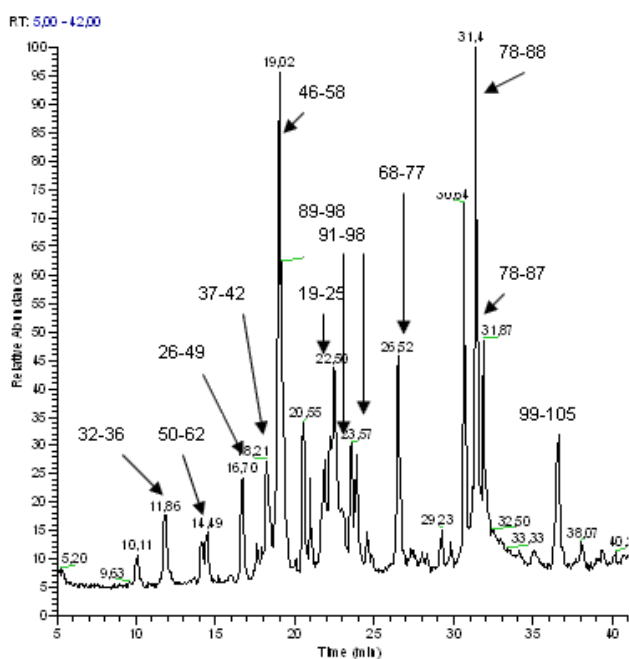


**Figure 4:** LC-MS chromatogram of digested CARD domain with the identified sequences.

For the assay purpose, the lyophilized fractions were reconstituted in water, properly diluted with buffer and subsequently assayed as competitors in the BCL10-CARD self-association test. Screening results are expressed as percentage of inhibition of self-association and are summarized in Table I. As expected, fractions F1 and F2 where no peptides were detected, provided no binding reduction. Among the remaining fractions, only fraction F8 containing the peptides BCL10 [91-98] (sequence: TQNFLIQK, relative abundance 63%) and the homolog BCL10 [89-98] (sequence: EKTQNFLIQK, abundance 37%), produced a relevant binding reduction (about 50%). The sequence EKTQNFLIQK, compared to the most abundant [91-98] fragment only contained two additional residues at the N-terminus and was not considered for further investigations, while the peptide BCL10 [91-98] (Peptide I) was re-prepared by chemical synthesis as a C-terminally amidated and N-terminally acetylated variant.

**Table I**

<i>Fraction</i>	<b>BCL10-CARD domain fragments</b>	<b>Relative distribution of fragments within fractions (%)</b>	<b>Relative composition of the fraction (%)</b>	<b>Extent of inhibition of self-association (%)</b>
<b>F1</b>	//	//	//	//
<b>F2</b>	//	//	//	//
<b>F3</b>	I46-R49	100	24	20
	I32-R36	100	41	
	E50-R58	100	35	
<b>F4</b>	K45-R49	100	7	0
	L111-K115	100	44	
	V26-K31	100	56	
<b>F5</b>	G78-R88	100	100	16
	G78-R87	100	8	
<b>F6</b>	H37-R42	100	0.7	10
	T91-K105	100	0.3	
	I99-K105	93	88	
	D19-R25	22	3	
	K18-R25	100	19	
<b>F7</b>	D19-R25	88	83	7
	N108-K115	100	15	
	E89-K98	32	2	
<b>F8</b>	E89-K98	68	37	45
	T91-K98	100	63	
<b>F9</b>	L68-K77	100	100	10
<b>F10</b>	E89-K115	100	87	12
	I99-K105	7	10	
	I46-R58	100	3	

### III.4.3 Design of BCL10 peptides

A model for the BCL10-CARD, retrieved from the ModBase server of the University of California at San Francisco (<http://modbase.compbio.ucsf.edu/>) and visualized by the WebLab ViewerPro software, vers. 3.7 (Molecular Simulations Inc.), was used to localize the putative structure of the selected peptide [91-98] within the CARD structure. The model, obtained using as template the X-ray crystallography structure of the apoptotic protease activating factor 1 CARD (pdb code: 1cy5 [48]) despite the very low sequence identity (17%), has a very low E-value ( $2 \times 10^{-8}$ ) and a model score of 0.99. This putative homology model of CARD domain shows that the segment [91-98] is inserted in the 6<sup>th</sup> helix of the bundle.

To also investigate the influence of the structured flanking region of the selected peptide on CARD self-association, two additional BCL10 peptides containing the 91-

98 stretch at the C-terminus were designed and synthesized. These peptides, named Peptide II and Peptide III, contained residues 78-98 and 68-98, respectively (table II). Thus, on examination of this model, it can be seen that the 91-98 region is inside the modelled sequence and virtually corresponds to the 6<sup>th</sup> helix (partially distorted); the sequence 78-98 instead, covers the 5<sup>th</sup> and the 6<sup>th</sup> helix, and the 68-98 fragment corresponds to the protein region including helices 5 and 6, the loop between helix 5 and helix 4 and part of the helix 4.

<b>Peptide I</b>	<b>TQNFLIQK</b>	<b>BCL10 [91-98]</b>	<b>M.W.1031.58</b>
<b>Peptide II</b>	<b>GLDTLVESIRREKTQNFLIQK</b>	<b>BCL10 [78-98]</b>	<b>M.W.2746.41</b>
<b>Peptide III</b>	<b>LLDYLQENPKGLDTLVESIRREKTQNFLIQK</b>	<b>BCL10 [68-98]</b>	<b>M.W.3731.01</b>

**TABLE II:** The three peptides used to identify residues involved in protein-protein interactions.

### III.4.3.1 Synthesis, purification and characterization of BCL10 peptides

Peptides I-III were synthesized by SPPS following Fmoc chemistry, purified by RP-LC and characterized by LC-MS.

Far UV-Circular dichroism experiments were carried out to investigate their structural behaviour. CD experiments were performed in 10 mM phosphate pH 7.0 buffer at room temperature, using all peptides at the concentration of 20  $\mu$ M. The spectra do not show the occurrence of canonical structures for the three synthetic fragments (Fig.5). However, negative bands at 208 nm and shoulders at 222 nm are indicative of a tendency to adopt  $\alpha$ -helical conformations.

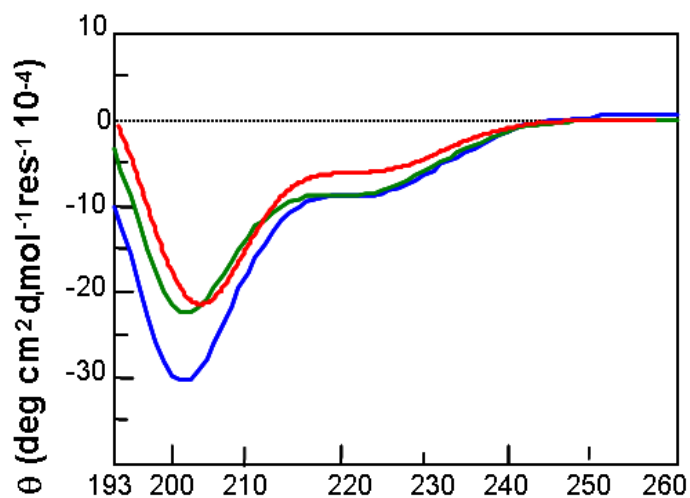


**Figure 5:** Far-UV CD spectrum of the BCL10-CARD peptides: Peptide I BCL10[91-98] (red), Peptide II BCL10[78-98] (green) and Peptide III BCL10[68-98] (blu).

### III.4.3.2 Competitive ELISA assay with BCL10 peptides

The synthetic peptides I-III were utilized in a dose response competition assay under the same conditions used for the protein fragments screening (coating 0.12  $\mu\text{M}$ ; biotinylated protein 0.80  $\mu\text{M}$ ). They were utilized at increasing concentrations between 0.03  $\mu\text{M}$  and 15  $\mu\text{M}$ . Results are reported in Fig. 6. Data show that the shorter Peptide I BCL10[91-98] strongly reduces protein self-association in a dose-dependent fashion, whereas, unexpectedly, the longer polypeptides II and III, containing this active sequence, only slightly interfered with the interaction. In particular, Peptide I inhibited the protein association by 90% at the highest dose of 15  $\mu\text{M}$  and exhibited an  $\text{IC}_{50}$  of 70 nM. Conversely, Peptides II and III exhibited an efficacy between 30% and 40% only at the highest concentration tested this result being suggestive of a tendency of peptides to self-aggregation.

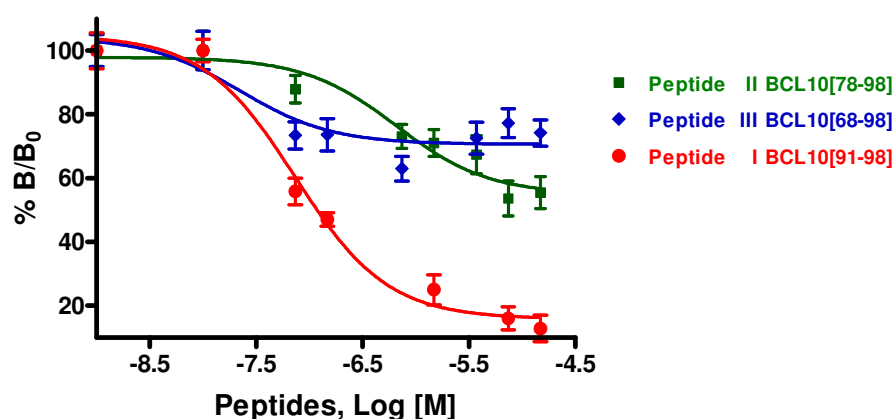


**Figure 6:** Dose-dependent competitive ELISA assay with synthetic Peptide I-III corresponding to fragments [91-98], [78-98] and [68-98] of BCL10-CARD domain, respectively.

### III.4.3.3 Characterisation of the oligomeric state of Peptide I and Peptide II by SEC analysis

The oligomerization state of peptides and their apparent molecular weight were determined by Size Exclusion Chromatography analysis. Peptide I and Peptide II were loaded onto the Biosep/SEC/S 2000 column at five different concentrations (5  $\mu\text{M}$ , 10  $\mu\text{M}$ , 50  $\mu\text{M}$ , 100  $\mu\text{M}$ , 400  $\mu\text{M}$ ) using phosphate 50 mM, pH 6.8 buffer. A calibration curve was built using molecular mass markers under the same conditions. Data analysis, reported in table III, shows that, while the Peptide I BCL10[91-98] appeared invariably monomeric, the [78-98] variant eluted as a dimer even at the lowest concentration of 5  $\mu\text{M}$  (Log M = -5.3). This property, together with the inability to efficiently suppress the BCL10-CARD domain self association at concentrations higher than about 1  $\mu\text{M}$ , suggests that the presence of residues 78-90 may favour the formation of peptide oligomers or that the longer structure might induce a conformation more suitable for self-recognition.

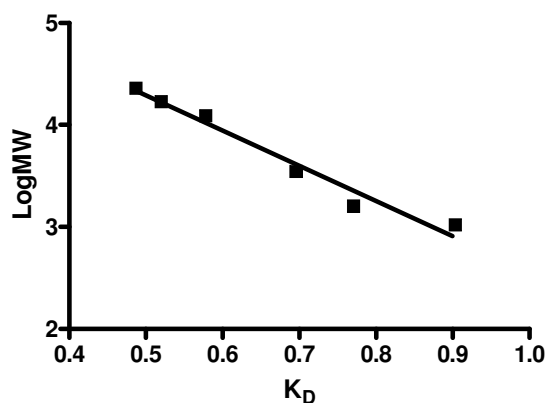


**Figure 7:** Calibration curve used to determine the apparent  $M_r$  of Peptide I and Peptide II.  $K_D$  is the partition coefficient, calculated as  $(V_t - V_o)/(V_t - V_o)$ , where  $(V_t)$  is the elution volume at the elution time of the peptide,  $V_o$  is the column void volume, while  $V_t$  is the column total volume.

Conc ( $\mu\text{M}$ )	Peptide I	Peptide II
	$MW_{\text{exp}}(\text{Da})/MW_{\text{th}}= 1032$	$MW_{\text{exp}}(\text{Da})/MW_{\text{th}}= 2746$
400	1314	5802
100	1322	5470
50	1309	5352
10	1294	4981
5	1245	5045

**TABLE III:** Characterisation of the oligomeric state of Peptide I and Peptide II. Gel-filtration analysis of synthetic peptides on Biosep/SEC/S 2000 buffer phosphate 50 mM, pH=6.8. Gel-filtration analyses were performed at five different concentrations between 400 and 5  $\mu\text{M}$  (each run was repeated at least twice). A calibration curve was used to determine the MWs. Calibrants were: Trypsinogen, 23.0 kDa; Myoglobin, 17.0 kDa; Cytochrome C, 12.4 kDa; Angiotensin II, 1.0 kDa; an unrelated synthetic peptide I, 3.5 kDa; an unrelated synthetic peptide II, 1.67 kDa.

### III.4.3.4 Ala-scanning assay

To further investigate the inhibiting properties of Peptide III and to explore residues involved in protein-protein interactions, four mutated variants of Peptide III, where adjacent residue pairs were substituted by alanines, were next designed and synthesized, as reported in table IV.

These peptides were synthesized by SPPS following Fmoc chemistry, purified by RP-LC and characterized by LC-MS.

<b>Peptide IV</b>	<b>AANFLIQK</b>	<b>BCL10[91-98]T91A,Q92A</b>	<b>M.W. 945.14</b>
<b>Peptide V</b>	<b>TQAALIQK</b>	<b>BCL10[91-98]N93A,F94A</b>	<b>M.W. 913.09</b>
<b>Peptide VI</b>	<b>TQNFAAQK</b>	<b>BCL10[91-98]L95A,I96A</b>	<b>M.W. 948.05</b>
<b>Peptide VII</b>	<b>TQNFLIAA</b>	<b>BCL10[91-98]Q97A,K98A</b>	<b>M.W. 918.03</b>

**TABLE IV:** The four double alanine mutated peptides used to identify residues involved in protein-protein interactions.

The mutated variants, Peptides IV, V, VI and VII were tested in a dose-response assay along with the parent BCL10[91-98] again using pre-saturation conditions (coating 0.12  $\mu\text{M}$ ; biotinylated protein 0.80  $\mu\text{M}$ ). For this assay, competitor concentrations ranged between 0.03  $\mu\text{M}$  and 15  $\mu\text{M}$ . Subsequent steps were carried out as described. The results are summarized in Fig. 8. As shown, Peptides I, V, VI and VII still reduced the BCL10-CARD domain self-association, whereas Peptide IV with Thr91 and Gln92 changed to alanine was almost ineffective even at the highest dose (15  $\mu\text{M}$ ). Notably, Peptide VI, having residues Leu95 and Ile96 changed to alanines, exhibited only a reduced efficacy, being able to lessen the interaction to 50% only at the highest concentration. Also the Peptide V, with substitutions on residues N93 and F94, had a ten folds lower efficacy (about  $10^{-6}$  M) than Peptides IV and VII. Together, these data suggest that residues BCL10 [91-98] can have a relevant role in BCL10-CARD domain self-association and that the side chains of Thr91, Gln92, Leu95 and Ile96 may represent key contact points between protein monomers.

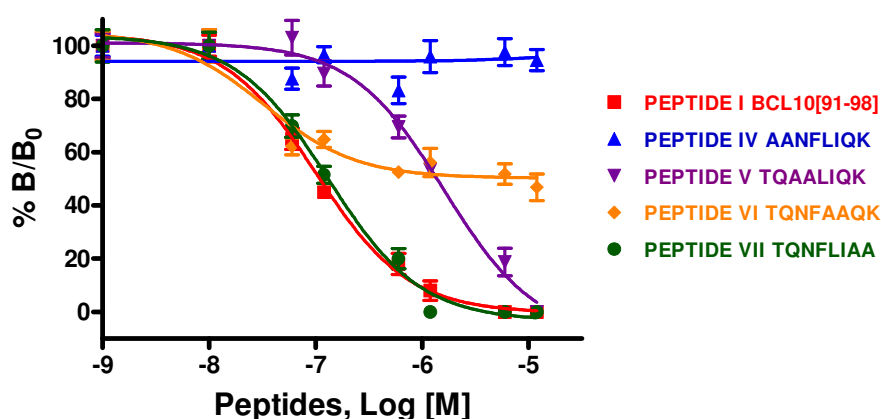


**Figure 8:** Dose-dependent competitive ELISA assay with synthetic Peptides I, IV, V, VI, VII. Peptides IV-VII are doubly-mutated synthetic variants of the most active [91-98] fragment.

### III.4.4 Cellular assays

In order to confirm the efficacy of the selected peptide to block self-association between CARDS of BCL10 and possibly the association between BCL10 and other protein partners, we planned cellular experiments of co-immunoprecipitation and luciferase activity. For this purpose the peptides BCL10[91-98] and BCL10[91-98]T91A,Q92A were opportunely prepared using TAT-conjugated variants to favour cell entry [49]. Peptides were also labelled with fluorescein to confirm quantitative peptide cellular viability.

#### III.4.4.1 Synthesis, purification, serum stability and characterization of TAT-conjugated and FITC-TAT-conjugated Peptide VIII and IX

Peptides BCL10[91-98] and BCL10[91-98]T91A,Q92A were prepared fused to the basic region of the HIV TAT protein (fragment 48-60) [41]. These peptides, reported in table V, were synthesized by SPPS following Fmoc chemistry, purified by RP-LC

and characterized by LC-MS. Aliquots of Peptides VIII and IX were also prepared with N-terminal fluorescein labelling to monitor cell delivery.

---

<b>Peptide VIII</b>	<b><i>FITC-βA-GRKKRRQRRRPPQ-AA-TQNFLIQK</i></b>	<b><i>TAT-BCL10[91-98]</i></b>
<b>Peptide IX</b>	<b><i>FITC-βA-GRKKRRQRRRPPQ-AA-AANFLIQK</i></b>	<b><i>TAT-BCL10[91-98]T91A,Q92A</i></b>

---

**TABLE V:** Sequences of TAT-conjugated peptides utilized in the cellular assays.

The stability of TAT-fused Peptides VIII and IX was determined by RP-HPLC analysis of peptide samples incubated with serum. The samples, serially diluted in PBS pH 7.4 buffer containing 10% FCS were incubated at 37°C for 24 h. Aliquots were removed at different times (0, 4 h, 8 h, 12 h, 16 h and 20 h) and were analyzed after centrifugation. In Fig.9, a plot of peak area (%) versus time is reported and shows that peptides resulted stable in serum for at least 24 hours.

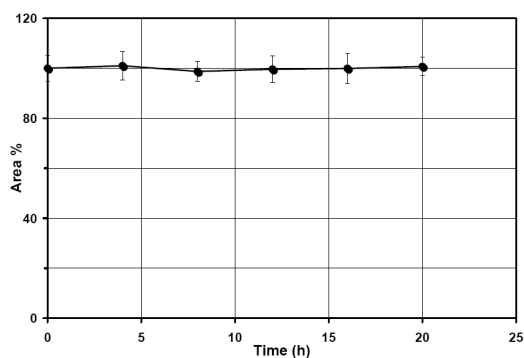


**Figure 9:** Stability of the TAT-fused Peptide VIII in serum.

### III.4.4.2 Immunoblotting and co-precipitation analysis

HEK293 cells were co-transfected with plasmids encoding for two tagged versions of BCL10 (1-127) bearing the HA and the FLAG epitope. Lysates from transfected cells were immunoprecipitated with anti-FLAG antibodies either in the absence or presence of increasing concentrations of Peptide VIII added at concentrations ranging between 5 and 100  $\mu$ M. Co-precipitating HA-tagged BCL10 (1-127) was detected by immunoblot assay. Importantly, the peptide repressed self association of BCL10 (1-127) in a dose dependent manner and at 100  $\mu$ M the binding was totally abolished (Fig.10).

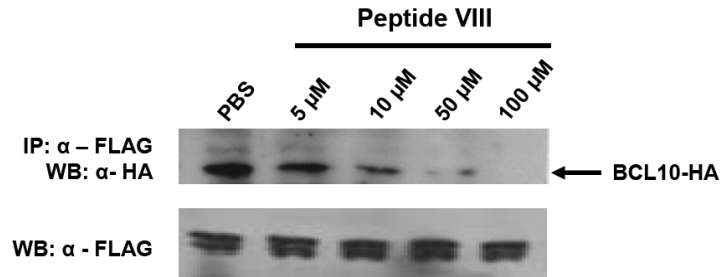


**Figure 10:** In vitro inhibition of BCL10-CARD (region 1-127) self-association in lysates of BCL10-overexpressing HEK293 cells. Two differentially tagged protein constructs were utilized in these assays. Roughly 50% binding inhibition was achieved at 5  $\mu$ M Peptide VIII.

### III.4.4.3 Assessment of peptide entry into HEK 293 cells

HEK293 cells transfected with BCL10 (1-127) were treated for 5 h at R.T. with FITC and TAT-conjugated Peptides VIII and IX (used as a control) at 100  $\mu$ M, 200  $\mu$ M and 300  $\mu$ M. Samples were analyzed by fluorescence microscopy. Under these conditions, both peptides appeared uniformly distributed in HEK293 cells at the concentration of 200  $\mu$ M (Fig. 11).

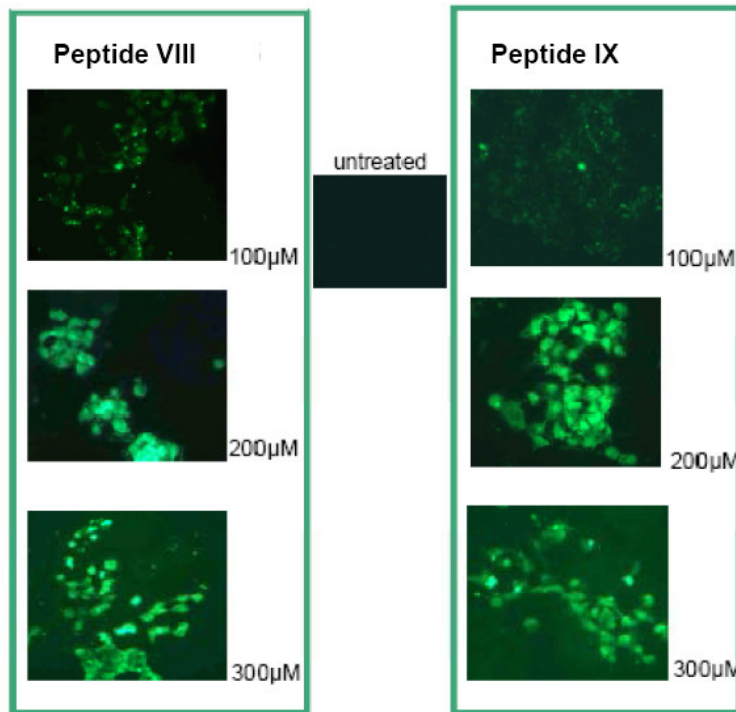


**Figure 11:** Assessment of peptide entry within BCL10-transfected HEK293 cells. Cells were incubated with peptide solutions at different concentrations (100  $\mu$ M, 200  $\mu$ M and 300  $\mu$ M) and subsequently analyzed by fluorescence microscopy. A picture of the untreated cells is also reported in the middle.

### III.4.4.4 NFκB luciferase reporter gene assay

The ability of the selected peptides to inhibit NF-κB activation induced by BCL10 (1-127) over-expression and PKC activation was determined by luciferase activity measurement using HEK293 cells. This system provides a reporter gene containing the NF-κB promoter (the DNA sequence that regulates NF-κB-induced genes) cloned upstream of the luciferase gene. The protein encoded by the luciferase gene fluoresces strongly when the NF-κB promoter is active, making it easy to determine the level of activation based on the level of luminescence.

HEK293 cells were transiently co-transfected with an expression vector encoding BCL10 (1-127), together with an NF-κB-luciferase and β-galactosidase reporter vector. After 16 h, the cells were treated for 5 h with TAT-Peptide VIII and TAT-Peptide IX, used as a control, at 5 μM, 10 μM and 50 μM. Luciferase activity was determined from cell extracts using a luciferase assay system and a luminometer. The results of these experiments, shown in Fig.12, indicated that Peptide VIII repressed the activation of NF-κB promoted by BCL10 over-expression in a dose dependent manner with a maximum efficacy of about 50% at the highest dose of 50 μM. In the same experiment, treatment of cells with the control Peptide IX had no effect on NF-κB activity.

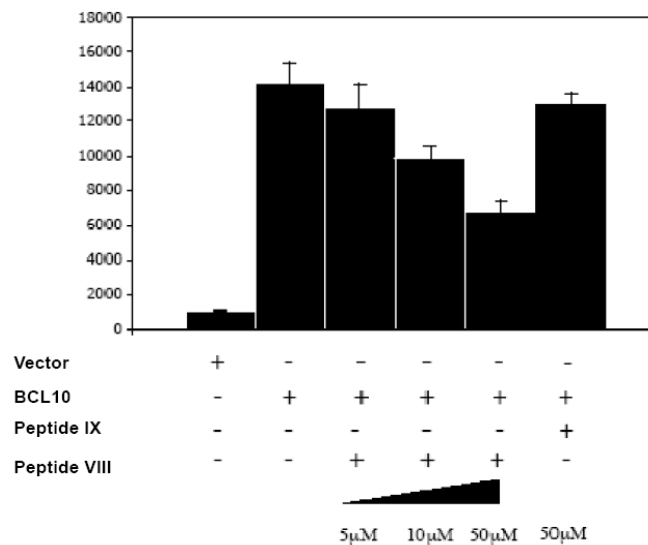


**Figure 12:** Luciferase assay: TAT-BCL10[91-98] peptide inhibits in a dose dependent manner BCL10 overexpression-mediated NF-κB activation.

Since PKC activity is required for LPA-induced NF-κB activation, we also tested whether Peptide VIII inhibited activation of NF-κB following PKC activation [42].

HEK293 cells were transiently transfected with an NF-κB-luciferase and β-galactosidase reporter vector. In a preliminary experiment, a dose dependent assay was carried out adding the TAT- Peptide VIII and control at 5 μM, 10 μM and 50 μM to cells left untreated or stimulated with 40 ng/mL PMA, a surrogate of 1,2-diacylglycerol (the natural activator of conventional and novel PKCs) and 1 μM ionomycin, a calcium ionophore. After 5 h luciferase activity was measured, as previously described. Data analysis shows that the TAT-Peptide VIII repressed the activation of NF-κB following PKCs activation in a dose dependent manner (Fig.13). 50 μM TAT-Peptide VIII was able to block NF-κB activation by about 70%.

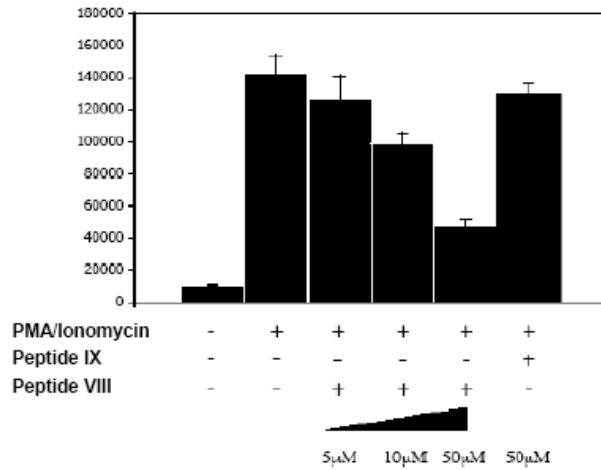


**Figure 13:** Luciferase assay: TAT-BCL10[91-98] peptide inhibits PKC-mediated NF-κB activation in a dose-dependent manner.

Subsequently a time dependent assay was carried out by adding the TAT-Peptide VIII and the control at 50 μM to cells left untreated or stimulated with ionomycin and PMA. Luciferase activity was measured after 1h, 3h and 5 h (Fig.14). In agreement with the previous results, data confirmed that the TAT-BCL10[91-98] peptide inhibits at 50 μM PKC-mediated NF-κB activation in a time-dependent and dose-dependent way.

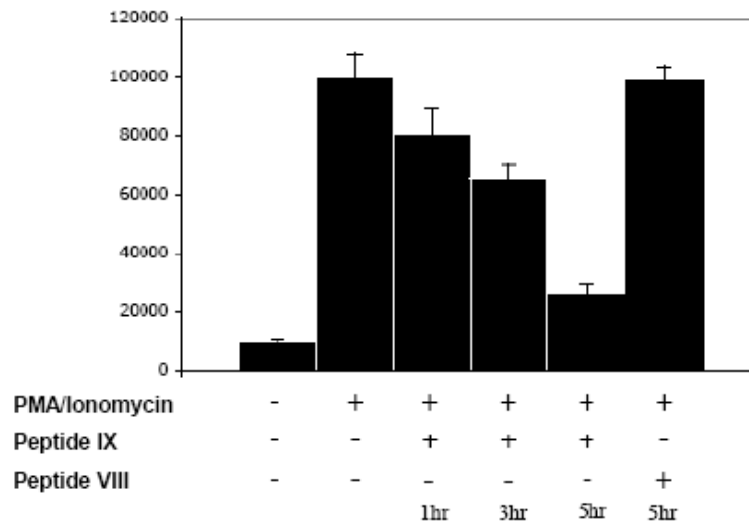


**Figure 14:** Luciferase assay: TAT-BCL10[91-98] peptide inhibits at 50 μM PKC-mediated NF-κB activation in a time-dependent manner

### III.5 CONCLUSIONS AND PERSPECTIVES

In lymphocytes, the N-terminal CARD domain of BCL10 binds to the CARD domain of CARMA1, this interaction is necessary for the correct transduction of the NF- $\kappa$ B activating signal [26].

Accordingly, the experimental hypothesis addressed here is that disruption of the pattern of interactions involving the CARD of BCL10 should down-regulate BCL10-dependent NF- $\kappa$ B activation.

Given these premises, knowledge of regions involved in protein-protein interactions becomes of utmost importance for the design of BCL-10-targeted NF- $\kappa$ B inhibitors. Hence, by means of a procedure described in a previous paper [40]. The CARD domain of BCL10 has been fragmented with trypsin and the peptides obtained following HPLC fractionation have been used as competitors in a CARD-CARD interaction assay. Using this method, a fragment corresponding to residues 91-98 of the protein (Peptide I), that strongly abolishes protein self-association both in vitro and in a BCL-10-overexpressing cell line, has been isolated. Noticeably, Peptide I has an  $IC_{50}$  of about 70 nM, although when fused to the basic region of the TAT protein (Peptide VIII) it is less effective, and shows an  $IC_{50}$  of only about 5  $\mu$ M (see Fig.10 ). This result implies both a reduced affinity of the modified peptide for the protein domain and to a higher stability of the complexes formed by BCL10 in the presence of other proteins. This hypothesis is confirmed by the cellular assays, where a concentration of about 50  $\mu$ M is needed to block NF- $\kappa$ B activation by 70% (Fig.12,13,14). Importantly, the loss of activity of Peptide VIII is not due to peptide degradation within the cell medium, as it appeared highly stable when in contact with serum for over 24 h. Also Peptides II and III, designed to account for adjacent CARD helices and containing the wild type sequence 91-98 at the C-terminus, resulted poorly effective in reducing the BCL10-CARD self-association in vitro. This behaviour can be explained by the propensity of the longer polypeptides to self-aggregation and by a consequent, inaccessibility of contact residues even at low concentrations. This hypothesis is supported by the observation that the 78-98 segment is dimeric even at 5  $\mu$ M and a similar dimeric structure can be also expected for the 68-98 peptide. Indeed, the oligomeric organization of these peptides reflects the CARD tendency to self-associate and corroborates the view that recognition is mediated by the C-terminal helix of the globular domain. However the possibility that other residues within the 78-90 stretch mediates self-recognition or that the longer peptides likely adopt a conformation which is closer to that within the full length CARD, can not be ruled out. These biochemical data also provide evidence that the side chains of Thr91, Gln92, Leu95 and Ile96 are implicated in the pattern of interactions involving CARD self-recognition of BCL10 and the inability of the ThrGln91,92AlaAla synthetic mutant to activate NF- $\kappa$ B even after PMA/ionomycin stimulation, suggesting a critical role for these amino acids in mediating CARD-CARD contacts. Notably, residues 91, 92, 95 and 96, given their alternate distribution along the sequence, could be part of an extended surface on one side of the putative helix 6. It is well known that BCL10 forms a large protein complex known with CARMA1 and MALT1 known as CBM (**CARMA1-BCL10-MALT1**), which is the ultimate effector of BCL10 activity [46]. Several studies have reported direct interactions between the CARDS of BCL10 and CARMA1 and between the Ig-like domain of MALT1 and residues 107-119 of BCL10. Very recently it has also been reported that residues from the putative helix 5 of the BCL10 CARD (D80 and E84) mediate the binding to the death domain (DD) of MALT1 and are essential for downstream NF- $\kappa$ B activation; furthermore it has been

demonstrated that mutations within the 6<sup>th</sup> helix (Q92, L95, I96) preclude this binding by seemingly altering the CARD structural stability [13]. Our findings essentially agree with these data as they fit with a model of multiple interactions between CARDS and between CARD and the MALT1 DD, whereby helix 5 mediates the recognition with MALT1 and residues from the adjacent helix 6 are involved in CARD self association.

This work offers the proof of concept that blocking the CARD domain of BCL10 (and possibly the association with other interacting partners) is an effective way to selectively reduce NF- $\kappa$ B activation and can be a valuable therapeutic approach for treatment of specific pathologic conditions associated with inappropriate NF- $\kappa$ B activation.

### III.6 REFERENCES

1. Steller H. Mechanisms and genes of cellular suicide. *Science* (1995) 267(5203):1445-9.
2. Thompson C.B. Apoptosis in the pathogenesis and treatment of disease. *Science* (1995) 267(5203):1456-62.
3. Weber C.H. and C. Vincenz The death domain superfamily: a tale of two interfaces? *Trends Biochem. Sci.* (2001) 26(8):475-81.
4. Hofmann K., Bucher P., and J. Tschopp The CARD domain: a new apoptotic signalling motif. *Trends Biochem. Sci.* (1997) 22(5):155-156
5. Park H., Lo Y.C., Lin S.C., Wang L., Yang J.K. and H. Wu The death domain superfamily in intracellular signalling of apoptosis and inflammation. *Annu. Rev. Immunol.* (2007) 25:561-586
6. Guet, C. and P. Vito Caspase recruitment domain (CARD)-dependent cytoplasmic filaments mediate bcl10-induced NF-kappaB activation. *J. Cell. Biol.* (2000) 148(6):1131-40
7. Boldin MP, Goncharov TM, Goltsev YV and D. Wallach Involvement of MACH, a novel MORT1/FADD-interacting protease, in Fas/APO-1- and TNF receptor-induced cell death. (1996) *Cell.* 14; 85(6):803-15
8. Adrain C. and S.J. Martin The mitochondrial apoptosome: a killer unleashed by the cytochrome seas. *Trends Biochem. Sci.* (2001) 26(6):390-7
9. Bouchier-Hayes L. and S.J. Martin CARD games in apoptosis and immunity. *EMBO Rep* (2002) 3(7):616-21.
10. Liang H. and S.W. Fesik Three-dimensional structures of proteins involved in programmed cell death. *J. Mol. Biol.* (1997) 274(3):291-302.
11. Zhou, P., Chou J., Olea R.S., Yuan J. and G. Wagner Solution structure of Apaf-1 CARD and its interaction with caspase-9 CARD: a structural basis for specific adaptor/caspase interaction. *Proc. Natl. Acad. Sci. U. S. A.* (1999) 96(20):11265-70.
12. Lucas P.C., Yonezumi M., Inohara N., McAllister-Lucas L.M., Abazeed M.E., Chen F.F., Yamaoka S., Seto M. and G. Nunez Bcl10 and MALT1, independent targets of chromosomal translocation in malt lymphoma, cooperate in a novel NF-kappa B signaling pathway. *J. Biol. Chem.* (2001) 276(22):19012-9
13. Langel F.D., Jain N.A, Rossman J.S., Kingeter L.M., Kashyap A.K. and B.C. Schaefer Multiple protein domains mediate interaction between Bcl10 and MALT1. *J. Biol. Chem.* (2008) Sep 19. Epub ahead of print
14. Ruefli-Brasse A.A., Lee W.P., Hurst S. and V.M. Dixit Rip2 participates in Bcl10 signaling and T-cell receptor mediated NF-kappaB activation. *J. Biol. Chem.* (2004) 279(2):1570-4.
15. Gaide O., Martinon, F., Micheau O., Bonnet D., Thome M. and J. Tschopp Carma1, a CARD-containing binding partner of Bcl10, induces Bcl10 phosphorylation and NF-kappaB activation. *FEBS* (2001) 496(2-3):121-127
16. Pomerantz J. L., Denny E.M. and D. Baltimore CARD11 mediates factor-specific activation of NF-kappaB by the T cell receptor complex. *Embo J.* (2002) 21(19), 5184-5194
17. McAllister-Lucas L. M., Inohara N., Lucas P. C., Ruland J., Benito A., Li Q., Chen S., Chen F.F., Yamaoka S., Verma I. M., Mak T. W. and G. Nunez Bimp1, a MAGUK family member linking protein kinase C activation to Bcl10-mediated NF-kappaB induction. *J. Biol. Chem.* (2002) 276:30589-30597
18. Wang L., Guo Y., Huang W. J., Ke X., Poyet J. L., Manji G.A., Merriam S., Glucksmann, M.A., Di Stefano P.S., Alnemri E. S. and J. Bertin Card10 is a novel caspase recruitment domain/membrane-associated guanylate kinase family member

that interacts with BCL10 and activates NF-kappa B. *J. Biol. Chem.* (2001) 276(24):21405-21409

19. Bertin J., Guo, Y., Wang L., Srinivasula S. M., Jacobson M. D., Poyet J. L., Merriam S., Du M.Q., Dyer M.J., Robison K.E., Di Stefano P.S. and E.S. Alnemri CARD9 is a novel caspase recruitment domain-containing protein that interacts with BCL10/CLAP and activates NF-kappa B. *J. Biol. Chem.* (2000) 275(52):41082-41086

20. Gaide O., Favier B., Legler D. F., Bonnet D., Brissoni B., Valitutti S., Bron C., Tschopp, J. and M. Thome CARMA1 is a critical lipid raft-associated regulator of TCR-induced NF-kappa B activation. *Nat. Immunol.* (2002) 3(9):836-843

21. Hara H., Wada T., Bakal C., Koziaradzki I., Suzuki S., Suzuki N., Nghiem M., Griffiths E. K., Krawczyk C., Bauer B., D'Acquisto F., Ghosh S., Yeh W. C., Baier G., Rottapel R. and J. M. Penninger The MAGUK family protein CARD11 is essential for lymphocyte activation. *Immunity* (2003) 18(6):763-775

22. Wang D., You Y., Case S.M., McAllister-Lucas L.M., Wang L., Di Stefano P.S., Nunez G., Bertin J., and X. Lin A requirement for CARMA1 in TCR-induced NF-kappa B activation. *Nat. Immunol.* (2002) 3(9):830-835

23. Stilo R., Liguoro D., Di Jeso B., Formisano S., Consiglio E., Leonardi A. and P. Vito Physical and functional interaction of CARMA1 and CARMA3 with I-kappa kinase gamma-NFkappaB essential modulator. *J.Biol. Chem.* (2004) 279(33):34323-34331

24. Zhou H., Wertz I., O'Rourke K., Ultsch M., Seshagiri S., Eby M., Xiao W. and V. M. Dixit. Bcl10 activates the NF-kappaB pathway through ubiquitination of NEMO. *Nature* (2004) 427(6970):167-71

25. Sun L., Deng L., Ea C.K., Xia Z.P. and Z.J. Chen The TRAF6 ubiquitin ligase and TAK1 kinase mediate IKK activation by BCL10 and MALT1 in T lymphocytes. *Mol. Cell.* (2004) 14(3):289-301

26. Egawa T., Albrecht B., Favier B., Sunshine M.J., Mirchandani K., O'Brien W., Thome, M. and D.R. Littman Requirement for CARMA1 in antigen receptor-induced NF-kappa B activation and lymphocyte proliferation. *Curr. Biol.* (2003) 13(14):1252-1258

27. Jun J.E., Wilson L.E., Vinuesa C.G., Lesage S., Blery M., Miosge L.A., Cook M.C., Kucharska E.M., Hara H., Penninger J.M., Domashenz H., Hong N.A., Glynne R.J., Nelms, K.A. and C.C. Goodnow Identifying the MAGUK protein Carma-1 as a central regulator of humoral immune responses and atopy by genome-wide mouse mutagenesis. *Immunity* (2003) 18(6):751-762

28. Xue L., Morris S. W., Orihuela C., Tuomanen E., Cui X., Wen R., and D. Wang Defective development and function of Bcl10-deficient follicular, marginal zone and B cells. *Nat. Immunol.* (2003) 4:857-865

29. Willis T.G., Jadayel D.M., Du M.Q., Peng H., Perry A.R., Abdul-Rauf M., Price H., Karra, L., Majekodunmi O., Wlodarska I., Pan L., Crook T., Hamoudi R., Isaacson P. G. and M.J. Dyer Bcl10 is involved in t(1;14)(p22;q32) of MALT B cell lymphoma and mutated in multiple tumor types. *Cell* (1999) 96:35-45

30. Newton K., and Dixit V. M. *Curr Biol* (2003) 13(14):1247-1251

31. Grabiner B.C., Blonska M., Lin P.C., You Y., Wang D., Sun J., Darnay B.G., Dong C., and X. Lin CARMA3 deficiency abrogates G protein-coupled receptor-induced NF-kappa B activation. *Genes Dev* (2007) 21(8):984-996

32. Wang D., You Y., Lin P.C., Xue L., Morris, S.W. Zeng, H. Wen, R. and X. Lin Bcl10 plays a critical role in NF-kappaB activation induced by G protein-coupled receptors. *Proc. Natl. Acad. Sci. U. S. A.* (2007) 104(1):145-150

33. McAllister-Lucas L.M., Ruland J., Siu K., Jin X., Gu S., Kim D. S., Kuffa P., Kohrt D., Mak T.W., Nunez G. and P.C. Lucas CARMA3/Bcl10/MALT1-dependent NF-kappa B activation mediates angiotensin II-responsive inflammatory signaling in non immune cells. *Proc. Natl. Acad. Sci. U. S. A.* (2007) 104(1):139-144
34. Schulze-Luehrmann J. and S. Ghosh Antigen-receptor signaling to nuclear factor kappa B. *Immunity* (2006) 25:701-715
35. Wegener E. and D. Krappmann CARD-Bcl10-Malt1 signalosomes: missing link to NF-kappaB. *Sci STKE* (2007) 21
36. Willis T.G., Jadayel D.M., Du M.Q., Peng H., Perry A.R., Abdul-Rauf M., Price H., Karran L., Majekodunmi O., Wlodarska I., Pan L., Crook T., Hamoudi R., Isaacson, P.G., and M.J. Dyer Bcl10 is involved in t(1;14)(p22;q32) of MALT B cell lymphoma and mutated in multiple tumor types. *Cell* (1999) 96(1):35-45
37. Zhang Q., Siebert R., Yan M., Hinzmann B., Cui X., Xue L., Rakestraw K.M., Naeve, C. W., Beckmann G., Weisenburger D.D., Sanger W.G., Nowotny H., Vesely M., Callet-Bauchu E., Salles G., Dixit V.M., Rosenthal A., Schlegelberger B. and S.W. Morris Inactivating mutations and overexpression of BCL10, a caspase recruitment domain-containing gene, in MALT lymphoma with t(1;14)(p22;q32). *Nat. Genet.* (1999) 22(1):63-68
38. Lu F., Chi S.W., Kim D.H., Han K.H., Kuntz I.D. and R.K. Guy Proteomimetic libraries: design, synthesis, and evaluation of p53-MDM2 interaction inhibitors. *J. Comb. Chem.* (2006) 8(3):315-25
39. Hershberger S.J., Lee S.G. and J. Chmielewski Scaffolds for blocking protein-protein interactions. *Curr Top Med Chem.* (2007) 7(10):928-42)
40. Tornatore L., Marasco D., Dathan N., Vitale R.M., Benedetti E., Papa S., Franzoso G., Ruvo M. and S.M. Monti. Gadd45 beta forms a homodimeric complex that binds tightly to MKK7. *J. Mol. Biol.* (2008)18;378(1):97-111
41. Richard J.P., Melikov K., Vives E., Ramos C., Verbeure B., Gait M.J., Chernomordik, L.V. and B. Lebleu Cell-penetrating peptides. A re-evaluation of the mechanism of cellular uptake. *J. Biol. Chem.* (2003) 278(1): 585-590
42. Grabiner B.C., Blonska M., Lin P.C., You Y., Wang D., Sun J., Darnay B.G., Dong C. and X. Lin. CARMA3 deficiency abrogates G protein-coupled receptor-induced NF- $\kappa$ B activation. *Genes Dev.* (2007) 21(8): 984-996
43. Bradford M. A rapid and sensitive method for the quantization of microgram quantities of protein utilizing the principle of protein-dye binding. *Anal. Biochem.* (1976) 72:248
44. Crowther J.R. The ELISA guidebook. *Methods Mol Biol.* (2000) 149:III-IV; 1-413:III-413 (2005) 6:195-205
45. Fields G.B. and R.L. Noble Solid phase peptide synthesis utilizing 9-fluorenylmethoxycarbonyl amino acids. *Int. J. Pept. Protein Res.* (1990) 35(3):161-214
46. Rebeaud F., Hailfinger S., Posevitz-Fejfar A., Tapernoux M., Moser R., Rueda, D., Gaide O., Guzzardi M., Iancu E. M., Rufer N., Fasel N. and M. Thome The proteolytic activity of the paracaspase MALT1 is key in T cell activation. *Nat. Immunol.* (2008) 9(3) : 272-281

## IV. ABBREVIATIONS INDEX

$\alpha$ Fc $\epsilon$ RI: alpha subunit of the human Fc $\epsilon$ RI  
Apaf 1: Apoptotic Protease-Activating Factor 1  
APC: antigen-presenting cells  
BCL10: B-cell lymphoma 10  
 $\beta$ Fc $\epsilon$ RI: beta subunit of the human Fc $\epsilon$ RI  
 $\beta$ tFc $\epsilon$ RI: truncated beta subunit of the human Fc $\epsilon$ RI  
BSA: Bovine Serum Albumin  
CARD: Caspase Recruitment Domain  
CC-CARD: coiled-coiled caspase recruitment domain  
CD: Circular Dichroism  
DD: Death Domain  
DCM: dichloromethane  
DED: Death Effector Domain  
DIPEA: diisopropyl-ethylendiammine  
DMEM: Dulbecco's Modified Eagle's Medium  
DMF: *N,N*-dimethylformamide  
DMSO: dimethyl sulfoxide  
DNP-HBS: 2,4-dinitrophenol conjugated human serum albumin  
DTT: 1,4-Dithiothreitol  
ECD: extracellular domain  
EDC: N-ethyl-N'-(dimethylaminopropyl) carbodiimide  
EDTA: ethylenediaminetetraacetic acid  
ELISA: Enzyme-Linked Immunosorbent Assay  
ER: Endoplasmic Reticulum  
FCS: fetal calf serum  
Fc-IgE: Fc fragment of immunoglobulin E  
Fc-IgG: Fc fragment of immunoglobulin G  
FPLC: Fast Protein Liquid Chromatography  
4-VP: 4-vinyl pyridine  
 $\gamma$ Fc $\epsilon$ RI:  $\gamma$ -chains of the human Fc $\epsilon$ RI  
hFc $\epsilon$ RI: human Fc $\epsilon$ RI  
h $\alpha$ Fc $\epsilon$ RI: alpha subunit of the human Fc $\epsilon$ RI  
HBS: HEPES buffer saline  
HPLC: High Performance Liquid Chromatography  
HRP: horseradish peroxidase  
IgA: immunoglobulins A  
IgE: monoclonal anti-DNP mouse IgE  
IgG: immunoglobulins G  
IgM: immunoglobulins M  
IPTG: isopropyl-beta-D-thiogalactopyranoside  
ITAM: immunoreceptor tyrosine-based activation motif  
LB: Luria-Bertani medium  
LC-MS: Liquid Chromatography-Mass Spectrometry  
MAGUK: Membrane-Associated Guanylate Kinase  
MALT: Mucosa-Associated Lymphoid Tissue  
MALT1: Mucosa-Associated Lymphoid Tissue Lymphoma Translocation Protein 1  
MHC: Major Histocompatibility Complex  
NBD: Nucleotide-Binding Domain

NFDM: Non Fat Dry Milk  
NF- $\kappa$ B: Nuclear Factor- $\kappa$ B  
NHS: N-hydroxysuccinimide  
NTA: nitrilotriacetic acid  
OD<sub>600</sub>: Optical Density at 600 nm  
OPD: ortophenyldiamine  
PBS: Phosphate Buffered Saline  
PCR: Polymerase Chain Reaction  
PDB: Protein Data Bank  
PKC $\delta$ : Protein kinase C  
PMSF: Phenylmethylsulphonylfluoride (Inhibitor of Serine proteases)  
*p*-NAG: *p*-nitrophenyl-*N*-acetyl- $\beta$ -d-glucosaminide  
RP-HPLC: Reverse Phase-High Pressure Liquid Chromatography  
R.T.: room temperature  
RU: response unit  
SDS: sodio-dodecil solfato  
SPR surface plasmon resonance  
TEV: Tobacco Etch Virus (TEV) Nla protease  
TFA: Trifluoroacetic acid  
TIS: triisopropylsilane  
TNF- $\alpha$ : Tumor Necrosis Factor- $\alpha$   
TPCK: Tosyl Phenylalanyl ChloromethylKetone 1-Chloro-3-tosylamido-4-phenyl-2-butanone (irreversible inhibitor of chymotrypsin)  
TRIS:tris(hydroxymethyl)aminomethane  
TTBS :Tween Tris-buffered saline

## V. SCIENTIFIC PRESENTATIONS

1. F. Viparelli, N. Doti, **A. Sandomenico**, S.M. Monti, N. Dathan, L. Tornatore, M. Pizzulo, M. Amoroso, F. Beguinot, C. Miele, D. Marasco, E. Benedetti, C. Pedone, M. Ruvo.

PED binds with high affinity to the D4 domain of PLD1.

10<sup>th</sup> Naples workshop on bioactive peptides, Napoli, 11-14 Giugno 2006

2. L. Tornatore, S.M. Monti, N. Dathan, **A. Sandomenico**, D. Marasco, N. Doti, F. Viparelli, M. Pizzulo, M. Amoroso, E. Benedetti, C. Pedone, M. Ruvo.

Expression, purification and characterization of Gadd45 $\beta$ .

10<sup>th</sup> Naples workshop on bioactive peptides, Napoli, 11-14 Giugno 2006

3. **Sandomenico A.**, Monti S.M., Tornatore L., Dathan N., Doti N., Viparelli F., Marasco D., Saporito A., Sabatella M., Pedone C., De Capua A., Saviano M., Benedetti E., Ruvo M.

Peptide mimics of the IgE high affinity receptor Fc $\epsilon$ RI.

6<sup>o</sup> Pharmaco-Bio-Metallics, Napoli, 30 Novembre-1 Dicembre 2006

4. L. Tornatore, S.M. Monti, N. Dathan, N. Doti, F. Viparelli, **A. Sandomenico**, D. Marasco, A. Saporito, M. Sabatella, C. Pedone, E. Benedetti, M. Ruvo.

Antagonists of Gadd45 $\beta$ -MKK7 interaction by screening of a synthetic peptide library.

9<sup>th</sup> International symposium on Applied Bioinorganic Chemistry, Napoli, 2-5 Dicembre 2006

5. **Sandomenico A.**, Monti S.M., Tornatore L., Dathan N., Doti N., Viparelli F., Marasco D., Ronga L., Saporito A., Sabatella M., Pedone C., DeCapua A., Benedetti E., Ruvo M.

Synthetic peptide ligands for  $\alpha_1$ AT.

6<sup>o</sup> Pharmaco-Bio-Metallics, Napoli, 30 Novembre-1 Dicembre 2006

6. **Sandomenico**, D. Marasco, S.M. Monti, M. Saviano C. Pedone, E. Benedetti, M. Ruvo.

Peptides binding the type E immunoglobulins.

2007 American Peptide Society Symposium, Montreal, Quebec, CANADA 26-30 giugno 2007

7. M. Ruvo, **A. Sandomenico**, D. Marasco, S.M. Monti, B. Tizzano, A. De Capua, C. Pedone, A. Saporito, R.M. Vitale, R. Stilo and R. Liguoro.

Self association regions in the CARD of Bcl-10

2007 American Peptide Society Symposium, Montreal, Quebec, CANADA 26-30 giugno 2007

8. Marasco D., Cutillo F., Saporito A., Tornatore L., **Sandomenico A.**, Sabatella M., Doti N., Viparelli F., Pedone C., Dathan N., Monti S. M., Ruvo M.

A simplified and automated perspective for the screening of universal synthetic peptide libraries.

EUROCOMBI 4, Firenze, 15-18 Luglio 2007

9. **Sandomenico A.**, Marasco D., Dathan N., Saviano M., Monti SM., Ruvo M.  
Polypeptides antagonists of IgE-FcεRI interaction.  
11<sup>th</sup> Naples workshop on bioactive peptides, Napoli, 24-27 Maggio 2008